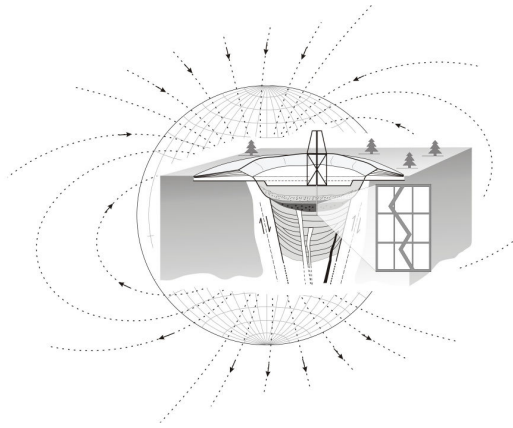


***Origin of magnetic anomalies in pyroclastic rocks  
of the Messel volcano: insights into a  
maar-diatreme-structure***



Dissertation zur Erlangung des  
naturwissenschaftlichen Doktorgrades  
der Julius-Maximilians-Universität Würzburg

vorgelegt von

**Diplom-Geologe Thomas Nitzsche**

Würzburg, Februar 2007

Eingereicht am:

1. Gutachter: Prof. Dr. Helga de Wall
2. Gutachter: Prof. Dr. Bernd Zimanowski

1. Prüfer: Prof. Dr. Helga de Wall
2. Prüfer: Prof. Dr. Reiner Klemd

Tag der Disputation:

Doktorurkunde ausgehändigt am:

Ich erkläre hiermit,

- a) dass ich die vorgelegte Dissertation selbst verfasst und mich dabei keiner anderen als der von mir ausdrücklich bezeichneten Quellen und Hilfen bedient habe,
- b) dass ich keiner anderen Stelle ein Prüfungsverfahren beantragt bzw. die Dissertation in dieser oder anderer Form bereits anderweitig als Prüfungsarbeit verwendet oder einer anderen Fakultät als Dissertation vorgelegt habe.

Würzburg, den 28.02.2007

# Curriculum vitae

## Persönliche Daten

Name: Thomas Nitzsche  
Geburtsdatum: 31.10.1975  
Geburtsort: Heilbronn  
Eltern: Dieter Nitzsche  
Renate Nitzsche, geb. Zügel  
Familienstand: ledig  
Staatsangehörigkeit: deutsch  
Konfession: evangelisch

## Ausbildungsdaten

Schulbildung:  
1982-1986 Grundschule Heilbronn-Horkheim  
1986-1990 Theodor-Heuss-Gymnasium Heilbronn  
1990-1995 Kreisgymnasium Riedlingen

Ersatzdienst:  
1995-1996 Kreiskrankenhaus Riedlingen

Studium:  
1996-2003 Studium der Geologie-Paläontologie and der Julius-Maximilians-Universität Würzburg  
1998 Vordiplom  
2000-2001 Post-graduate Student am Department of Geology und am Geothermal Institute der University of Auckland, Neuseeland  
2002-2003 Diplomkartierung und -arbeit am Stromboli Vulkan, Italien  
2003 Diplom  
2003-2007 Promotion in der Strukturgeologie, Institut für Geologie der Universität Würzburg  
2004-2007 Wissenschaftlicher Angestellter, Institut für Geowissenschaftliche Gemeinschaftsaufgaben (GGA), Hannover

## **Preface**

Maar volcanoes are commonly considered to be the phreatomagmatic equivalent of scoria cones and are the Earth's second most volcanic landforms in subaerial environments. They occur in volcanic fields, on ring plains surrounding composite cones and inside calderas of polygenetic volcanoes. On-going geoscientific investigations on maar-related deposits manifest their variety and complexity, despite the relatively small size and volumes of magma involved in maar-volcano systems. Maars consist of the crater that is incised in the former landscape and surrounded by a circular tephra ring, and the underlying diatreme (tuff pipe). The latter is the typical funnel-shaped sub-structure of maar volcanoes and is frequently buried beneath the surface.

Maar craters are frequently filled with lakes which are attractive sites for palaeoclimatic research because of their small surface catchments, simple basin morphology and rapid sediment accumulation. With respect to diamond-bearing kimberlites, understanding diatreme-facies has not only economic significance but also relevance in hazard assessment. The phreatomagmatic model of maar-diatreme formation frequently comprises highly explosive eruptions, which pose a threat to society in vicinity of inhabited areas. Experimental studies on volcanoclastic deposits with aspects of different geoscientific approaches provide the knowledge for understanding maar-related problems. Field and laboratory investigations on these rocks are the key to acquire knowledge of syn- and post-eruptive emplacement mechanisms.

This dissertation deals with experimental studies on volcanoclastic rocks of the Messel maar-diatreme-volcano to explain the origin of magnetic anomalies found during the research drilling project in 2001. Chapter 1 introduces the main topic and study site of the project. Chapter 2 deals with rock magnetic investigations on drilled volcanoclastic units. Chapter 3 covers pyroclastic fragment or particle investigations on a microscopic scale and assists to the rock magnetic results. Chapter 4 deals with combined gravity and magnetic field measurements and a computer-based 3D model of the Messel maar-structure. Chapter 5 closes the dissertation with its conclusions and perspectives.

## **Acknowledgements**

First of all I would like to thank my supervisor Helga de Wall for her excellent support and helpful ideas during the project. It was always a pleasure to me to acknowledge her critical and valued comments. I have been always fortunate to have had a particularly lively and competent person throughout my whole Ph.D. studies.

Many thanks deserve Christian Rolf (Laboratory of Rock Magnetism, Grubenhagen, GGA Institute) who supported me in rock magnetic concerns. Besides his professional assistance, he accompanied me with personal engagement and contributed to the success of the study.

Volker Lorenz and Bernd Zimanowski (University of Würzburg) are thanked for stimulating and teaching discussions on volcanism and volcanic particle problems. I profited from their professional competence, which inspired me during my whole study of geology.

I am grateful to the following colleagues and individuals for their help, encouragement and technical assistance: Rüdiger Schulz, Gerald Gabriel, Hermann Bunes, Helga Wiederhold, Kathrin Worm and Marianne Klick (GGA Institute); Gerhard Notbohm (BGR Institute); Marita Felder and Franz-Jürgen Harms (Senckenberg Research Institute); Valerian Bachtadse, Roman Leonhardt and Manuela Weiß (University of Munich); Ulrich Bleil and Thomas Frederichs (University of Bremen); Agnes Konty, Carsten Vahle and Luca Nano (University of Heidelberg); Jutta Lingstädt, Ulrike Martin, Frank Holzförster, Nina Dworazik, Daniela Renk, Verena Streit and Fabian Richard (!) (University of Würzburg).

Financial support was provided by the Deutsche Forschungsgemeinschaft (DFG).

The loveliest thanks deserve my parents Renate and Dieter Nitzsche, my sister Annette Nitzsche and my girlfriend Sabine Solinski.

## Summary

In 2001 the 433 m deep Messel 2001 borehole was drilled in the centre of the Messel Pit, 25 km south of Frankfurt (Germany). Geoscientific results from this drilling clarified the origin of the circular-shaped basin as a maar-diatreme-structure. Recovered deposits consist of lacustrine sediments (0-240 m) and volcanoclastic rocks such as lapilli tuffs (240-373 m) as well as rocks of the underlying diatreme breccia (373-433 m). The lapilli tuffs, as main interest here, show little differentiation on a macro- and microscopic scale and appear as a massive and unsorted volcanoclastic body with dominating juvenile lapilli and accidental clasts mostly in the range of (sub)millimetres to centimetres in diameter.

This study presents rock magnetic properties measured on core samples of the volcanoclastic units and explains the origin of downhole magnetic anomalies detected during the drilling project in 2001. Magnetic behaviour of the erupted material is related to fine-grained, Fe-rich (titano)-magnetites, which are dispersed within the juvenile lapilli. Temperature-dependent susceptibility experiments, isothermal remanent magnetisation and hysteresis investigations demonstrate similar ferrimagnetic properties throughout the volcanoclastic material, in terms of composition, coercivity and grain size (pseudo-single-domain particles) of the ferrimagnetic minerals. Thus, during emplacement of the erupted material, the ferrimagnetic minerals had the same remanence acquisition potential.

However, demagnetisation experiments show different magnetic stability behaviour of the acquired natural remanent magnetisation (NRM). Heating experiments prove the acquisition of thermal remanent magnetisation (TRM) dominated by temperature effects which could have been occurred during eruption and deposition of volcanic material, forming the Messel maar-diatreme. It is assumed that the upper half of the lapilli tuffs was deposited at relatively low depositional temperatures ( $<300\text{ }^{\circ}\text{C}$ ), whereas the material of the lower half took advantage of higher temperatures ( $>>300\text{ }^{\circ}\text{C}$ ). To understand the rock magnetic character within the Messel maar-diatreme-facies, particle grain sizes, the degree of the relative fraction dominance and the shape of the juvenile fragments have been studied in more detail. Image analytical methods as well as major and trace element analyses on the juvenile fraction support the clear subdivision of the lapilli tuffs. These findings in combination with rockmagnetic data indicate a separation into a relatively hot, geochemically undifferentiated eruption phase and a colder, differentiated phase. A two-condition eruption stage at the end of the Messel volcanic activity is suggested. The juvenile particles account for the temperature evolution and heat conditions during deposition of the Messel tuffs and contribute to the origin of magnetic field anomalies.

Based on gravity parameters and the results of magnetisation properties, the potential field 3D-model of the Messel subsurface explains the negative ground anomalies, calculates the mass and volume parameters of the drilled lithozones and shows the asymmetric appearance of the diatreme-structure.

## Zusammenfassung

Im Jahre 2001 wurde im Zentrum der Grube Messel, ca. 25 km südlich von Frankfurt gelegen, eine 433 m tiefe Bohrung abgeteuft. Geowissenschaftliche Ergebnisse, die durch die Bohrung gewonnen wurden, konnten die Herkunft des rundlichen Beckens durch eine Maar-Diatrem-Struktur erklären. Die erbohrten Kerne sind vom Hangenden zum Liegenden durch lakustrine Sedimente (0-240 m) und vulkaniklastische Gesteine gekennzeichnet, letztere werden durch Lapillituffe (240-373 m) und der Diatrem-Brekzie (373-433 m) beschrieben. Die Lapillituffe, auf die hier das Hauptaugenmerk gelegt wurde, sind makro- und mikroskopisch schwer differenzierbar und erscheinen als ein einzig massig auftretender, unsortierter vulkaniklastischer Körper, der hauptsächlich aus millimeter- bis zentimeter-großen juvenilen Klasten und Nebengesteinsbruchstücken aufgebaut ist.

Die hier vorliegende Arbeit präsentiert die gesteinsmagnetischen Eigenschaften von Kernproben der Messel Vulkaniklastika und erklärt die Herkunft der magnetischen Anomalien, die während des Bohrprojekts 2001 detektiert wurden. Das magnetische Verhalten des eruptierten Materials bezieht sich auf feinkörnige und eisenreiche (Titano)-Magnetite, die verteilt in den juvenilen Lapilli auftreten. Experimente der temperaturabhängigen Suszeptibilität sowie isothermale remanente Magnetisierungs- und Hystereseuntersuchungen an den vulkaniklastischen Proben zeigen im Sinne der Zusammensetzung, Koerzivität und Korngröße (Pseudo-Einbereichsteilchen) sehr ähnliche ferrimagnetische Eigenschaften. Das eruptierte Material mit seinen ferrimagnetischen Mineralen besaß bei der Ablagerung ein sehr ähnliches Potential zum primären Remanenzwerb.

Entmagnetisierungsversuche offenbaren Unterschiede im magnetischen Stabilitätsverhalten der erworbenen natürlich remanenten Magnetisierung (NRM). Aufheizexperimente beweisen die Akquisition einer thermisch remanenten Magnetisierung durch Temperatureffekte, die bei der Eruption und der Ablagerung des vulkanischen Gesteins im Diatrem auftraten. Die obere Lapillituffhälfte wurde bei relativ niedrigen Temperaturen ( $<300\text{ °C}$ ), die unter Hälfte bei hohen Temperaturen ( $\gg 300\text{ °C}$ ) abgelagert. Um den gesteinsmagnetischen Charakter der Messel Maar-Diatrem-Fazies besser zu verstehen, sind zusätzlich die Partikelkorngröße, der relative Anteil und die Form der juvenilen Fragmente sowie deren chemische Zusammensetzung näher untersucht und analysiert worden. Die Methodik der Bildanalyse sowie der Haupt- und Spurenelementanalyse des juvenilen Anteils ermöglicht eine klare Unterteilung der Lapillituffe. Die Kombination der Resultate der Partikelanalytik mit den gesteinsmagnetischen Befunden begünstigt die Einteilung der Vulkaniklastika in eine relativ heiße, geochemisch undifferenzierte und eine kältere, differenzierte Eruptionsphase. Somit liegt am Ende der vulkanischen Aktivität von Messel ein bivalentes Stadium zugrunde. Dabei sind die juvenilen Fragmente für die Temperaturentwicklung und Wärmebedingungen

innerhalb des vulkaniklastischen Materials verantwortlich und tragen zur Herkunft der magnetischen Feldanomalien bei.

Basierend auf gravimetrischen Parametern und den Ergebnissen der Magnetisierungseigenschaften der Pyroklastika ermöglicht ein 3D Potentialfeld-Modell der Messel Maar-Diatrem-Struktur die an der Erdoberfläche gemessenen negativen Anomalien zu erklären, sowie die Massen und Volumina der erbohrten Lithozonen zu berechnen.



# Contents

## Chapter 1 Introduction

1.1 Maar-diatreme volcanoes . . . . .	11
1.2 Motivation of the study . . . . .	15
1.3 Study site and Tertiary volcanism . . . . .	16
1.2 Messel drilling project 2001 . . . . .	17
1.4 Volcaniclastic rocks . . . . .	19

## Chapter 2 Rock magnetism

2.1 Fundamentals in paleo- and rock magnetism . . . . .	20
2.1.1 Earth's magnetic field . . . . .	20
2.1.2 Natural remanent magnetisation (NRM) . . . . .	22
2.1.3 Types of remanences . . . . .	25
2.1.4 Magnetic susceptibility (MS) . . . . .	26
2.2 Realisation of rock magnetic measurements . . . . .	27
2.2.1 Sampling and instruments . . . . .	28
2.2.2 Identification of magnetic minerals . . . . .	28
2.2.3 Demagnetization and thermal magnetic measurements . . . . .	30
2.2.4 Anisotropy of magnetic susceptibility (AMS) . . . . .	32
2.3 Results of rock magnetic measurements . . . . .	33
2.3.1 Magnetic signature of the volcaniclastic units . . . . .	33
2.3.2 Magnetic properties inside and outside the anomalies . . . . .	36
2.3.3 Magnetic susceptibility and magnetic fabric of the lapilli tuffs . . . . .	43
2.4 Interpretation of rock magnetic measurements . . . . .	46
2.4.1 Magnetic properties of the lapilli tuffs . . . . .	46
2.4.2 Magnetic fabric of the lapilli tuffs . . . . .	48

## Chapter 3 Pyroclastic fragments

3.1 Why study the Messel volcaniclastic particles? . . . . .	51
3.2 Analytical methods . . . . .	51
3.2.1 Image analysis . . . . .	51
3.2.2 Geochemical analysis . . . . .	52
3.3 Results of the fragment studies . . . . .	53
3.3.1 Image-analytical results . . . . .	53
3.3.2 Geochemical results . . . . .	56
3.4 Interpretation of the analytical measurements . . . . .	61
3.4.1 Heat source . . . . .	61
3.4.2 Magma source . . . . .	62

<b>Chapter 4</b>	<b>Potential field modelling</b>	
4.1	Potential field data of Messel Pit . . . . .	63
4.1.1	Gravity measurements . . . . .	63
4.1.2	Magnetic measurements . . . . .	64
4.2	Methodology . . . . .	65
4.2.1	Elevation model . . . . .	66
4.2.2	Modelling with IGMAS . . . . .	66
4.3	Results of 3D modelling . . . . .	69
4.4	Interpretation of 3D modelling . . . . .	72
<b>Chapter 5</b>	<b>Conclusions</b> . . . . .	74
<b>References</b>	. . . . .	79

## **Chapter 1 Introduction**

Volcanism has played and continues to play an important role in the early genesis and subsequent evolution of the Earth. It is a far-ranging phenomenon, addressing aspects from the generation of magma, its transport and migration, eruption and formation of volcanic deposits. Thereby, the study of volcanic rocks and minerals, their composition, history and constantly changing character combined with methods and techniques of physics are invaluable for the understanding of volcanic systems.

In the study presented here, geophysical and geological applications on volcanoclastic rock units of the Messel volcano explain the origin of magnetic anomalies, detected in the borehole and on the surface. The experimental results provide new insights into a maar-diatreme structure by estimations of emplacement temperatures, eruption and formation conditions as well as spatial and temporal distribution of intra-crater deposits.

### **1.1 Maar-diatreme volcanoes**

The term “maar” was first introduced by Steininger (1819, 1820, 1821 and 1822) who possibly re-used the name known from Roman times (Noll, 1967). As Steininger identified the round-shaped lakes of the West Eifel as volcanic craters, Scope (1825) introduced the definition of the geological term in the Anglo-Saxon literature and initiated the international usage of the word. In experimental studies, Daubree (1891 and 1893) pierced rock panels with gas and named these drill holes after the Greek word for perforation “la/une diatreme”. Daubree already compared these drill holes with kimberlite-pipes of South Africa as well as maars of the Eifel and Auvergne. Nowadays, the term pipe comprises the diatreme and underlying the root zone (transition zone between feeder dyke and the overlying diatreme) which are all sub-structures of a maar-volcano. The funnel-shaped pipe ends downwards in a feeder-dyke and opens upwards into the maar-crater. First introduced by Lorenz (1975), all terms are integral elements which correspond to a single type of a volcanic edifice – the maar-diatreme volcano.

#### *Formation and size of maars and diatremes*

The combination of field and laboratory methods is the key to understand maar-related eruption mechanisms. In this connection, the formation of maar-diatreme volcanoes has been analysed in a number of recent papers (e.g. Lorenz 1985, 1986, 1998 and 2000; Zimanowski, 1998; Lorenz and Kurszlaukis, 2007; Lorenz et al., 2002; Fröhlich et al., 1993; Zimanowski et al., 1997; Büttner and Zimanowski, 1998; Ort et al., 2000) and thus is described here very shortly.

Basically, maar-diatreme volcanoes form when magma of any chemistry rises from the magma chamber close to surface and interacts explosively with groundwater. The magma-

water interaction may lead to brittle fragmentation of the involved magma volume. Consequent shock waves generated by these thermohydraulic explosions have the quality to fragment the surrounding country rocks (Zimanowski et al., 1997; Kurszlaukis et al., 1998; Lorenz, 2000). The produced water vapour of the groundwater causes further fragmentation of the magma and the rise towards the surface generating an eruption cloud. Decompression of the eruption cloud and consequent condensation of large amounts of water vapour leads to tephra ejection and deposition of the material. The erupted rocks emplace on the crater floor and on the surrounding surface by base surges, ballistic transport and tephra fall. Tephra deposits may be primary thinly bedded base surges, thick beds of fall deposits or redeposited tephra of debris and mud flows. The different types of maar deposits with variable thickness are primarily influenced by the involved eruption volume, the interstitial water derived from the phreatomagmatic eruptions, rainfall, wind activity, distance to the maar crater and pre-eruptive topography. The most pronounced secondary effects on maar deposits mainly occur near the maar crater by syn-and post-eruptive collapse, resedimentation and subsidence processes.

Natural examples of maar crater are less than 100 m to over 2 km in diameter (measured from the crest of the tephra ring/wall) and several tens of metres to 300 m deep (measured from the crest of the tephra ring/wall) (Lorenz et al., 2003). The tephra ring is several metres to over 100 m high. Its inner slope dips towards the interior of the crater at about 33° (natural angle of rest) and the outer slope dips outward at a much shallower angle (e.g., 5–10°), both angles depending on the total volume ejected, the pre-eruptive topography, and, during and immediately after the eruptions of the volcano, also on the state of moisture content of the tephra and erosion processes (e.g., slumping). The tephra ring is built up by possibly a few tens to over of 1000 tephra beds, most of which are only a few mm, cm to 1–2 dm thick. These thinly bedded tephra beds of the tephra ring represent the proximal tephra deposits and point to the number of eruptions of the maar-diatreme volcano. From the foot of the tephra ring, very thinly bedded tephra extend outwards in a thin veneer for up to a few hundreds of km and represent the distal tephra deposits. Geophysical exploration and drilling as well as investigation of the country-rock clasts in the maar tephra give evidence that maars are underlain by diatremes (e.g., Hawthorne 1975, Lorenz and Büchel 1980, Lorenz 1982a, Büchel, 1987 and 1988, Büchel et al. 1987). Exposed diatremes may be several tens of metres to over 1.5 km wide and less than 100 m to over of 2.5 km deep. In hard rocks as is known from diamond-bearing kimberlite mines in South Africa they frequently dip inward at average angles of 82° (Hawthorne 1975). The diatreme fill consists of volcanoclastics, subsided blocks of country rocks and a variable amount of intrusive rocks. The rather regularly cone-shaped diatremes extend at depth into root zones, which can be 50 m in width and <500 m in vertical extend (Lorenz and Kurszlaukis, 2007). The root zone of a maar-diatreme is irregular in shape and overlies the magmatic feeder dyke of the volcano, typically less than 1 m in thickness (Lorenz and Kurszlaukis, 2007).

*Significance of maars and diatremes*

Maar eruptions can be highly explosive and pose a threat to society in vicinity of inhabited areas. Considering the geohazardous point of view solely, it is important to study maar-diatreme problems to guarantee a safer environment for human beings.

Young and well-preserved maar volcanoes, e.g. occurring in the western United States, Eifel region in Germany or Patagonia in Argentina, are impressive landforms which may attract thousands of tourists each year. For instance, the Eifel Volcano Park has various attractions worth seeing and is lucrative to be represented by Vulkanpark GmbH. Economic significance represents diatremes as important sites of deposits for building materials, diamond and ore deposits (Lorenz et al., 2003). Thereby, the exploration of diamondiferous kimberlite- and lamproite-diatremes has the highest economic relevance.

Maar crater depressions evolved after eruption and subsequent subsidence processes may serve as sediment entrapments. The formation of lacustrine sediments can provide important archives for terrestrial climatic and environmental reconstructions. For instance, composite varve dated sediment profiles from Lake Holzmaar and Lake Meerfelder Maar situated in the Eifel region have been used to investigate Holocene climate variability (Lücke et al., 2005). Stable carbon and nitrogen isotopes of bulk organic matter were determined continuously resulting in isotope records with a mean time resolution of 20-50 years. Differences in the isotopic response between these small maar lakes help to explore the sensitivity of different lake systems to similar environmental and climatic changes. The isotope records give evidence of major Holocene climate events in Europe around 9,600, 7,300, 5,500 and 2,700 years BP (Baier et al., 2000; Lücke et al., 2003,). Comparisons with marine records from the north-east Atlantic indicate a clear temporal synchronicity between terrestrial and marine signals. In addition, higher frequency oscillations in the order of several hundred years are revealed by the stable nitrogen isotope records from Lake Holzmaar and Lake Meerfelder Maar. The forcing factors for this behaviour can probably be found in atmospheric circulation changes or variations in solar activity.

Furthermore, within the framework of the International Continental Scientific drilling Program (ICDP) the Potrok Aike Maar Lake Sediment Drilling Project (PASADO) workshop held in March 2006 addressed several issues to Earth history and climate, natural hazards and volcanic systems during past glacial to interglacial cycles (Zolitschka et al., 2006). The topics included environmental reconstruction, paleosecular variation of the Earth's magnetic field, fire history, frequency of volcanic activity and tephra fallout, dust deposition, evolution of phreatomagmatic maar craters and the history of regional volcanic activity. It was concluded that dust and tephra records might provide important links between this terrestrial record and marine sediment archives and ice cores from Antarctica, enabling the resulting reconstruction of climate variability to be compared statistically with global circulation model simulations of this region. The planned drilling will make a contribution to maar-related volcanological

research and understanding of prevailing discussions on global climate change, which nowadays is not only a scientific subject but also hot topic in politics and mass media.

### *Exploration of maar-diatreme volcanoes*

The Exploration of maars and their underlying diatremes or diatremes solely, due to the erosive elimination of the maar crater and its sediments, can be carried out by conventional, geological methods (e.g., mapping, drilling, remote sensing), geochemical, petrological and geophysical exploration applications. Many known maars and diatremes are buried by post-genetic sediments and thus only approachable by potential field methods (gravity, magnetics, aeromagnetics, geoelectrics and seismics). Detailed investigations on preserved maar-structures by combined geophysical surveys have been performed in a few volcanic settings only, e.g. in the Eifel region in Germany (Büchel, 1987 and 1988; Büchel et al., 1987) the Auckland volcanic field in New Zealand (Cassidy and Locke, 2004; Cassidy et al., in press), the southern Slovakian basin (Puchnerova et al., 2000), and on German maars of Baruth and Messel (Schulz et al., 2005).

After Büchel (1987 and 1988), geophysical anomalies over maars and diatremes vary in their character and do not provide definitive evidence for a phreatomagmatic origin. However, geophysical methods are instrumental in the initial discovery of buried maars or diatreme-structures. Subsequent drilling and geological samples may confirm the phreatomagmatic origin. Interpretation of a single geophysical data set over a suspected maar or diatreme structure can be ambiguous. When combined, however, with complementary geophysical methods and the existing database over other known maar or diatreme structures, a more definite assessment can be made.

The most notable geophysical signature associated with maars or diatremes is a negative gravity anomaly. These gravity lows are generally circular and cover the whole structures. They are due to lithological and physical changes associated with the phreatomagmatic explosion. In well-preserved maar structures, low-density sedimentary infill of the topographic depression of the crater contributes to the gravity low.

Generally, magnetic anomalies associated with maar or diatreme structures are more complex than gravity anomalies. Their reasons may be very complex intrusion processes in the diatreme or in the sedimentary infilling of the maars. Depending on the groundwater involvement and the hydrostatic pressure in the maar-system, dykes and sills can get emplaced at relatively high levels in the pipe (Lorenz, 1986). Dykes can even reach the surface and erupt in magmatic fashion resulting in the formation of spatter cones in the maar crater. All these features inside and outside the diatreme pipe can cause a magnetic anomaly.

Further effective maar exploration methods are various electrical methods. Here, the presence of fluids in explosion-induced fractures and pore spaces of the maar and diatreme rocks leads to decreased resistivity levels that can be mapped. To study the maar structure morphology the best geophysical applications are reflection seismic surveys. These techniques provide

detailed information about subsurface layering and rock geomechanical properties by using seismic p- and s-waves. Moreover, well logging methods are very useful for detailed investigations of drill holes and the determination of lithozones in maar and diatreme structures.

## **1.2 Motivation of the study**

Completely preserved maar structures are restricted to areas of subsidence. Therefore, objective evidence for the existence of maar-diatreme structures can only be provided by geophysics and boreholes. As mentioned above, gravity and magnetics are the most common geophysical methods for prospecting maars (e.g. Wood, 1974); Quaternary dry maars in the Eifel area and some Tertiary maar structures in the German highlands have been investigated by gravity and magnetic methods (Büchel, 1993; Pirrung et al., 2003). Toth (1992) also included the resistivity method to detect hidden maars in the Slovakian Basin (Puchnerova et al., 2000). However, none of these methods give any information on the internal structure of the maar-lake sediments and intra-crater volcanoclastics.

In 2001 the geoscientific Messel research culminated in a 433m deep research drill hole. The preliminary interpretation of the potential field anomalies of several oil shale basins on the Sprendlinger Horst (Fig.1), discussed by Jackoby et al. (2000), turned out to be correct by the ultimately proof of drilled volcanoclastic sequences of a maar-diatreme volcano.

For the first time, the Messel research with its comprehensive geophysical ground survey, logging and core investigations serve as background information to clarify the origin of ground and borehole magnetic anomalies. In this way, volcanoclastic intra-crater maar-deposits have not been previously investigated by studies on vertical, successive core sections underlying lacustrine crater sediments. Rock magnetic and fragment analytical experiments in combination with the potential field investigations provide essential data sets for the interpretation of maar-related magnetic field anomalies and contribute to the understanding of the Messel maar genesis.

To clarify the Messel magnetic anomalies, rock magnetic experiments have been used to illuminate the logging data and the magnetisation properties of the volcanoclastic rock units (chapter 2). The results are supported by image-analytical and geochemical investigations on juvenile fragments to identify eruption phases and comment on depositional conditions. Rock magnetic and gravity parameters in combination with current geoscientific information of the Messel research allow reconstructing the subsurface dimensions of the Messel lithozones by computer-based 3D potential field modelling (chapter 4).

### 1.3 Study site and Tertiary volcanism

The Messel Pit, 25 km south of Frankfurt (Hesse, Germany), is world-famous since the discovery of its excellent fossils of animals and plants, and has been declared a UNESCO world heritage site in 1995. It is one of several proven Eocene basins (approx. 48 Ma) on the *Sprendlinger Horst*, which is part of the Upper Rhine Graben (URG) shoulder (Fig. 1).

Volcanic activity in this region occurred along faults systems which were formed during the Variscan orogeny and were reactivated in Permian and Tertiary times as extensional faults. Magma pierced through Rotliegend clastic sediments and crystalline rocks of the paleozoic basement, the latter cropping out mostly to the south of the Messel Pit (Fig. 1). Volcanic rocks are of Permian (melaphyres) and Tertiary (basalts) age. The occurrence of Tertiary “oil shales” (pelites) appear as isolated spots throughout this region and can be associated to the assumed SW-NE orientated “Messel-fault-zone” (Fig. 1).

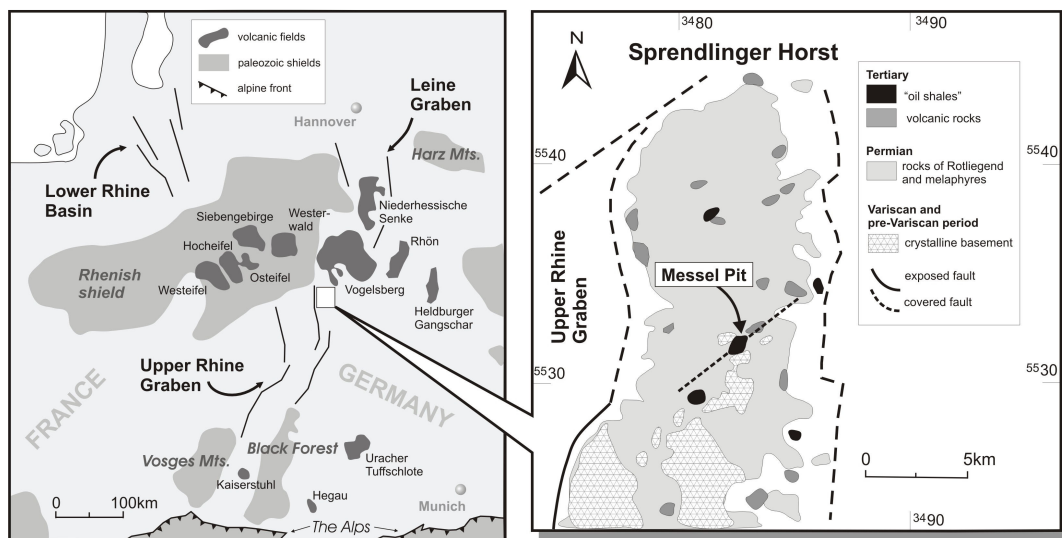


**Fig. 1** Tertiary (and Quaternary) volcanic fields in Germany and Central Europe (modified after Schmincke, 2004) and the geological situation around the Messel Pit (modified after Jackoby et al., 2005), which is located on the Sprendlinger Horst, a NE segment of the Upper Rhine Graben shoulder.

Most of Tertiary (and Quaternary) intraplate-volcanism in Germany can be associated to rift evolution of the URG (White and McKenzie, 1989; Ziegler, 1992; Goes et al., 1999; Wilson and Downes, 2006). The URG, Leine Graben and their north-western continuation of the Lower Rhine Basin reflect intermediate rift complexes of the Cenozoic Western European Rift system (Fig. 1), which extends from the North Sea to the Mediterranean Sea. Volcanic fields (e.g. Westerwald, Siebengebirge, Eifel) are mostly concentrated to uplifted and partly still uplifting blocks of the graben shoulders (Rhenish Shield, Vosges Mts., Black Forest) or are located within the graben or rift zones (e.g. URG and Leine Graben with Kaiserstuhl and Vogelsberg) adjoining to these graben shoulders (Schmincke, 2004).

Volcanic activity started with the onset of rift zone evolution in the lower/middle Eocene, concerning isolated volcanic centres of the Hocheifel (e.g. Eckfeld Maar) and the Sprendlinger Horst (e.g. Messel Maar) for instance. Extensional forces transitional to the



URG axis enabled the opening of the graben structure and its interrelated magma ascent, respectively, which is attributed to a meridional compressive stress field deriving from collision processes in the Alps region (Larroque and Laurent, 1988; Dèzes et al., 2004). The URG extension was localised on systems of pre-existing discontinuities and caused subsidence and sedimentation in the southern and intermediate parts of the graben (Schumacher, 2002). Extensional forces of the Oligocene established subsequent sedimentation throughout the rift structure with extensional directions ranging between WSW-ENE and WNW-ESE (Illies, 1975; Schumacher, 2002; Michon et al., 2003). Due to reorientation of the stress field in the Miocene and hence the WNW-ESE orientated formation of the Lower Rhine Basin, the URG has been reactivated in form of a strike-slip-fault system. Thereby, sedimentation was limited to parts of the northern graben system, whereas the other graben-related parts have been subject to uplift and erosion processes (Roll, 1979). Volcanism achieved its climax during Miocene epoch and formed most of the rift-associated volcanic field centres (Eifel, Siebengebirge, Westerwald, Vogelsberg, Niederhessische Senke, Vogelsberg, Rhön, Heldburger Gangschar, Kaiserstuhl, Uracher Tuffschlote, Hegau). The highly silica-undersaturated and alkaline magmas of the URG-associated volcanoes derive from sub-lithospheric depths of 80-100 km, but can be influenced by differentiation processes in shallow depths, too (Downes, 1987; Wilson and Downes, 1991; Wedepohl et al., 1994; Jung and Hoernes, 2000; Bogaard and Wörner, 2003; Frisch and Meschede, 2005; Wilson and Downes, 2006). Thus volcanic rocks accompanied by graben systems may feature high geochemical variability.

#### **1.4 Messel drilling Project 2001**

Since the discovery and excavations of the fossil-bearing “oil shales”, the origin of the Messel basin was controversial for a long time. As magnetic, gravimetric and seismic investigations suggested a maar-diatreme-structure beneath the surface (Buness, 2005; Schulz et al., 2005), the drilling project in 2001 proofed the maar-volcano hypothesis and allowed the Messel reconstruction (Fig. 2a). The 433 m deep bore hole was drilled in the centre of the Messel pit with discovery of lacustrine sediments (0-240 m) overlying volcanoclastic units with lapilli tuffs (240-373 m) and the diatreme-breccia (373-433 m). After Felder and Harms (2004), the moderately laminated, lacustrine sediments are divided into the middle (0-100 m) and lower (100-240 m) Messel formation. The latter shows within its lower parts some occurrences of juvenile and scoria fragments and is generally dominated by sandy, sometimes coarse-grained and breccious re-sediments (collapse breccia). The underlying, 133 m thick pyroclastic rocks (lapilli tuffs) represents a relatively homogeneous lithozone with a dominance of partly clast-supported juvenile and accidental fractions. The tuffs are frequently cemented by calcite which may also serve as a filling mineral within juvenile vesicles. The drilled sequences of the diatreme-breccia mostly consist of large clasts of granodiorites, amphibolites or

Rotliegend-sandstones. The breccia varies in clast components forming respective meter-thick layers of country rocks from the Messel area (Fig. 2a).

The Messel Pit today has a diameter of 700-1000 m. According to dimensions of maar-diatreme volcanoes (diameter of 1000 m and diatreme wall dip of c. 82°; Lorenz et al., 2003), approximately one fifth of the total maar-structure has been penetrated by the Messel 2001 borehole (Fig. 2a). The drilled lithozones confirm the well-described and proved model on formation of maar-diatreme volcanoes, mainly controlled by magma-water interactions (Lorenz, 1973 and 1986; Fischer and Schmincke, 1984; Wohletz 1986; Zimanowski et al., 1997; Vespermann and Schmincke 2000). From the bottom to the top, the Messel cores reflect volcanoclastic deposits of the last eruption phases and sedimentary deposits from the maar- to the lake-stadium.

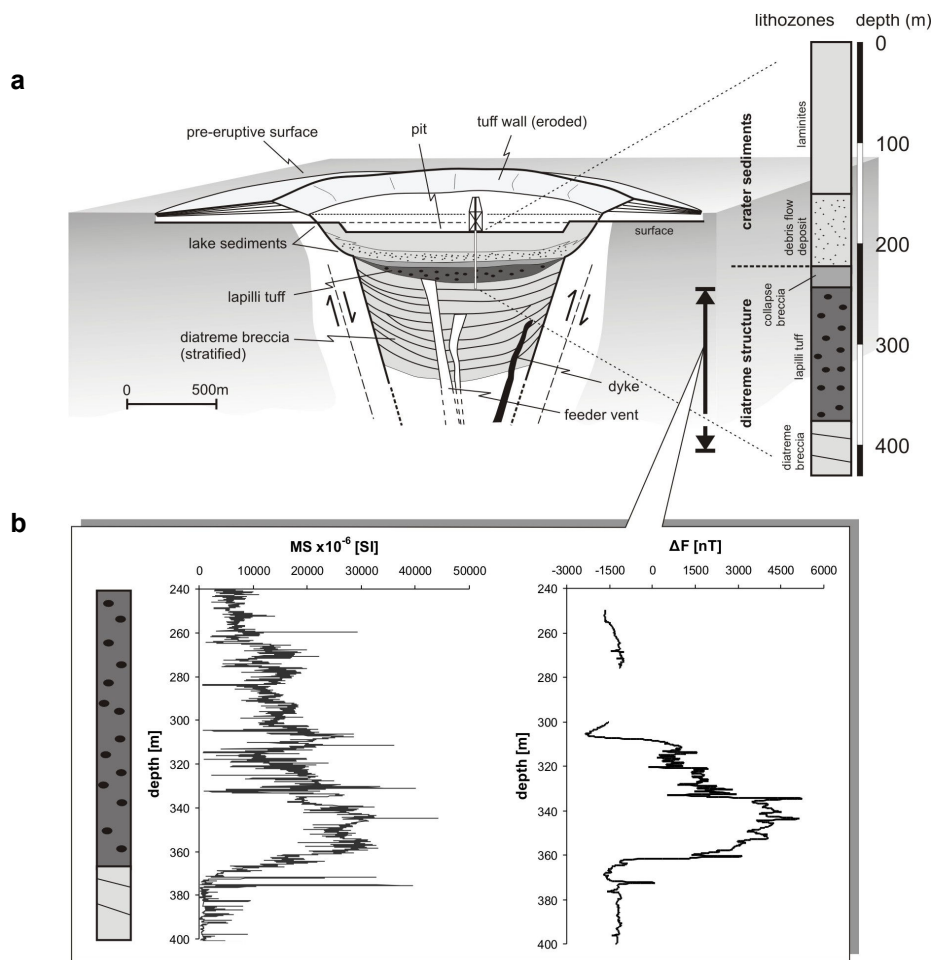


**Fig. 2 a)** Reconstruction of the Messel maar-diatreme volcano (modified after Lorenz, 2000; Harms et al., 2003) and its schematized lithozones (Harms et al., 2003) in depths of 0-433 m. **b)** Downhole magnetic data (Wonik and Salge, 2002) with magnetic susceptibilities MS (left) and deviations of the total magnetic field intensities  $\Delta F$  (right), performed during the drilling project in 2001.

One of the open scientific questions was the origin of the magnetic anomalies observed at the surface and within the borehole. Downhole magnetic measurements (Fig. 2b) performed during the drilling in depth between 240 m and 400 m (Wonik and Salge, 2000) display remarkable logs of the magnetic susceptibility (MS) and the deviations of the local magnetic

field intensities ( $\Delta F$ -anomalies) within the lapilli tuff units. While the MS log with varying intensities tend to increase with depths from the top to the bottom, it is remarkable that the downhole magnetic  $\Delta F$ -anomalies are mostly pronounced within the lower half of the lapilli tuffs (Fig. 2b).

### 1.5 Volcaniclastic rocks

The general term *volcaniclastic* was introduced by Fischer (1961) and includes all clastic volcanic materials formed by any process of fragmentation, dispersed by any kind of transport mechanism, deposited in any environment or mixed in any significant portion with nonvolcanic fragments. Because Messel volcanic fragments are vent-oriented particles formed by the explosive fragmentation of magma, it can be synonymously termed *pyroclastic*. After definition the term *tephra* is applied to pyroclastic accumulations blown into the air above an erupting volcano with any kind of particle size. The term is often used when dealing with relatively fresh and loose pyroclasts. In the case of Messel, the volcanic particles form relatively dense and old pyroclastic rock units, thus the word *tephra* is avoided in the text.

After Fischer (1961), the best criteria describing volcaniclastic rocks are to characterise their particles on the basis of grain size (Fig. 3a). There are three main types – *ash* (<2 mm), *lapilli* (2-64 mm) and *bombs* or *blocks* (>64 mm). *Tuff* is the consolidated equivalent of ash and pyroclastic *breccia* is a consolidated aggregate of blocks containing less than 25 % lapilli and ash. Moreover, there are several other criteria to describe pyroclasts in more detail, including origin, vesicularity and composition; they are specified in textbooks by Fischer and Schmincke (1984) or Heiken and Wohletz (1985). Figure 3b shows exemplarily photographs of typical Messel volcaniclastic rocks. The grain size difference between lapilli tuffs and diatreme breccia is remarkable. A more detailed description and investigation on the Messel particles will be given in the pyroclastic fragment chapter (3).

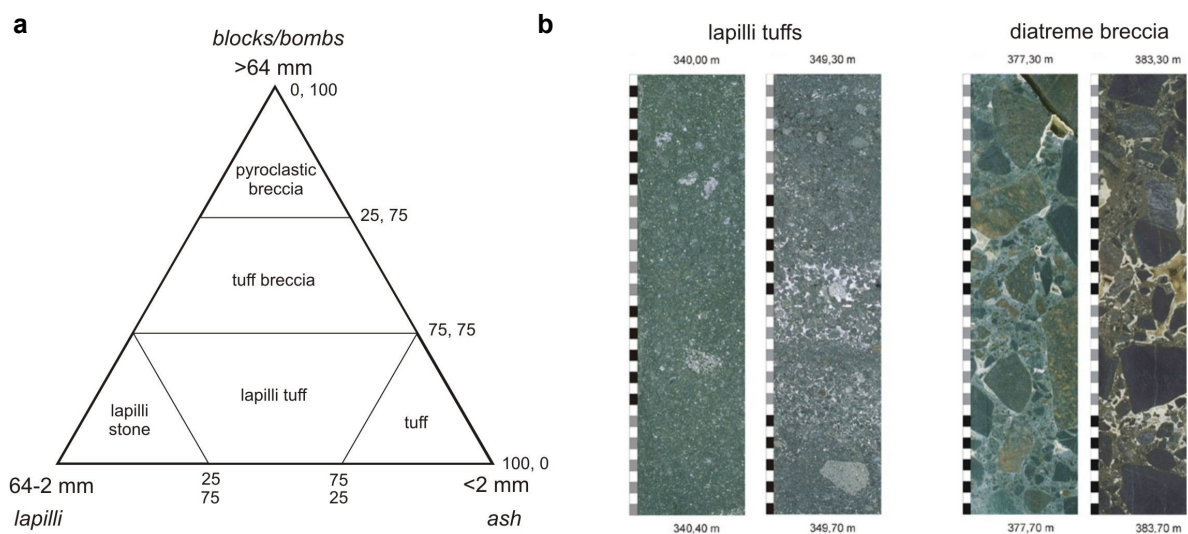


**Fig. 3 a)** Mixture and end member rock terms for pyroclastic fragments (after Fischer, 1966). **b)** The Messel volcaniclastic rocks with obvious grain size differences of the lapilli tuffs and the diatreme breccia.

## Chapter 2 Rock magnetism

### 2.1 Fundamentals in paleo- and rock magnetism

Paleomagnetism utilises the fossil magnetism in rocks. One major application is to measure movements of rocks since they were magnetised, which can be due to plate movements or tectonic tilting. Another important application is to measure the thermal history of a rock, such as reheating or the temperature of emplacement of pyroclastic deposits. Successful applications require understanding the magnetic field of the Earth and how rocks become magnetized, and detecting whether this magnetisation has changed subsequently. Rock and/or mineral magnetism utilises the variation of the magnetic properties of rocks to study processes such as deposition which may characterise magnetic field anomalies in volcanic bodies. The following chapter describes some fundamentals of rock magnetic applications which are essential for understanding the magnetic character within the volcanoclastic sequences of the Messel maar-diatreme.

#### 2.1.1 Earth's magnetic field

Magnetic fields are produced by the motion of electrical charges. The magnetic field of a bar magnet, for example, results from the motion of negatively charged electrons in the magnet. This can be made more visible by sprinkling iron filings on a sheet of paper placed over the magnet. The iron particles become tiny magnets which trace the magnetic field lines. A compass needle reacts in the same way to the Earth's magnetic field, which behaves as a magnetic dipole (Fig. 4a). The geomagnetic north (dipole) differs from the geographic north (Earth's rotation axis) and is presently tilted by  $11.5^\circ$  (Fig. 4b).

The magnetic field is measured in nano Teslas (nT) and its intensity varies from roughly 30,000 nT at the magnetic equator to 60,000 nT near the magnetic poles. As illustrated in figure 4b, it is distinguished between the geomagnetic poles, the real magnetic north and south poles, where inclinations (deviation from horizontal) are highest ( $I = \pm 90^\circ$ ). Thus, a geomagnetic and a real magnetic equator ( $I = 0^\circ$ ) also exist. Global isomagnetic maps of inclinations and other corresponding magnetic parameters can be deduced by Merrill et al. (1996).

The origin of the Earth's magnetic field is not completely understood, but is thought to be associated with electrical currents produced by convective effects within the liquid outer core. This mechanism is termed the *dynamo effect* (Bloxham and Gubbins, 1989)

Intensity and directions of the Earth's magnetic field or magnetization in rock samples can be described by three magnetic components (Fig. 4c). A horizontally oscillating needle points to a certain direction (magnetic north); the angle between this direction and the geographic north is called declination (D). A vertically oscillating needle deviates to this horizontal plane in a certain angle called inclination (I). It is positive when the north-searching end or the vector arrow of the total field intensity (F) is dragged down and negative when it is pulled up.

Relations and corresponding equations of the magnetic and geographic components can be deduced from figure 4c.

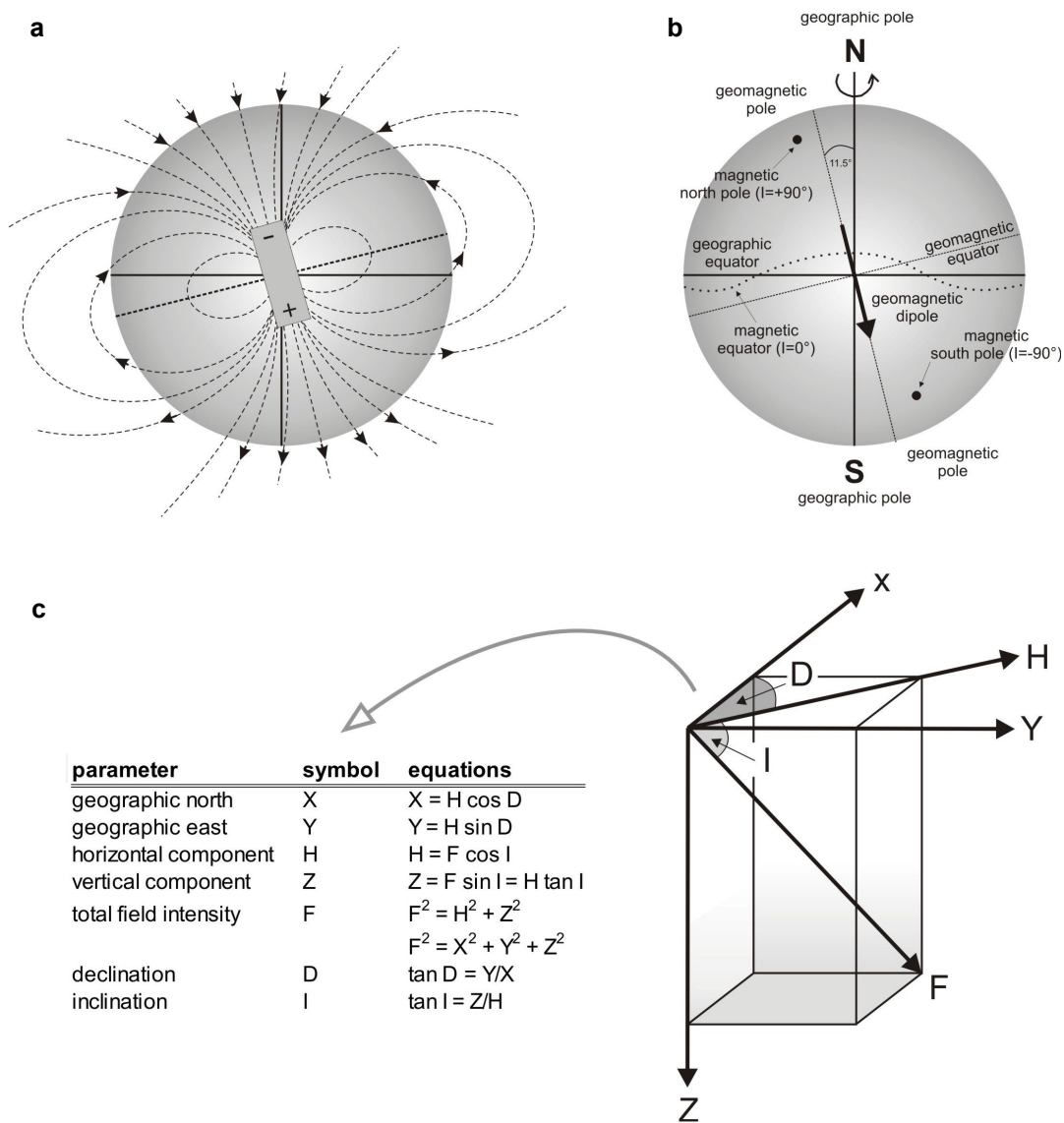


**Fig. 4 a)** Schematised Earth's magnetic dipole field and **b)** the corresponding magnetic field components. **c)** Definition of the Earth's magnetic elements and their mathematical relations. Knowing the inclination (I), the dipole location can be calculated.

It is known that the Earth's magnetic field with its different magnetic components appears to drift westward when measured at different places for a certain length of time (i.e. hundreds of years). This trend turns out to be different for the northern and southern hemisphere. The gradually spatial and temporal variation of all magnetic parameters, which result from non-dipole portions of the Earth's magnetic field, is called *secular variation*.

According to paleomagnetic measurements both the direction and the intensity of the field can vary enormously, up to a reversal of the Earth's magnetic field. Such polarity changes (normal and reversed polarity) have been recorded for a geological timescale from Upper Jurassic to present day. The current Earth's magnetic field is defined as normal polarity and

exists for about 780,000 years. Modelling magnetic field structures is a challenging subject for many scientists. It is proved that the Earth's magnetic field is about 10 percent weaker than it was 150 years ago (Glatzmaier and Roberts, 1996). If this fading trend continues, the field may collapse altogether and then reverse (Song and Richards, 1996). The volcanoclastic material of the Messel maar-diatreme has been erupted in such a period of reverse polarity at about 48 Ma ago (chapter 2.3).

### 2.1.2 Natural remanent magnetisation

*Diamagnetic* minerals are not important in paleomagnetism, because their atoms do not possess a magnetic moment without an applied magnetic field; whereas within an applied field, a magnetic field is induced (LENZ's law) which counteracts and weakens it. In the frame of rock magnetic investigations diamagnetism plays a minor important role. In some materials electrons, which surround an atomic nucleus and rotate around themselves (spin), produce a permanent magnetic moment and behave as small elementary magnets. In this case, when applying a magnetic field, the magnetic moments align to the induced field and slightly intensify it. Removing the applied field reproduces the original disarrangement of the magnetic moments. This weak and temperature-dependent magnetism is called *paramagnetic*. Dia- and paramagnetic materials lose their acquired magnetisation as soon as the field does not exist anymore.

Some rocks, however, consist of minerals which are able to acquire remanences. Thereby, when applying a magnetic field, the previously non-magnetised rocks get a remanent magnetisation after removing the magnetic field. Generally, remanence carriers are iron-bearing minerals, the so-called *ferro-* and *ferrimagnetic* minerals, respectively. The pure ferromagnetism is generally limited to metals or alloys, and rarely occurs in rocks. The pure *antiferromagnetic* component (e.g. illmenite), which is characterised by exactly antiparallel aligned magnetic moments, is not of great relevance in paleomagnetism, too. However, when

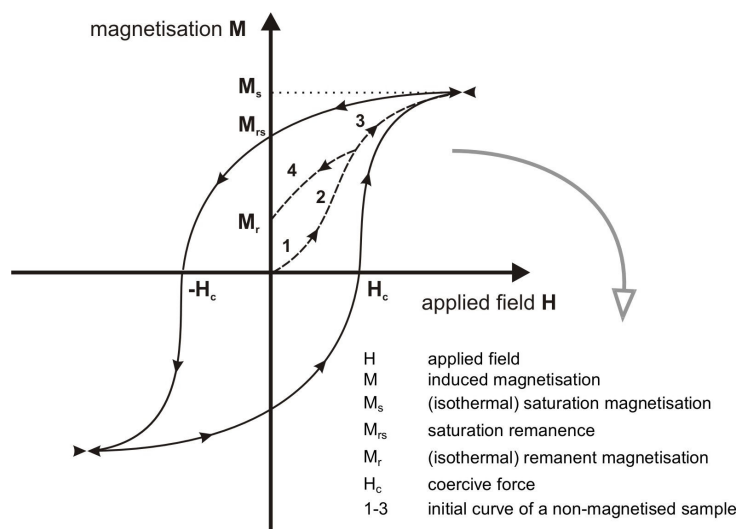


**Fig. 5** Exemplary magnetisation curve of ferromagnetic materials exposed to an applied magnetic field.

the antiparallel magnetic moments are not aligned exactly in the same strength, the *ferrimagnetic* component (e.g. magnetite) has an enormous effect. Chanted antiferromagnetic minerals (e.g. hematite), i.e. minerals which do not possess exactly parallel magnetic moments with the same strength, are also of interest for paleomagnetic investigations.

Subsequently, all (anti)ferro(i)magnetic states are simply summarised as ferrimagnetism.

Exposing a demagnetised ferrimagnetic sample to an applied field  $H$ , its magnetisation increases nearly linearly (Fig. 5). The initial susceptibility  $\kappa$  ( $\kappa = M/H$ ) corresponds to the gradient of the curve (stage 1) and is totally reversible in this section. The further increase of the applied field causes a higher gradient of the curve (stage 2) and leaves behind an isothermal remanent magnetisation ( $M_r$  or IRM) when removing field  $H$  (stage 4). Following stage 3, the saturation magnetisation ( $M_s$  or SIRM) is achieved at sufficiently high magnetic fields.

At decreasing fields to  $H=0$  a saturation remanence  $M_{rs}$  may be produced; when the field is applied to the opposite direction, the coercive force  $H_c$  is required to annihilate this magnetisation. At sufficiently high field strengths of the reverse direction the saturation may be pronounced, too. A fully evolved magnetisation curve is called *hysteresis loop*. Its shape is dependent on magnetic properties of the material and describes the most important rock magnetic parameters (Fig. 5). Further magnetic parameters and units can be deduced by Soffel (1991).

### *Magnetic domains*

Magnetisation of a rock sample results from numerous magnetic moments (dipoles). Due to energetic and geometric reasons, they are willing to align in groups of uniform magnetisation, the so-called *magnetic domains* which are confined by *Bloch walls*. Large mineral grains consist of several domains, the multi-domain (MD) particles, whereas below a certain grain size the particles are too small for carrying more than one domain; they are called single-domain (SD) particles. In between these end members the pseudo-single-domain (PSD) particles are effectively characterised by two, three or four domains. A more detailed description of the properties of magnetic domains can be deduced by Dunlop and Özdemir (1997).

Increasing temperature produces enhanced mobilisation of magnetic moments, mainly at a certain material specific temperature - the *Curie temperature* ( $T_C$ ). Above  $T_C$  the material becomes paramagnetic, so that magnetic moments are totally mobile. Here, the relaxation time  $\tau$  (quantity for the possible span of time in which remanent magnetisation of an assemblage of grains decays with time) is minimal, i.e. the magnetic moments align and react to the external magnetic field. Decreasing temperatures below the Curie temperature result in a spontaneous magnetisation and an increase in the relaxation time, so that the magnetic moments are fixed above the material specific temperature, the so-called *blocking temperature*  $T_B$  ( $T_B \leq T_C$ ). Thus, the relaxation time depends on blocking temperatures and the grain volumes. Appropriately, SD particles with  $\tau = 100$  Ma to 1 Ga assure the highest stability against remagnetisation and are able to retain paleomagnetic information over a geological time span. The even smaller superparamagnetic (SP) particles have very short relaxation times ( $<1$ s) and do not possess stable remanence directions at room temperatures.

Magnetisation of MD particles is carried out by movements of domain walls (Bloch walls) which require a relatively small energy input. They are easy to magnetise in contrast to PSD particles, which Bloch walls are considerably influenced by their grain shapes. Additionally, an enhanced energy input is needed for magnetisation of SD particles. According to this phenomenon, the domain structure is of elementary importance because only SD and PSD particles have the ability to retain rock magnetic information over geological time spans.

*Magnetic minerals*

Remanences of rocks are caused paramount by iron-titanium-oxides, iron-sulphides and iron-hydroxides (goethite). The most important remanence-bearing minerals belong to the ternary system of iron-titanium-oxides with notably two considerable oxidation lines (Fig. 6). First, the oxidation line of titano-magnetites with the end members ulvoespinel and magnetite, second, the oxidation line of titano-hematites with the end members of ilmenite and hematite. Curie temperatures indicate the most stable remanences close to the end members of magnetite and hematite. Titano-magnetites occur very frequently within the Earth’s crust, particularly in basalts, intrusions, sandstones and carbonates, but accessory in many other rock suites, too. Titano-magnetites form during rapid cooling, i.e. in ocean basalts, lava flows or juvenile fragments.  $T_c$  for magnetite is at about 578 °C and for titano-magnetite mostly between 150-400 °C. Maghemite forms as a result of oxidation processes of titano-magnetites at temperatures below 250 °C. Its  $T_c$  is difficult to determine because it decays to hematite above 400 °C.  $T_c$  for hematite is quoted 680 °C.

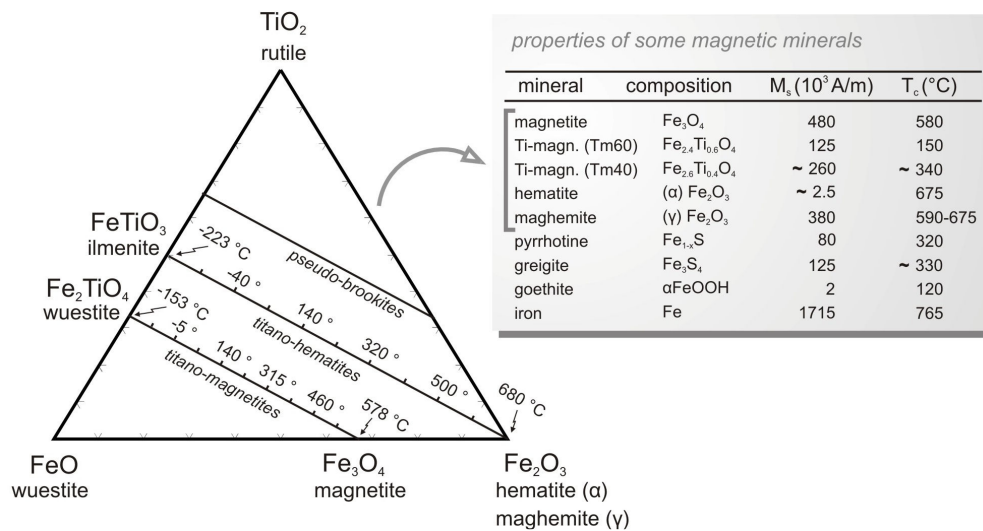


**Fig. 6** Ternary diagram of the iron-titanium-oxides after McElhinny and Mc Fadden (2000). Between the end members of  $\text{TiO}_2$ ,  $\text{FeO}$  and  $\text{Fe}_2\text{O}_3$ , titano-magnetites, titano-hematites and pseudo-brookites are illustrated. The chemical composition of the ferrites can be deduced by their Curie temperatures. Pseudo-brookites are paramagnetic under room temperature conditions.

Both hematite and titano-hematite occur very frequently in silica-rich magmatites such as granites, quartz-porphyrines or rhyolites, respectively. However, hematites may possess



remanent magnetisation and appear as important chromophoric pigments or isolated grains in red sediments, too. Anti-ferrimagnetic hematite may form due to oxidation of magnetite and dehydration of goethite, or it is precipitated from iron-rich solutions. Besides the Curie-temperature of 680 °C, it achieves just 0.5 % of the saturation magnetisation of magnetite (Soffel, 1991). Solid solutions of titano-hematite just develop at high temperatures, whereas their intermediate composition remains, for instance, by rapid cooling of pyroclastic material (McElhinny and McFadden, 2000). The solid solution line of pseudo-brookite occurs in the ternary diagram above the titano-hematites, with a stronger chemical influence of rutile composition, but in this context it is of no importance and will not be discussed in detail.

The iron-sulphides greigite and pyrrhotin may develop during anoxic conditions, alike the paramagnetic pyrite, but alter easily into pyrite when exposed to an oxygen-rich environment.

### **2.1.3 Types of remanences**

Nowadays, very sensible and modern magnetometers enable the proof of remanent magnetisation of practically all rock types. It is called the natural remanent magnetisation (NRM) and is accomplished by a small content of ferrimagnetic minerals. The acquisition of NRM is produced by physical and physical-chemical effects. Thereby, series of rock types with characteristically physical remanence types can be determined. The formation of a certain remanence type is strongly dependent on different grain fractions, and thus on different coercivity forces or blocking temperatures of ferrimagnetic minerals. It is the aim to characterise and analyse the NRM, and to determine magnetic directions and intensities in a rock sample. In this context three different remanence types will be discussed in the following paragraphs.

#### *Thermoremanent magnetisation (TRM)*

TRM is acquired during emplacement of volcanic rocks (effusive or explosive) and intrusive bodies or nearby their contact zones, which reflects a “snapshot” of the Earth’s magnetic field. It can be very stable and produced by the process of cooling below the Curie temperature  $T_C$  of ferrimagnetic material. The grain size-dependent blocking temperature  $T_B$  (see 2.1.2, magnetic domains) is a discrete temperature, when ferrimagnetic minerals exist in one grain size fraction. However, most rock samples possess a wide grain size spectrum, resulting in wide blocking temperature spectra. If  $T_C$  is not achieved when temperatures are too low, a partial TRM (PTRM) may remain. It compromises the acquired remanences of all mineral grain sizes when their blocking temperatures have been exceeded. Consequently, TRM is composed of many PTRMs.

#### *Chemical remanent magnetisation (CRM)*

CRM evolves in ferrimagnetic minerals when they grow in an external magnetic field and exceed a certain grain size (blocking volume  $V_B$ ; analogical to  $T_B$ ). Superparamagnetic single-

domain particles (SD particles) with a short relaxation time ( $\varnothing = 0.1 \mu\text{m}$ ,  $\tau = 100\text{s}$ ) exist below  $V_B$ , whereas above  $V_B$  the relaxation time achieves very quickly geological time spans (magnetite with  $\varnothing = 0.13 \mu\text{m}$ ,  $\tau = 1 \text{ Ga}$ ; after McElhinny and McFadden, 2000). CRM may acquire a similar stability to TRM, but feature a lower magnetic intensity. Thus, discrimination between CRM and TRM turns out to be sometimes not very easy. CRM may form due to weathering processes and is very often acquired by goethite, hematite and (Ti)-maghemite.

*Detrital remanent magnetisation (DRM)*

Ferrimagnetic particles may align to the external magnetic field and behave as compass needles, when they were deposited within a very settled milieu (e.g. lake sediments). The embedding of these particles is primarily controlled by their grain shapes. Thus some magnetic moments may align not exactly to the external field, but on average the remanence directions correspond to the magnetic field, which exists during rock formation. Platy particles mostly tend to embed very flat and falsify the intrinsic magnetic inclination to smaller values. This effect is amplified due to compaction of the material and thus the inclination error can be averaged up to  $10^\circ$  (Soffel, 1991). Further secondary chemical processes can alter or remove original detrital ferrimagnetic minerals and/or precipitate new minerals, which can have a large effect on paleomagnetic record. According to these complexities, DRM is less well understood than is TRM, and there are uncertainties of the accuracy of paleomagnetic record in sedimentary rocks (Butler, 1992).

**Table 1** Overview of natural remanence types (after McElhinny and McFadden, 2000).

Short form	Magnetisation type	Description
<b>NRM</b>	natural remanent magnetisation	insitu remanent magnetisation (RM) which a sample possess in its natural environment
<b>TRM</b>	thermoremanent magnetisation	RM which a sample acquires during cooling below $T_c$ within an external magnetic field
<b>PTRM</b>	partial thermoremanent magn.	RM which a sample acquires when heated and cooled below $T_c$
<b>CRM</b>	chemical remanent magnetisation	RM which a sample acquires due to transformation or regeneration of magnetic minerals
<b>DRM</b>	detrital remanent magnetisation	RM which acquires a sediment when its ferrimagnetic particles sink/deposit within an external magnetic field

**2.1.4 Magnetic Susceptibility (MS)**

In section 2.1.2 the connection of magnetic susceptibility (MS) and magnetisation curve or hysteresis loop has been shortly introduced. Generally, the MS is the degree of magnetization of a material in response to a magnetic field. The dimensionless volume magnetic susceptibility, represented by the symbol  $\kappa$  (or  $k$ ), is defined by the relationship

$$\kappa = M/H,$$

where M is the magnetization of the material (the magnetic dipole moment per unit mass), measured in amperes per meter (A/m), and H is the applied field, also measured in amperes per meter (A/m). Consequently, MS is a unitless constant that is determined by the physical properties of the magnetic material.

Paramagnetic materials (2.1.2) become magnetised only when a field is present, but ferrimagnetic materials also increase their magnetisation while a field is applied. This temporary magnetisation is called *induced magnetisation*. It can take on either positive (paramagnetic and ferrimagnetic) or negative (diamagnetic) values. Positive values imply that the induced magnetic field M is in the same direction as the inducing field H. Negative values imply that the induced magnetic field is in the opposite direction as the inducing field.

If magnetite is present, it is likely to dominate the MS (as well as the remanence). MS is measured by applying a known magnetic field to a sample and measuring the increased magnetism of the sample by the extra magnetic field it produces. These measurements can be made in the field (with a kappameter) or in the laboratory (with a kappabridge), the latter giving more sensitive results.

The application of MS in geosciences is used for all rock types. It is, for example, instrumental in mapping rocks which are macroscopically very difficult to distinguish. Furthermore, downhole MS measurements as a stratigraphic marker may provide information of lithological changes. They can be very useful in volcanology recording different eruption styles due to changing mineral phases or assemblages in the volcanic system. Thereby, when forming these rocks with their magnetic content and/or magnetic quantities, the geological situation (subaeric or subaquatous conditions) plays an important role. There are many other MS applications (e.g. record of climatic changes), but they are not subject in this study and thus will not be discussed in more detail. Studying magnetic fabrics of rocks, the anisotropy of magnetic susceptibility (AMS) provides information about geometries which are indicative for the internal structure of the material. This and other rock magnetic methods will be subject in the next chapter.

## **2.2 Realisation of rock magnetic measurements**

Samples used for rock magnetic measurements need to be prepared carefully in the laboratory before instrumental treatment. When studying magnetic properties of the drilled rock specimens, it is essential to identify and characterise the dominating magnetic mineral phase. In doing so, ferrimagnetic crystals and their domain status may explain how they lead to magnetic memory in the form of thermal, chemical or other remanent magnetisations. The (paleo)magnetic stability behaviour of the dominating ferrimagnetics can be tested by demagnetisation experiments which classifies their *in situ* magnetic record. Dealing with volcanic rocks, heating experiments can be crucial to understanding thermal conditions

during/after emplacement of the material. Besides the classic paleo/rock magnetic methods which may explain magnetic anomalies detected, AMS measurements are used for magnetic fabric indication and provide information about the internal structure of the erupted material. The following paragraphs are supposed to introduce the rock magnetic applications and proceedings used for elucidating the magnetic signature found within the volcanoclastic sequences of the Messel maar-diatreme.

### **2.2.1 Sampling and instruments**

Sample preparation and rock magnetic measurements have been performed in the Laboratory of Rock Magnetism in Grubenhagen (GGA Institute, Leibniz Institute for Applied Geosciences), unless otherwise noted. One-meter half-cores of the Messel drilling project 2001 have been used for receiving standard cylinders (1-inch in diameter and 2.2 cm in length) with a water-cooled drilling and sawing apparatus. In doing so, 4-10 plugs have been drilled from one selected half-core section. Magnetic susceptibilities have been measured with a Bartington apparatus MS2. Temperature-dependent MS experiments (using a KLY2/CS2 kappa-bridge, AGICO, in an argon atmosphere) were performed in the Magnetic Laboratory of the Geology Department at the University of Heidelberg. Magnetisation measurements have been realised with a 2G-cryogen magnetometer (Goree and Fuller, 1976; Fuller, 1987) or with a mini-spin magnetometer (Fuller, 1987) for samples with very high NRM intensities. Isothermal remanent magnetisation (IRM), alternating field (AF) and thermal (TH) demagnetisation as well as thermal remanent magnetisation (TRM) experiments have been carried out with instruments from Magnon GmbH (PM I, MI AFD 200 and MI TD 700). Hysteresis experiments at 5 K and 300 K have been measured on small mm-sized samples with MPMS-XL7 (Magnetic Properties measurement System XL-7) at the Department of Geosciences at the University of Bremen and with a variable field translation balance (VFTB), equipment of the Paleomagnetic Laboratory at Niederlippach (LMU, Munich). AMS measurements were performed with a KLY-4S kappa-bridge (AGICO) in the Structural Laboratory at the Institute for Geology of the University of Würzburg. Thin sections were produced at the Institute for Mineralogy of the University of Würzburg for microprobe analyses (CAMECA SX51), whereas magnetic minerals have been analysed at the Mineralogical Institute of the University of Heidelberg.

### **2.2.2 Identification of magnetic minerals**

Besides the visualisation of magnetic components on a microscopic scale and their geochemical identification via microprobe analyses, remanence-bearing minerals can be distinguished on the basis of the determination of Curie temperatures (compare table in figure 6). The combination of magneto-mineralogical and rock magnetic investigations is essential for a precise identification of the magnetic minerals.

*Determination of Curie temperatures*

Temperature-dependent MS experiments are investigated on pulverised samples. The fine-grained material is heated up stepwise (10 °C) to 700 °C and then cooled down to room temperature again. The originated heating and cooling curves (k/T-curves) of the samples reflect mineral-specific variations of the susceptibility. The temperature and material dependency of the MS for para- and ferrimagnetics as well as their calculated percentages in the material derives from the Curie-Weiss law which is documented by Houdra (1994).

During heating, thermomagnetic curves of rocks dominated by ferrimagnetic components frequently show a characteristic MS increase with a maximum directly below  $T_C$ , the so-called *Hopkinson-Peak*. When achieving  $T_C$ , a mineral-specific MS decrease occurs; this can be used for mineral identification. The variation of blocking temperatures in rocks, however, signifies that the MS (grain-size dependent!) with increasing temperatures declines in a different broad range, depending on the dominating domain status of the material (Fig.7 a-c).

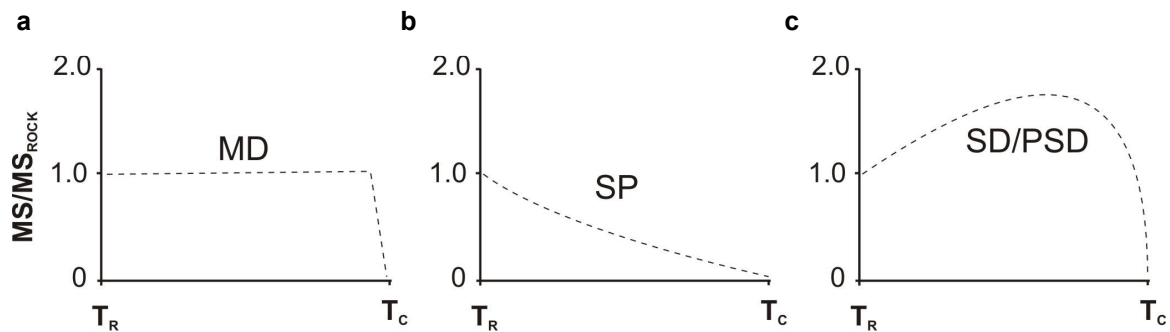


**Fig. 7 a-c** Thermomagnetic MS curves (k/T-curves) of synthetic magnetites after Radhakrishnamurty et al. (1982). Grain size dependency is reflected by MD, PSD, SD and SP (superparamagnetic) particles from their room ( $T_R$ ) to Curie ( $T_C$ ) temperatures.

Correlating heat and cooling sections of thermomagnetic curves point to an absence of mineral changes within the material. During heating, newly formed magnetite frequently occurs and results in an intense MS increase, noticeable by the shifted cooling curve to higher MS intensities. Furthermore, different ferrimagnetic mineral phases may transform into thermally stable minerals. These temperature-dependent mineral changes are highlighted in McElhinny and McFadden (2000) and will not be specified here because of the single ferrimagnetic component dominance within the volcanoclastic rocks of Messel.

#### *IRM and hysteresis measurements*

Isothermal remanent magnetisation (IRM) and hysteresis experiments are very instrumental in gaining the most important magnetisation parameters of the ferrites in order to state the mineral phase and domain status dominant within a sample (compare Fig. 5).

IRM experiments are carried out with a pulse magnetiser. Thereby, rock specimens, which are previously demagnetised, are exposed to an inducing field (peak fields up to 500 mT) at a constant temperature (room temperature) for stepwise acquisition of IRM. The acquired IRM curves may display a plateau, when saturation remanence (SIRM) is achieved. IRM and back

field curves inform about coercivity and domain state parameters. After Palmer et al. (1996), the latter can be deduced by IRM curves of a known mineral phase (Fig. 8a).

With respect to hysteresis experiments, the measured material initially behaves similar to IRM acquisition, magnetised in one direction. After removing the inducing field, applying a driving field to the material in the opposite direction and vice versa, its magnetisation will trace out a fully evolved hysteresis loop. The lack of retraceability of the magnetisation curve is the property called hysteresis and it is related to the existence of magnetic domains in the material. For further rock magnetic classifications, temperature-dependent hysteresis investigations can separate the ferri- and paramagnetic components.

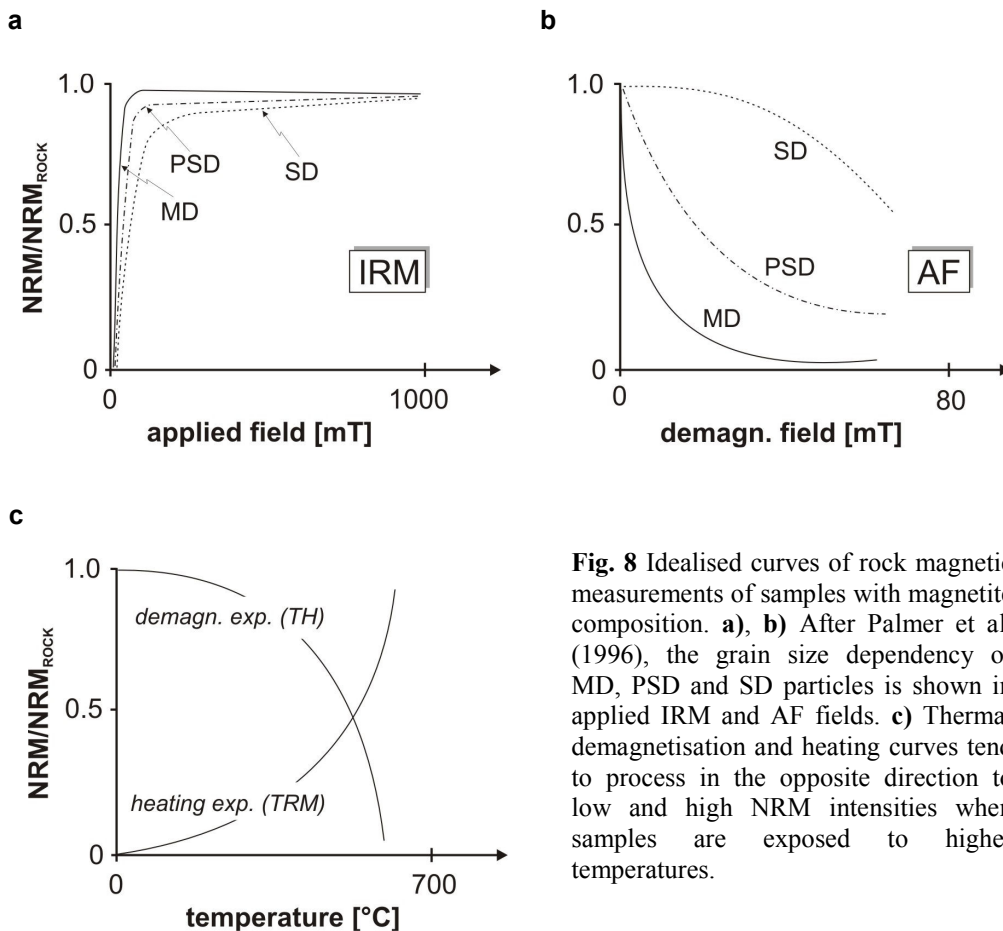


**Fig. 8** Idealised curves of rock magnetic measurements of samples with magnetite composition. **a), b)** After Palmer et al. (1996), the grain size dependency of MD, PSD and SD particles is shown in applied IRM and AF fields. **c)** Thermal demagnetisation and heating curves tend to process in the opposite direction to low and high NRM intensities when samples are exposed to higher temperatures.

### 2.2.3 Demagnetisation and thermal magnetic measurements

Demagnetisation techniques (alternating field (AF) and thermal (TH) demagnetisation) allow a further detailed magnetic characterisation of the material investigated. They inform about the magnetic stability behaviour. Laboratory-controlled heating experiments, such as thermoremanent magnetisation (TRM) experiments, are used to assess thermal history conditions during or after deposition of the volcanic material. Thereby, it is the action of the magnetic field (i.e. the applied field in the laboratory) at respective blocking temperatures

which are distributed downward from the Curie temperatures to produce TRM (or additive PTRM = partial thermoremanent magnetisation) within the rock specimens.

#### *AF demagnetisation experiments*

For stepwise AF demagnetisation, rock specimens were magnetically shielded and exposed to a 60 Hz alternating field. The higher the coercivity forces of the magnetic minerals within the material, the higher are AF fields needed for complete demagnetisation ( $H_{\text{dem}}$ ). The AF intensity being used to reduce the initial remanence by one half is called the median destructive field, or MDF. Generally, AF curve progressions also provide information about the remanence carriers (MD, PSD, SD particles), due to the magnetic stability behaviour of a known magnetic mineral phase (Fig. 8b).

#### *TH demagnetisation and TRM experiments*

Ferrimagnetic minerals, such as magnetite, acquire their remanence as they cool below their Curie temperatures ( $\sim 580$  °C) in a crystallising melt. Immediately below their Curie temperatures minerals respond to changes in the ambient field very quickly (their relaxation time is short). Below their “blocking” temperatures this time increases rapidly until the thermoremanent magnetisation (TRM) is permanently retained. Therefore, between the blocking temperature and the Curie temperature, the remanence remains after the external field is removed but is still relatively sensitive. Cooling below blocking temperatures “locks” the remanence in place. This phenomenon can be reproduced by TH and TRM experiments in the laboratory.

Dealing with both thermal magnetic methods, the samples are exposed to increasing temperatures (from 20 °C to 700 °C) and are set out in a 30 minute interval at each temperature step selected (Fig. 8c). While NRM intensities of the TH demagnetisation samples are measured directly after cooling, TRM-treated samples, previously AF-demagnetised, are exposed to induced fields (similar to the today’s magnetic field intensities) during cooling. In doing so, TH demagnetisation curves mostly display a trend to decreasing NRM intensities, due to stepwise loss of the initial remanence record with increasing temperatures. TRM curves behave the other way around and are signalled by the acquisition of remanent magnetisations with increasing NRM intensities. Thermal magnetic curves provide information about their magnetic stability behaviour and blocking temperature spectra.

#### **2.2.4 Anisotropy of magnetic susceptibility (AMS)**

Almost all rocks are magnetically anisotropic and their susceptibility intensities vary with direction of the applied field. Magnetic anisotropy is directly related to petro-fabric, and has become one of the most rapid, sensitive and widely used tools for its characterization. Anisotropy of magnetic susceptibility (AMS) is often called *magnetic fabric* and its

relationship to petro-fabric is complex and depends on various factors, including the composition, concentration, grain size and alignment of mineral grains (Houdra, 1994; de Wall, 2005). Ongoing research in geological applications is paralleled by studies of the fundamental mineral magnetic phenomena involved.

Generally, the bulk magnetic susceptibility  $k$  in first approximation can be determined as a scalar and directionally independent parameter. However, in reality it can be illustrated as a second order tensor (MS ellipsoid) with a maximal, intermediate and minimal axis, analogical to the susceptibilities of  $k$ -max,  $k$ -int and  $k$ -min (Fig. 9a).

In this study the highly magnetic (ferrimagnetic) minerals are of most interest. Their grain shape and mineral alignment have a high influence to AMS. The mean susceptibility is given by its arithmetic average of the three single values:  $k = (k\text{-max} + k\text{-int} + k\text{-min})/3$ . The three determined axes describe the degree of the anisotropy of the magnetic susceptibility and the magnetic susceptibility ellipsoid (Fig. 9a,b.). An *oblate* (disc-shape) ellipsoid is given, when  $k\text{-max} \approx k\text{-int} > k\text{-min}$  and *prolate* (cigar-shape), when  $k\text{-max} > k\text{-int} \approx k\text{-min}$ .

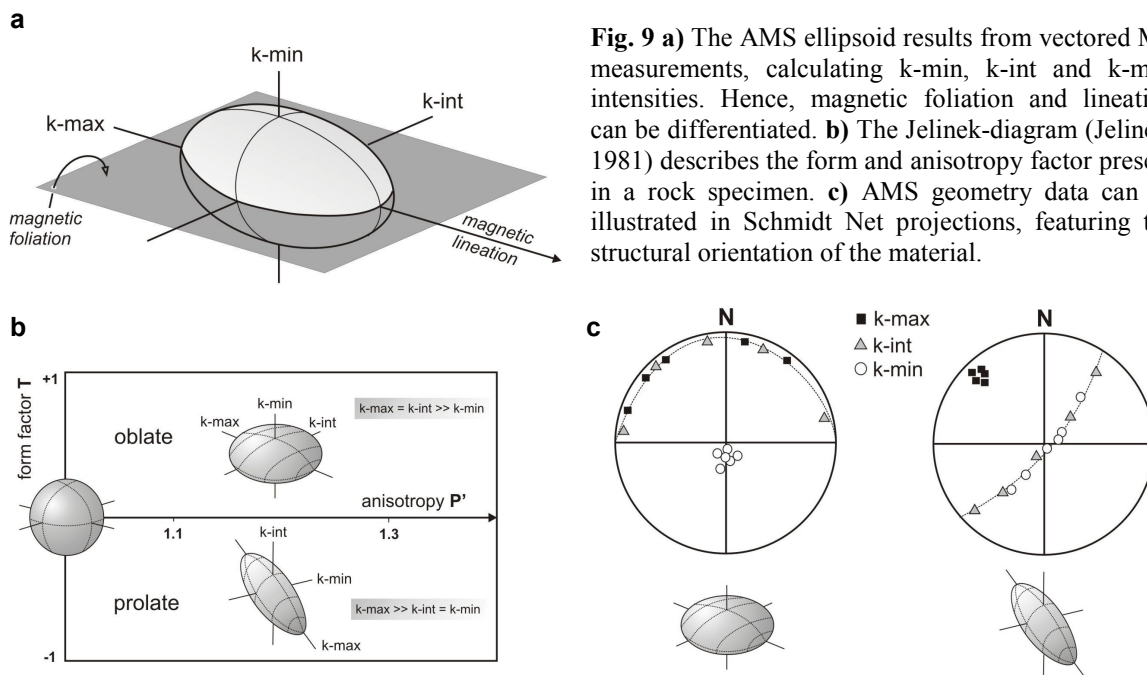


**Fig. 9 a)** The AMS ellipsoid results from vectored MS measurements, calculating  $k$ -min,  $k$ -int and  $k$ -max intensities. Hence, magnetic foliation and lineation can be differentiated. **b)** The Jelinek-diagram (Jelinek, 1981) describes the form and anisotropy factor present in a rock specimen. **c)** AMS geometry data can be illustrated in Schmidt Net projections, featuring the structural orientation of the material.

Magnetic fabrics can be expected in all rock types, magmatic, metamorphic and sedimentary rocks. Alignment of para- and ferrimagnetic minerals (ore grains) in magmatic rock types is indicative for flow directions during emplacement of intrusions (pluton, dyke or sill) or extrusions (lava or pyroclastic flow). Metamorphic rocks reflect AMS geometries due to highly anisotropic silicates (i.e. amphibole or biotite) or secondarily formed ferrimagnetic minerals with disc- or spicule-like shapes. Due to tectonic stress, deformation processes can be studied with AMS application. The alignment of elongated ferrimagnetic particles in sedimentary rocks results from deposition within a flowing system. Pyroclastic rocks are concerned with volcanic and sedimentary rocks, respectively. Thereby, alignment of



ferrimagnetic minerals is mainly bound to the juvenile fraction, but occurs also accessory within the ash matrix. AMS geometry data derived from fine-grained volcanoclastic material is normally used for the reflection of flow directions and subsequent information of vent locations. Evaluations of AMS data are illustrated most suitably by the so-called *Jelinek-diagrams* (Fig. 9b), using form and anisotropy factors ( $T$  and  $P'$ ), whereas geographic directions can be demonstrated easiest with *Schmidt Net* projections (Fig. 9c), a classic method used in structural geology.

## **2.3 Results of rock magnetic measurements**

In the following paragraphs the rock magnetic results of induced and remanent magnetisation of the volcanoclastic units will be discussed. Thereby, the pronounced downhole magnetic anomalies found during the drilling project 2001 provide the basis for the rock magnetic investigations. Besides the characterisation of the magnetic signature within the lapilli tuffs, the magnetic properties of the material will be distinguished with respect to deposits formed inside and outside the magnetic anomalies. To keep the data illustrations in a concise way, most of the rock magnetic results are presented on exemplary samples only. The creation of reliable AMS data and the magnetic fabric results, respectively, are given in the last paragraph.

### **2.3.1 Magnetic signature of the volcanoclastic units**

The magnetic anomalies found within the lapilli tuffs between 240 m and 373 m can be partitioned into at least 5 different units (I-V), which are separated by transition zones with conspicuous peaks deduced from the  $\Delta F$ -curve (Fig. 10). Deviations of the local intensity (including background anomaly of the regional field) from the reference intensity 47650 nT are in a range from -2500 nT to +5000 nT. The shape of the  $\Delta F$ -curve suggests a remanence inverse to the present field direction in the drilled cores. The negative  $\Delta F$  -anomalies from 240 m to 307 m convert subsequently to strongly positive values between 307 m and 360 m. It corresponds properly to a potential field at a boundary layer within a reversely magnetised body (Eberle 1985). The volcanic material appears to have been deposited at a time when the Earth's magnetic field was inversely polarised relative to today's magnetic field (Rolf et al., 2005).

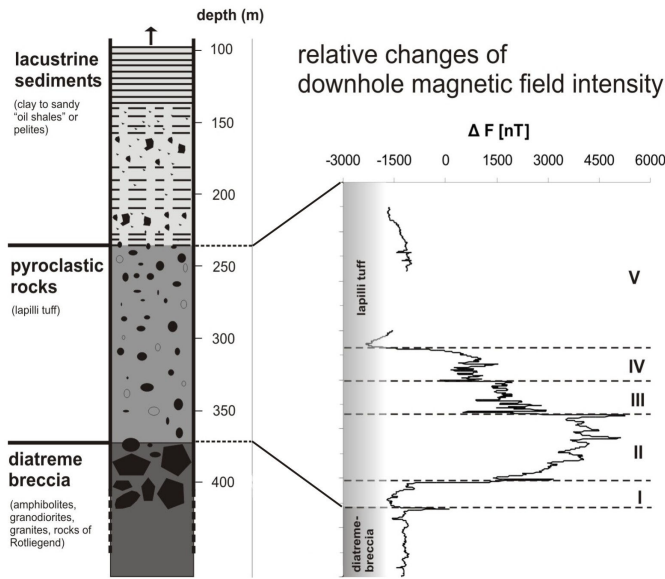


**Fig. 10** Results of downhole measurement of magnetic field intensity ( $\Delta F$  = total magnetic field intensity – normal field of 47650 nT). Due to pronounced peaks of the  $\Delta F$ -curve, the pyroclastic rocks can be divided into 5 different units (I-V). The strongest magnetised rocks are restricted to the lower half of the lapilli tuff between unit II and IV.

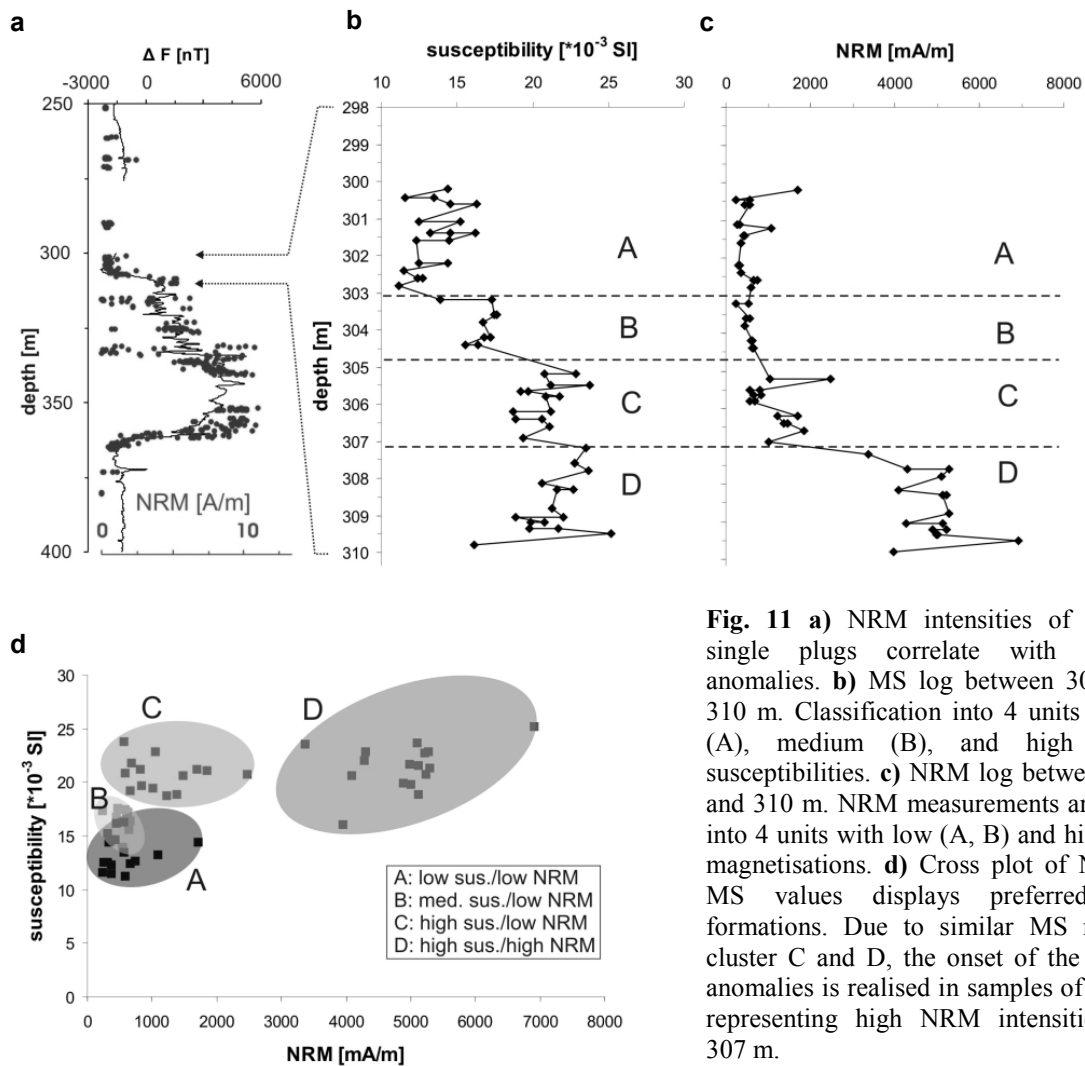


**Fig. 11 a)** NRM intensities of measured single plugs correlate with the  $\Delta F$ -anomalies. **b)** MS log between 300 m and 310 m. Classification into 4 units with low (A), medium (B), and high (C, D) susceptibilities. **c)** NRM log between 300 m and 310 m. NRM measurements are divided into 4 units with low (A, B) and high (C, D) magnetisations. **d)** Cross plot of NRM and MS values displays preferred cluster formations. Due to similar MS results in cluster C and D, the onset of the magnetic anomalies is realised in samples of cluster D representing high NRM intensities below 307 m.

Positive values up to +5000 nT are assigned only to the lower half of the lapilli tuffs, from unit II to IV. Here the volcanoclastic body is most strongly magnetized, whereas unit I and V as well as rocks of the diatreme-breccia display lower intensities. Following the  $\Delta F$ -curve downwards, increasing negative absolute values up to -2500 nT (at roughly 300 m) are due to the so-called “edge-effect”; this is typical for downhole magnetic field intensity measurements when entering a strongly magnetised body (Eberle 1985). Due to remarkable  $\Delta F$ -peaks within the lower half of the lapillituffs which are assigned to unit transitions of the  $\Delta F$ -anomalies, investigations on single plugs have been dominantly performed at depths between 300-370 m (Fig. 11a). The reversal point from negative to positive values arises first within units V and IV at depths between 300 m and 310 m. Therefore the rocks deposited here are of special interest in order to clarify the abrupt increase of these magnetic field anomalies.

Single plug measurements of the NRM intensities show a direct dependency to the  $\Delta F$ -anomalies (Fig. 11a). Laboratory magnetisation measurements agree with the magnetic field intensity data and show the anomalies pronounced to the lower half of the lapilli tuffs. The relatively low NRM values inside the most magnetised part reveal measurements of plugs drilled from blocks of accidental material in the volcanoclastics. These rock accumulations are scarce and have a weak magnetisation character which was not deduced by the downhole magnetic measurements, due to different data sampling rates. The transition into the anomalies (unit V to IV, Fig. 10) was studied in detail by 55 single plugs from cores between 300 m and 310 m depth. The nature of the magnetic structure can be illustrated by measurements of the susceptibility (MS) and natural remanent magnetisation (NRM). A log (Fig. 11b) of MS measurements displays values which can be subdivided into low (300-303 m), medium (303-305 m) and high (305-310 m) intensities, roughly in the range of  $10\text{-}15 \times 10^{-3}$  [SI],  $15\text{-}17 \times 10^{-3}$  [SI] and  $18\text{-}26 \times 10^{-3}$  [SI], respectively. NRM measurements (Fig. 11c) in contrast show low and high intensities (0-2000 mA/m and 2000-6000 mA/m) between 300-307 m and 307-310 m. A cross plot of MS and NRM within the transition zone from unit V to IV does not show a linear dependency between both parameters, but rather forms distinct clusters (A, B, C and D; Fig. 11d). Cluster A and B (300-305 m) can be considered a common unit due to the cluster overlaps. They feature relatively low MS ( $10\text{-}17 \times 10^{-3}$  [SI]) and relatively low NRM intensities (200-1000 mA/m). Cluster C (305-307 m) displays NRM intensities similar to the clusters of A and B, but shows higher susceptibilities between 18 and  $24 \times 10^{-3}$  [SI]. The onset of the effective magnetic anomalies is realised in samples of the cluster D. There, MS is in similar range as in cluster C ( $16\text{-}26 \times 10^{-3}$  [SI]), but NRM intensities are significantly higher (3400-5000 mA/m).

These analyses clearly indicate a remanence partitioning in the volcanoclastic units within the Messel maar-structure. Despite the same susceptibility for acquisition of a NRM, distinct differences in the magnetisation are realised. This is evident when comparing section C and D

in the core logs of MS and NRM in figure 11b, c. The deduced NRM/MS sub-structuring of the volcanoclastic units cannot be proofed by lithological or petrological observations.

### 2.3.2 Magnetic properties inside and outside the anomalies

The following paragraphs deal with rock magnetic studies to clarify the remanence partitioning pattern in the Messel volcanoclastic rocks. Both the juvenile and the accidental fragments can contribute to the magnetisation behaviour. It is the aim to characterise the ferrimagnetic minerals by their composition, grain size and magnetic stability. All parameters may influence the magnetic character of the material, explaining the occurrence of the magnetisation signature within the lapillituff units. Therefore, single plug measurements from inside and outside the  $\Delta F$ -anomalies are compared.

#### *Magneto-mineralogy*

In reflected light, iron oxides appear strictly bound and disseminated within the juvenile lapilli. Figure 12a shows photomicrographs of typical juvenile lapilli with their ferrimagnetic content. Displayed particles are zoomed in on a centimetre to (sub)millimetre scale. Mostly, backscatter images solely enable the visualisation of the very small ferrimagnetic (titano)-magnetites. These minerals occur as tiny individual grains in the lapilli matrix as well as rims around cores of Cr-Al spinels and frequently show skeleton-like textures (Fig. 12a). Table 2 outlines the chemical composition of the dominating ferrites by microprobe analyses. It is obvious that the element oxide analyses of Ti and Fe of the (titano)-magnetites and magnetites are very similar for samples inside and outside the  $\Delta F$ -anomalies.

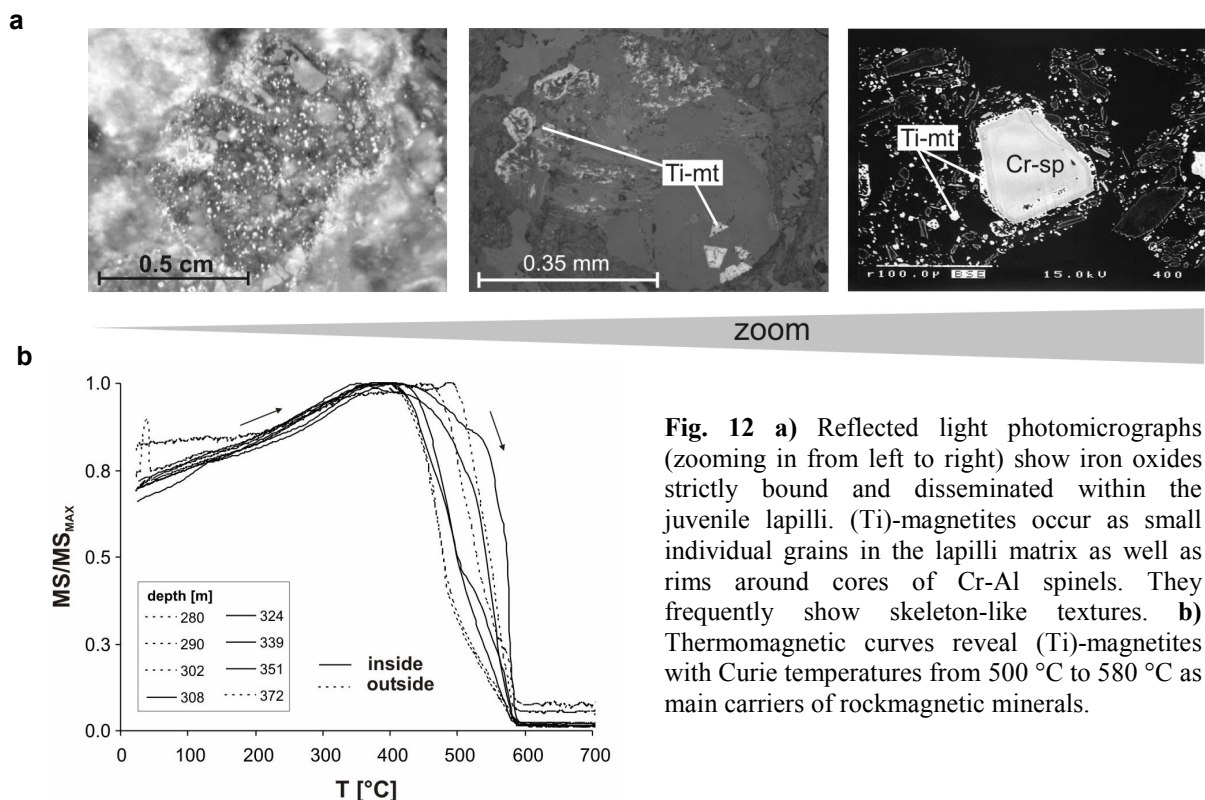


**Table 2** Exemplary element analyses of ferrimagnetic minerals inside and outside the anomalies

element	(titano)-magnetite		magnetite		Cr-sp. (middle)	Cr-sp. (rim)
	outside	inside	outside	inside	inside	
SiO <sub>2</sub>	0.16	2.14	0.42	0.18	0.22	2.26
TiO <sub>2</sub>	<b>12.99</b>	<b>9.97</b>	<b>0.30</b>	<b>0.34</b>	<b>1.18</b>	<b>21.12</b>
Al <sub>2</sub> O <sub>3</sub>	1.00	2.15	0.53	0.13	29.86	1.02
Cr <sub>2</sub> O <sub>3</sub>	0.00	0.03	0.03	0.03	26.11	0.71
MgO	1.90	2.62	8.13	0.04	15.55	0.91
CaO	0.27	0.70	0.16	0.08	0.11	0.66
MnO	2.29	0.67	1.24	0.13	0.00	0.16
FeO	<b>73.32</b>	<b>73.22</b>	<b>83.70</b>	<b>92.20</b>	<b>23.15</b>	<b>62.11</b>
NiO	0.01	0.08	0.03	0.03	0.24	0.00
ZnO	0.22	0.00	0.27	0.14	0.00	0.04
total	92.16	91.58	94.81	93.30	96.43	88.99

Because of polishing problems of the volcanoclastic samples during thin section preparation for microprobe analyses and the predominance of very small-sized Fe-oxides (<5  $\mu\text{m}$ ), the identification of the main ferrimagnetic mineral phase turned out to be very difficult on this scale. To handle this problem, the method of temperature-dependent susceptibility measurements has been used to support the geochemical analyses. It integrates all magnetic mineral phases of a sample and is a very sensitive method for the detection of variable mineral compositions. As shown in recent studies (e.g. Kontny and de Wall, 2000; Kontny et al., 2003; de Wall et al. 2004), the record of so-called  $k(t)$ -curves reflects the Ti-content of (titano)-magnetites. Distinct Ti-variability in magnetites may influence the rock magnetic properties and thus the remanent magnetisation behaviour.

Temperature-dependent susceptibility measurements identified (titano)-magnetites as main carriers of rockmagnetic properties. Curie temperatures of the lapilli tuffs are 500-580 °C indicating a near-magnetite composition (Fig. 12b). All  $k(t)$ -curves resemble idealised curves of small-sized magnetites (SD/PSD particles) illustrated in figure 7. The measured curves show an MS increase with increasing temperatures from 20 °C to roughly 400 °C. The curves lose their ferrimagnetic character in the temperature range between 500-580 °C without systematic distinction of the samples deposited inside and outside the  $\Delta F$ -anomalies. In addition to microscopic information, all identified magnetic iron-oxides bound to the juvenile fragments do not show distinct differences in their chemical composition, which may affect the magnetic properties of the lapilli tuffs.

#### *IRM and hysteresis experiments*

Isothermal remanent magnetisation (IRM) experiments have been carried out on six samples from different depths inside (unit II, III and IV) and outside (unit I and V) the anomalies.

Specimens at depths from 290 m, 302 m and 363 m represent IRM-curves outside, whereas samples from 309 m, 337 m and 355 m are from inside the anomalies. In addition, the samples differ in their susceptibility intensity, a parameter discussed in the following main paragraph.

The samples have been exposed to inducing fields from 0-500 mT. As shown in figure 13, all specimens already acquire their saturated remanence magnetisation at approximately 150 mT by illustration of a plateau with absolute maximum values of 335 A/m (290 m), 272 A/m (302 m), 561 A/m (309 m), 466 A/m (337 m), 615 A/m (355 m) and 353 A/m (363 m). According to the normalised IRM curves, all these (titano)-magnetite-bearing samples reveal very similar curve progressions. When applying the same magnetic field, samples from inside the anomalies acquired an insignificantly lower remanence than material deposited outside the anomalies. All these IRM-curves show similarities with idealised magnetite IRM-curves (PSD curve) measured by Palmer et al. (1996) (Fig. 8).

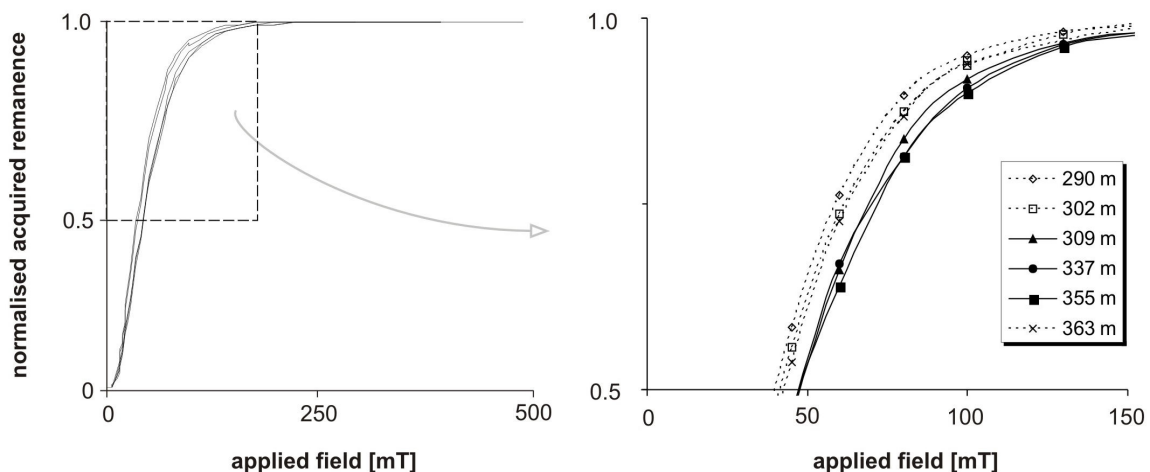


**Fig. 13** Acquisition of isothermal remanent magnetisation (IRM) of samples inside (black lines) and outside (dotted lines) the  $\Delta F$ -anomalies. Peak fields up to 150 mT close to their saturation remanence (SIRM). Samples inside the anomalies display a shift to slightly lower remanences than material deposited outside, but differences are not significant.

As mentioned in the introduction chapter, hysteresis studies are very qualified for investigating the rock magnetic character of a material. In this connection, magnetic fields with changing directions (0 mT to +300 mT and 0 mT to -300 mT) have been applied to volcanoclastic samples inside and outside the  $\Delta F$ -anomalies, producing (remanent) magnetisations (Fig. 14a). The hysteresis parameters, saturation remanence ( $M_{rs}$ ), saturation magnetisation ( $M_s$ ), remanent coercivity ( $H_{cr}$ ) and coercivity ( $H_c$ ) are calculated, which can serve for characterisation of domain states of ferrimagnetic particles. The data are plotted in a so-called Day-plot (Day, 1977) favouring pseudo-single-domain particles (Fig. 14a). Considering near-magnetite composition, they are intermediate in grain size (approx. 1-5  $\mu\text{m}$ )

between magnetically stable single-domain particles (SD; approx.  $<1 \mu\text{m}$ ) and relatively instable multi-domain particles (MD, approx.  $>5 \mu\text{m}$ ) (Soffel, 1991; Butler, 1992).

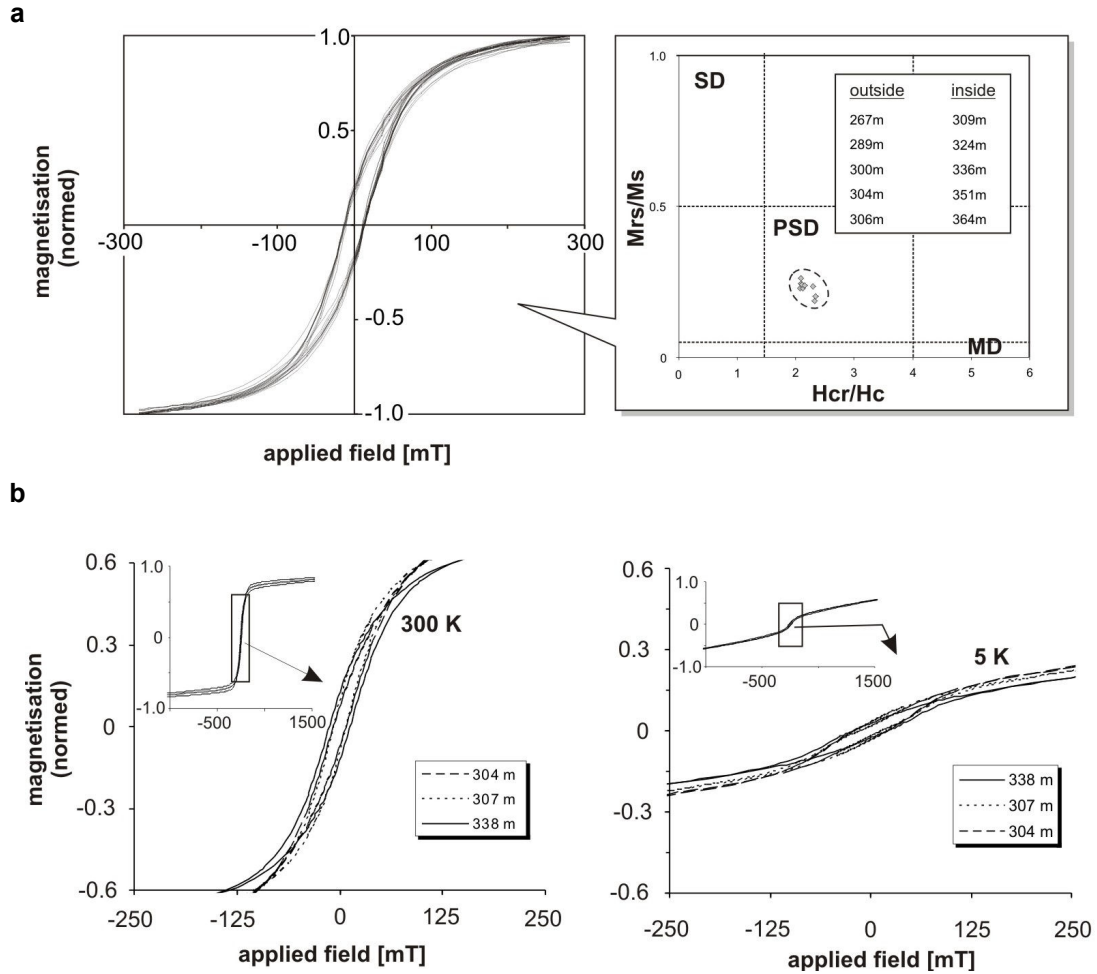


**Fig. 14** Hysteresis measurements. **a**) After Day (1977) hysteresis curves and calculated rockmagnetic parameters ( $M_{rs}$ ,  $M_s$ ,  $H_{cr}$ ,  $H_c$ ) show similarities in ferromagnetic properties by the grain size spectra of PSD particles (right). **b**) Similar hysteresis behaviour of samples inside (black line) and outside (dotted lines) the  $\Delta F$ -anomalies at 5 K and 300 K. Flat slopes of the curves (right) are controlled by the paramagnetic components, dominant at very low temperatures.

In order to study the hysteresis behaviour in even more detail, three samples with different NRM intensities have been investigated at different temperatures (Fig. 14b). Two samples are of the transition zone IV-V from depths at 304 m (outside the  $\Delta F$ -anomalies and low NRM intensity) and 307 m (inside the  $\Delta F$ -anomalies and higher NRM intensity), as well as one specimen from zone III at 338 m (inside the  $\Delta F$ -anomalies and very high NRM intensity). The hysteresis loops are illustrated in temperature ranges at 5 K and 300 K. With decreasing temperatures, the paramagnetic influence of a sample increase. Therefore, it is possible to state and recognize different ferrimagnetic components and the paramagnetic proportion in the material. However, all curves of the volcanoclastic samples show a similar acquired remanence ( $M_{rs}$ ), which is the remaining magnetisation when the driving field is dropped to zero. The coercivity forces ( $H_c$ ) are similar for rocks inside and outside the  $\Delta F$ -anomalies, roughly at about 10 mT (drawn from hysteresis loops). Saturation remanence ( $M_s$ ) develops

more precisely at the temperature of 300 K due to presence of the ferrimagnetic components, allowing a relatively rapid remanence acquisition. Comparing low and high temperatures, hysteresis loops at 5 K have lower slopes than curves at 300 K, whereas the closing of all curves ( $H_{cr}$ ) occurs between 100-125 mT. The area of each hysteresis loop is related to the amount of energy dissipation upon reversal of the field which is very similar for all rock specimens inside and outside the anomalies. The volcanoclastic material deposited inside and outside the  $\Delta F$ -anomalies feature similar magnetic behaviour, in terms of retraceability of their magnetisation and thus their ferri- and paramagnetic components.

#### *AF demagnetisation experiments*

While in the previous sections the ability of remanence acquisition has been characterised, the observed in situ remanence magnetisation in the subdivided units of the volcanoclastics is studied in more detail. Alternating (AF) field demagnetisation experiments in fields up to 100 mT are presented here on eight samples, five samples outside and three inside the anomalies – or more precisely, specimens from unit V (250 m, 260 m and 303 m), unit IV (315 m), unit III (322 m), unit II (356 m) and unit I (361 m), as well as one specimen close to the diatreme breccia (372 m). Generally, residual magnetisations at 100 mT are between 1-7 % and averages 3 % of the initial NRM (Fig. 15a), reflecting an almost total destruction of the magnetic information of the samples. Besides the specimen near the diatreme-breccia (372 m) and the sample close to unit IV (303 m), curves outside the  $\Delta F$ -anomalies show their MDF at about 20 mT, whereas samples inside the anomalies have values between 30 mT and 40 mT.

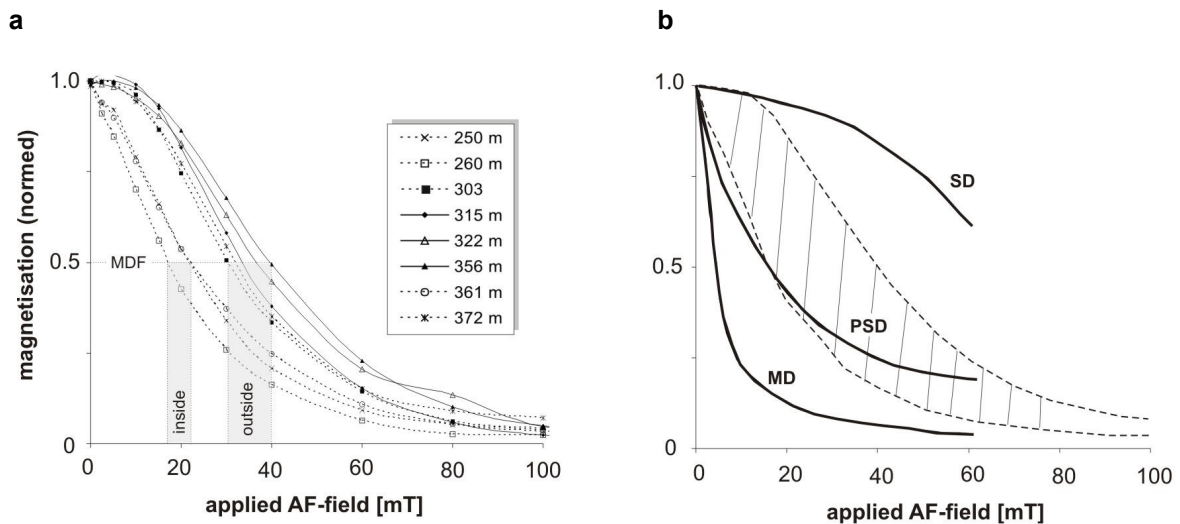


**Fig. 15 a)** Alternating field (AF)-curves display different demagnetisation behaviour for samples in and outside the  $\Delta F$ -anomalies. Median destructive field (MDF) values are basically lower for the material deposited outside, whereas rock specimens inside the anomalies (lower half of the tuff) reveal stronger remanent magnetisations and higher MDF values. Residual magnetisation of all rock specimens averages 3 % of the initially acquired NRM. **b)** After Palmer et al. (1996), AF-curves (hatched area) prefer domain states of PSD particles due to constructed magnetite AF-curves.



Obviously, the former samples have slightly lower coercivity intensities and thus show more unstable demagnetisation behaviour; the latter initially retain their acquired magnetisation up to 10-15 mT and are magnetically more stable. In terms of NRM acquisition during or after rock formation, the material inside the anomalies possesses a higher stability of its in situ acquired remanent magnetisation than the rocks deposited outside. According to the constructed magnetite AF-curves (Palmer et al. 1996), all measured rock samples plot in a distribution field which prefers an approximation of PSD particles (Fig. 15b). The favoured domain status is in agreement with hysteresis investigations.

#### *Thermal demagnetisation and TRM experiments*

Understanding the magnetic stability behaviour of the previous section, thermal magnetic experiments have been performed and illustrated here on seven samples from depths of 250 m, 290 m and 302 m (unit V), 309 m (unit IV), 337 (unit III), 355 m (unit II) and 363 m (unit I) (Fig. 16a). The thermal (TH) demagnetisation and heating (TRM) experiments are illustrated and discussed in more detail on two samples (267 m and 351 m; Fig. 16b, c), which are exemplary for the material deposited outside and inside the  $\Delta F$ -anomalies (Fig. 16a). According to the TH demagnetisation curve (Fig. 16b), the material of the upper half of the lapilli tuff (267 m) loses its magnetisation relatively quickly when exposed to temperatures stepwise from 20 °C to 600 °C. It shows broad blocking temperature spectra, pronounced between 20 °C and 550 °C. The material from the lower half of the lapilli tuff (351 m) is more likely to retain stable remanence. This is in coincidence with the narrow blocking temperature spectra, most effective between 400-600 °C.

For realisation of TRM experiments, the specimens, which acquired different NRM of 0.4 A/m (267 m) and 9.9 A/m (351 m) prior to TRM treatment, had to be demagnetised first. Subsequently, the rock specimens were heated up in the same temperature steps as for demagnetisation experiments. After each step, the samples were cooled down to room temperature within the present magnetic field intensity of 48,000 nT, in order to determine their acquired magnetisation. Although both rock samples inside and outside the anomalies revealed different initial NRM intensities, TRM curves indicate the same acquired magnetisation during stepwise heating and represent the same blocking temperature spectra (Fig. 16c). The acquired TRM intensities at 600 °C are 15.2 A/m (267 m) and 22.3 A/m (351 m), respectively.

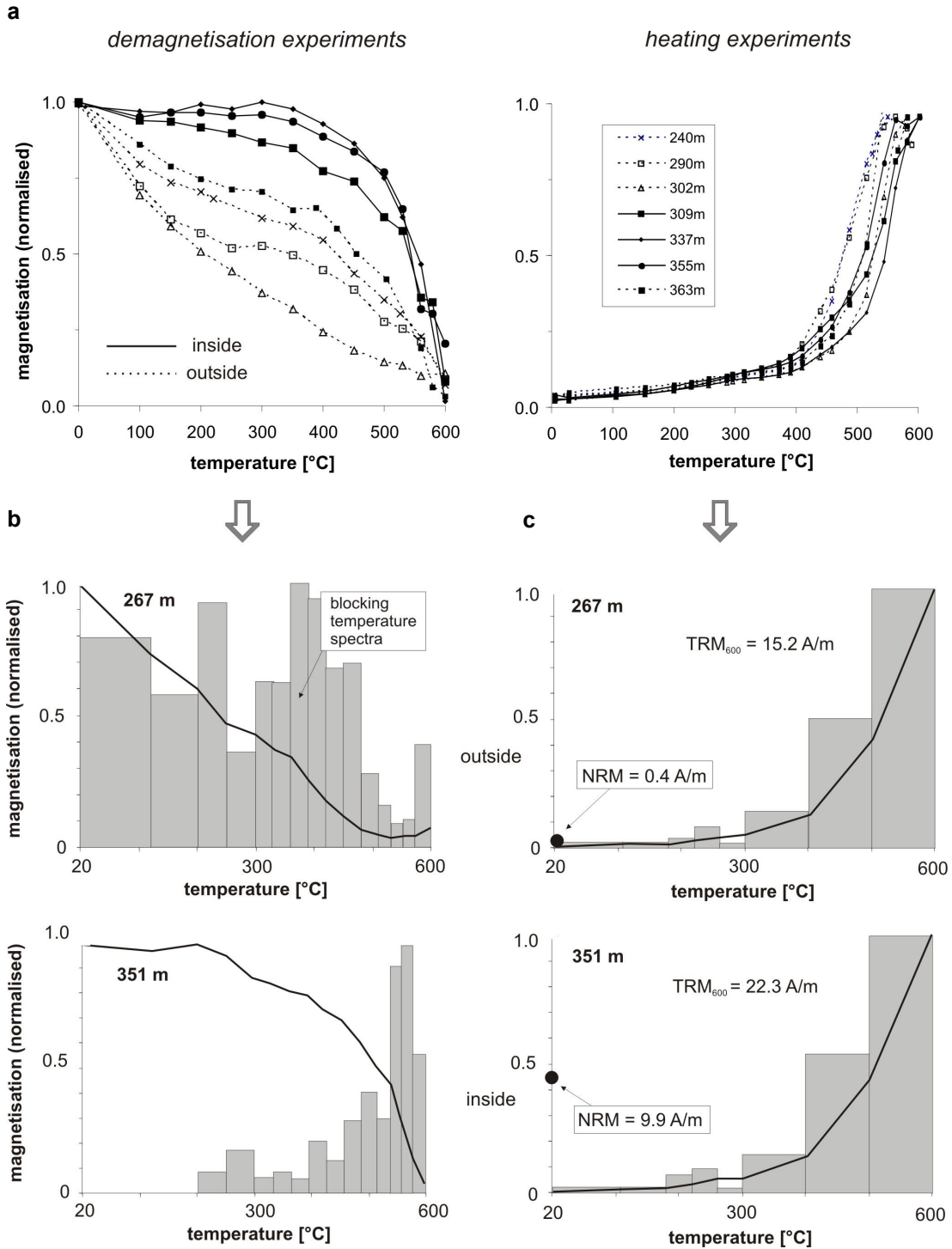


**Fig. 16 a)** Thermal magnetic experiments illustrated on seven exemplary samples deposited out- and inside the  $\Delta F$ -anomalies. **a)** Thermal demagnetisation experiments of the sample from 267 m (outside  $\Delta F$ -anomalies) the reveal a broad range of blocking temperatures and a relative weak remanence behaviour, due to a quick loss of magnetisation during stepwise heating. The Blocking temperature spectra of the sample from 351 m depth (inside  $\Delta F$ -anomalies) are relatively narrow, reflecting a strong acquired remanence. **c)** TRM experiments inside and outside the anomalies result in very similar stepwise acquisition of their magnetisation and blocking temperature spectra. The samples differ in their initial NRM and show small differences in their absolute TRM at 600 °C.

### 2.3.3 Magnetic susceptibility and magnetic fabric of the lapilli tuffs

For verifying the magnetic susceptibility (MS) trend of the lapilli tuff units to the transition to the diatreme-breccia within the maar-diatreme-structure, bulk MS measurements have been carried out in the laboratory on approximately 250 single plug specimens. Thereby, special attention is paid to the transition zones I-V, into the  $\Delta F$ -anomalies (high-NRMs) and from the anomalies to low-NRM volcanoclastics. The linear trend with strongly varying, but increasing MS values to the diatreme-breccia could be proved (Fig. 17a).

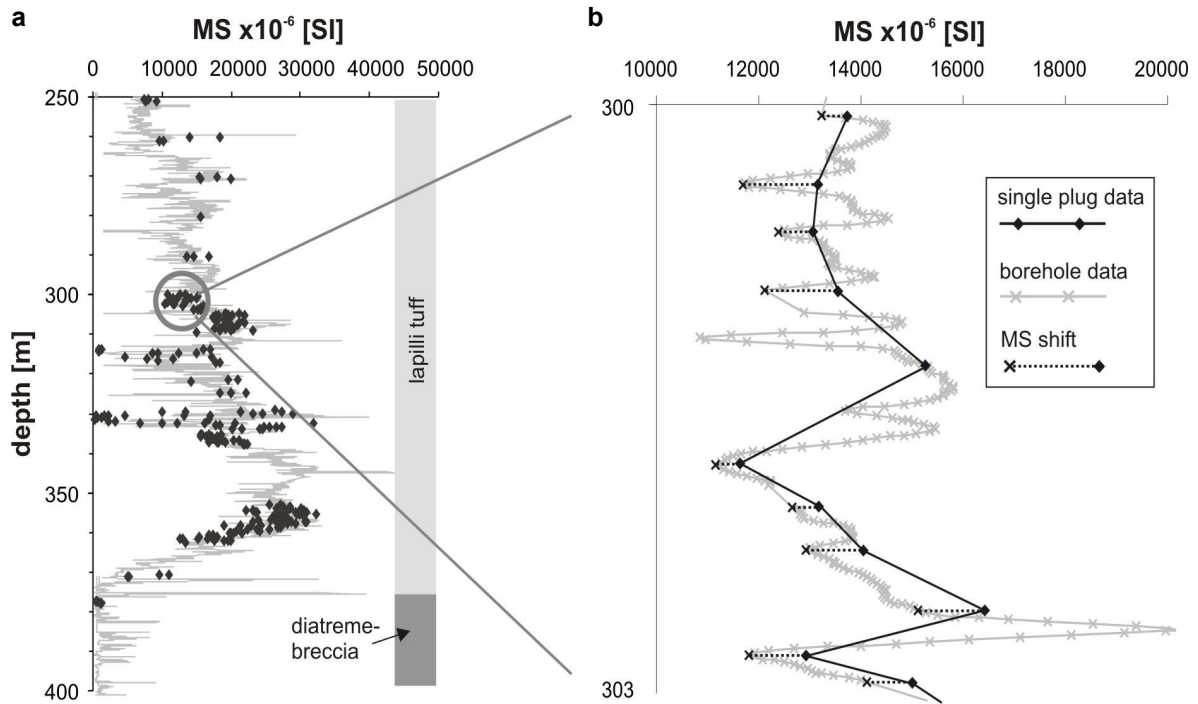


**Fig. 17** Magnetic susceptibility measurements. **a)** Bulk MS log of rock specimens correlates with MS intensities measured in the borehole. **b)** Comparison of borehole and plug data. Due to different applied MS methods, the plot shows an insignificant MS shift between 500-2000  $\text{SI} \times 10^{-6}$ .

The MS values within the lapilli tuff roughly increase from  $10,000 \times 10^{-6}$  SI to  $30,000 \times 10^{-6}$  SI in depths between 250-360 m. The remarkable drop of the curve occurs in a transition zone to the diatreme-breccia in depths between 360-373 m, with approximated values starting from 30,000 to  $<1,000 \times 10^{-6}$  SI. The lowest susceptibilities of the whole volcanoclastic rocks are shown in the diatreme breccia with roughly  $<1,000 \times 10^{-6}$  SI. This is due to the occurrence of large fragmented blocks of the country rocks and the lack of the juvenile material. Comparing the MS pattern between 250-400 m, borehole and single plug data are in agreement. Observing the MS data within a few meters, single plug data shows an insignificant shift to higher values ( $500-1000 \times 10^{-6}$  SI), due to the different surveying methods applied within the borehole and on single rock specimens (Fig. 17b). The exemplary section in depths between 300-303 m reveals the high MS variation (here:  $11,000-20,000 \times 10^{-6}$  SI) of the volcanoclastic units, carried out by single plug and borehole data.

Even though petrographical studies on the Messel volcanoclastic rocks do not show preferred orientations of the particles, the implementation of oriented MS measurements is particularly suitable for studying structural properties of these rocks (e.g. Le Pennec et al., 1998; Zanella et al., 1999 and 2001; Ort et al., 1999; Alva-Valdivia et al., 2005). Here, the magnetic fabric investigations are not subject for identifying vent locations, but for structural studies on vertical successions, indicating possible debris flow directions or local stress situations of Messel.

Unfortunately, the cores of the Messel drilling project were not recovered with respect to their orientation in the borehole. Thus, an absolute, geographic reorientation of the AMS data of the measured plugs was not possible. The single bench mark of the vertical drilling is the core-axis considered as the z-axis. Because of stable paleofield vectors in many sections of the volcanoclastic profile (mainly in rocks deposited inside the  $\Delta F$ -anomalies), the magnetic declinations of the NRM measurements (declination = azimuth  $000^\circ$ ) have been selected as point of reference; the AMS main axes have been reoriented to this value, i.e.

*AMS-decl. – NRM-decl. = reorientation of reliable AMS data*

Measurements of 100 samples have been mainly performed on rocks in depth between 300-310 m, 330-340 m und 355-365 m. Here, it is assumed that the volcanoclastic material acquired its *in situ* magnetisation during or after deposition (Buness et al., 2004; Rolf et al., 2005). Furthermore, eight samples between 240-290 m have been measured in addition, four from the transition of the lower lake sediments to the volcanoclastic sequences and four from the upper half of the lapilli tuffs.

Shape and anisotropy of the AMS ellipsoids are illustrated in standardised diagram for AMS (Jelinek, 1981) (Fig. 18a). The samples generally show a weak magnetic anisotropy with maximum  $P'$ -values of 1.06, whereas the majority of the samples have  $P'$ -values  $<1.02$ . The AMS ellipsoids display shapes between clearly oblate and prolate geometries. A dependency of the oblate and prolate forms with depths could not be proved.

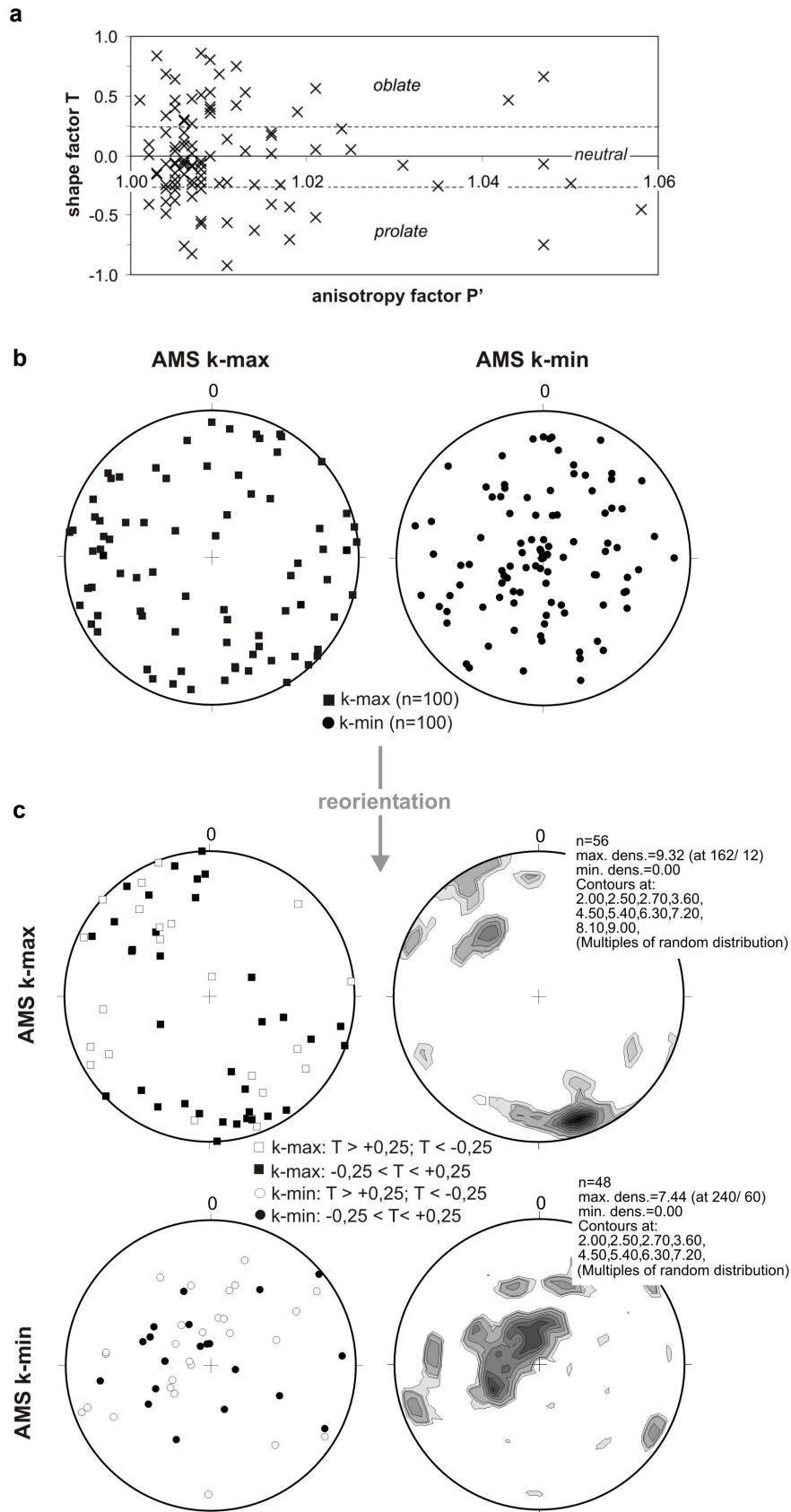


**Fig. 18 a)** Rock specimens show weak magnetic anisotropies. The AMS ellipsoids range from strongly oblate to strongly prolate forms. **b)** Equal-area lower hemisphere projection of non-orientated data of AMS axes (left: k-max, right: k-min). **c)** Equal-area lower hemisphere projection of orientated data of AMS axes (left) and density contour calculation (right). Linear (prolate fabrics) are shown in the upper, planar (oblate) fabrics in the lower diagrams. Black coloured signs represent the orientation data of the neutral AMS-ellipsoids.

Figure 17c classifies a neutral field ( $T = +0.25$  bis  $-0.25$ ) and oblate and prolate fields ( $T > +0.25$  und  $T < -0.25$ ). The orientation of the smallest axis of the AMS ellipsoid (pole to the magnetic foliation,  $k$ -min) is well-defined in oblate textures, whereas the longest axis of the AMS ellipsoid (magnetic lineation,  $k$ -max) mainly determines the prolate textures (Tarling and Hrouda, 1993; Fig. 18b). All three axes within the neutral field are well-defined and have a triaxial geometry, when  $k\text{-max}/k\text{-int} = k\text{-int}/k\text{-min}$ . The samples of the Messel drilling project possess very weak anisotropies, therefore samples with oblate geometries are supposed to illustrate the orientation of the magnetic foliation and the prolate geometries are used for the depiction of magnetic lineations. Both data sets show the structural trends in preferred orientation of the AMS axes within Schmidt-net projections (Fig. 18c). The  $k$ -max axes generally have flat inclinations. After reorientation with respect to NRM declinations, the axes arrange in a sub-horizontal NW-SE oriented cluster (Fig. 18c). This trend approximately corresponds to the real geographic orientation of the lineation, because paleo-declinations (approx. 48 Ma) differ only in  $10^\circ$  from the today's oriented declination (McElhinny and Lock, 1990). Observing  $k$ -min declinations/inclinations, an obvious trend also occurs. Here, the declinations appear in a NE-SW oriented belt with a predominance of steep foliation poles and thus flat orientation of the magnetic foliations. Although the volcanoclastic rocks of the Messel maar-diatreme do not show any indication to internal structures, the method of AMS application provides textural details of the erupted rock formations.

## 2.4 Interpretation of rock magnetic measurements

### 2.4.1 Magnetic properties of the lapilli tuffs

Table 3 outlines the magnetic properties inside and outside of the anomalies, which will be interpreted in the following:

Rock magnetic studies on volcanoclastic rocks of the Messel maar-diatreme volcano resemble in ferrimagnetic properties inside and outside the  $\Delta F$ -anomalies. Using the methods of magneto-mineralogy, the acquisition of IRM and hysteresis experiments, the ferrites within the juvenile lapilli point to very similar compositions (Curie temperatures and geochemical analyses), coercivities and grain sizes. According to AF-demagnetisation curves, the (titano)-magnetites with a near magnetite composition are characterised by pseudo-single-domain particles (PSD), which are intermediate in grain size between magnetically stable SD and instable MD particles (Soffel 1991). Despite the similarities in ferrimagnetic properties of the volcanoclastic material, the magnetic signature illustrated by log-comparison of NRM and MS measurements reveals a remanence partitioning. The onset of the clearly reverse magnetisation is realised below 307 m depth and generally greatest within the lower half of

the lapilli tuff, up to the appearance of the underlying diatreme-breccia. This can also be demonstrated by a log of NRM measurements and their magnetic inclinations (Fig. 19).

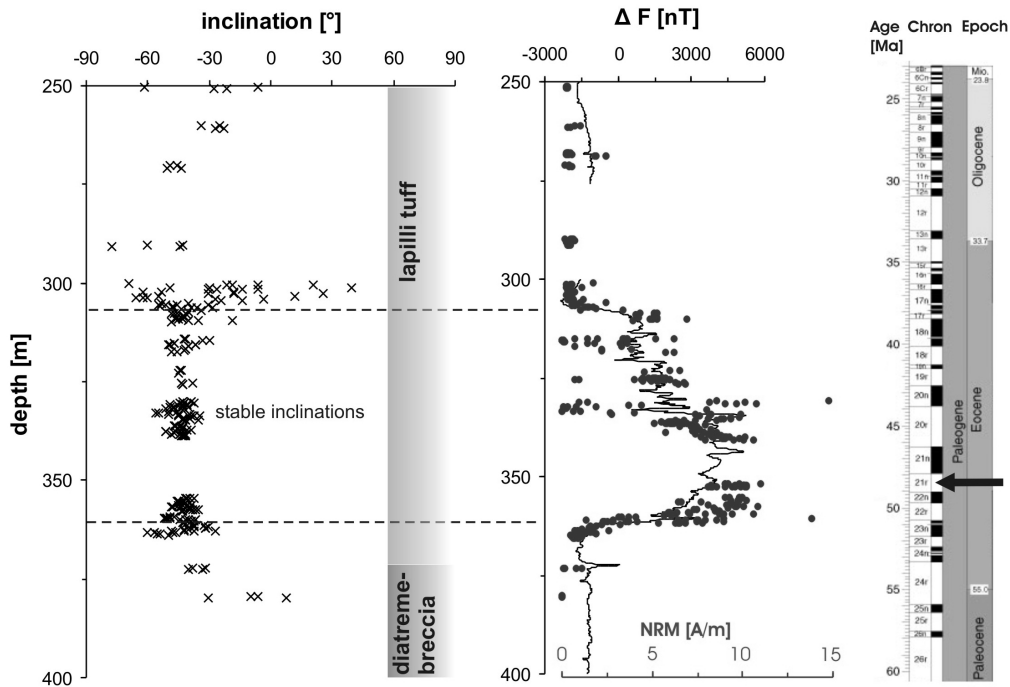


**Fig. 19** Comparison of the NRM inclinations log with the  $\Delta F$ -curve and the NRM intensities. Stability or dispersion of negative inclinations signalises the strength of magnetisation highest within the lower half of the lapilli tuff. NRM intensities trace the  $\Delta F$ -curve and are also highest within the lower half of the lapilli tuff. The dominant negative inclinations correspond to the reverse polarity in the Eocene Chron C21r (c. 48 Ma).

NRM values trace the anomalies of the  $\Delta F$ -curve in a range from 0-15 A/m. The lower half of the lapilli tuffs depicts stable negative inclinations between  $-30^\circ$  and  $-56^\circ$ , whereas in units I and V and the diatreme-breccia inclinations are more dispersed between  $-77^\circ$  and  $+39^\circ$ . In coincidence with the Eocene age of Messel calculated after Mertz and Renne (2005), the reverse magnetisation of the volcanoclastic deposits suggests a remanence acquisition earliest during the ocean anomaly C21r (47,907-49,036 Ma) (Fig. 19). The Messel averaged inclinations of  $I = -40^\circ$  are too low when compared with volcanic Tertiary rocks of Southwest Germany, possessing paleo-inclinations of  $I = 61.5^\circ$  (Nairn and Negendank, 1967). The magnetic inclination flattening most likely resulted from compaction and subsidental processes (Lorenz, 2003), occurred after deposition of the intra-crater volcanoclastics. Differences in the magnetization of the material have been demonstrated in the demagnetisation experiments. AF demagnetisation measurements signal different magnetic stabilities, whereby samples inside the anomalies ( $\Delta F$ ) appear to be more stable than material deposited outside. Thermal demagnetisation experiments also indicate that magnetic remanence destruction is greatest within the upper part of the lapilli tuffs (unit V).

The differently acquired or “locked” magnetisations of the volcanoclastic material can be interpreted by differently availed depositional temperatures. In this context, heating experiments may explain the origin of the magnetic partitioning. Although the whole

volcaniclastic material was able to acquire similar remanent magnetisations (due to similarities in ferrimagnetic properties), only the lower half of the lapilli tuff shows high remanence magnitudes. This is because unit II-IV has been exposed to higher temperatures than units I, V and the diatreme breccia. Thus the temperature effect was most pronounced between 307 m and 373 m, where the erupted lapilli tuff acquired its strongest TRM. Heating experiments compared to the initially acquired NRM (Fig. ?) favour depositional temperatures <300 °C for the material outside the anomalies, whereas material inside the anomalies most likely was deposited at temperatures >300 °C. Slightly different absolute values of acquired TRM at 600 °C (15.2 A/m and 22.3 A/m) can be explained by the occurrence of different susceptibilities. Increasing magnetic susceptibilities with depth (240-360 m) point to an increasing volume portion of juvenile components. Considering the heat source within the volcaniclastic units, the abundance of different sized juvenile lapilli and their frequency of occurrence give reason to study the juvenile fragments in more detail. This will be subject in the next main chapter.

**Table 3** Major rock magnetic properties inside and outside the  $\Delta F$ -anomalies

magnetic properties		inside	outside
downhole measurements	$\Delta F$ intensities [nT]	0 to +5000	-2500 to -1200
magneto-mineralogy	Curie temperatures [°C]	500-580	500-580
IRM curves	SIRM [mT]	~150	~150
hysteresis loops	$H_c$ [mT]	~10	~10
	$H_{cr}$ [mT]	100-125	100-125
AF curves	MDF [mT]	~30-40	~20
	$H_{dem}$ [mT]	100	100
	domain state	PSD	PSD
heating experiments	(TH) blocking temp. spectra [°C]	400-600	20-550
	TRM <sub>600</sub> [A/m]	~22	~15
NRM measurements	inclination [°]	-30 to -56	-77 to +39
	NRM [A/m]	3.5-15	<2.5

### 2.4.2 Magnetic fabrics of the lapilli tuffs

The drilled lapilli tuffs of the Messel maar-diatreme reveal increasing MS intensities with depth, proved by borehole measurements and laboratory measurements on single rock specimens. The approximately 130 m thick, volcanic body with its magnetic subdivisions is very difficult to distinguish on a macro- and microscopic scale. Except for a few sections within the lithological profile, represented by large blocks of the crystalline basement (<0.5 m in diameter), the erupted rocks with its dominant juvenile, accidental and ash particles appear as unsorted and structurless pyroclastics. Nevertheless, AMS measurements reveal magnetic fabrics in these rocks. Their preferred magnetic foliations and lineations are clearly pronounced by occupancy densities of 9.3 and 7.4 of multiples of random distribution. With



respect to the data reorientation and when evaluating the structural orientations, it has to be considered that declination variations occur and can be incorrect. According to the rock magnetic properties and high bulk MS intensities ferrimagnetic components are dominant throughout the lapilli tuffs. Hence, the AMS is affected by shape or distribution anisotropies of the ferrimagnetic particles (de Wall, 2005). The assumption of form anisotropies within the measured samples can be neglected, because the crystallised Fe-(Ti) oxides with skeleton-like structures are isometric (Fig. 12). Furthermore, it is assumed that the juvenile lapilli possessed a spheroid shape during deposition, i.e. primary form anisotropy of the lapilli did not exist. Distinct form changes of the lapilli by means of compaction, for instance, can occur after deposition of the pyroclastic rocks. Transport and relocation mechanisms may result in distribution anisotropies by linear or planar arrangement of the juvenile particles. Pronounced AMS geometries, for instance, have been found on pyroclastic flow deposits (Zanella et al., 1999). Indeed, there is not any indication of directional flow processes within the investigated lapilli tuff deposits. The oblate geometries with steep pole axes possibly reflect a compaction texture (“sandwich effect”) caused by the load of the overlying lake sediments. However, the prolate geometries of the rock samples and the filtered k-max data with a preferred NW-SE oriented lineation, respectively, point to a different causation. Considering the total AMS geometries, it can be deduced that the distribution field of the foliation poles lie upon a steep NW-dipping plane which acts as the  $\pi$ -circle with a flat NW-SE striking lineation cluster in  $\pi$ -pole direction. Such AMS patterns are typical for deformation textures which develop by relative compression to the striking direction of the  $\pi$ -plane and extension in direction to the  $\pi$ -pole (de Wall, 2001).

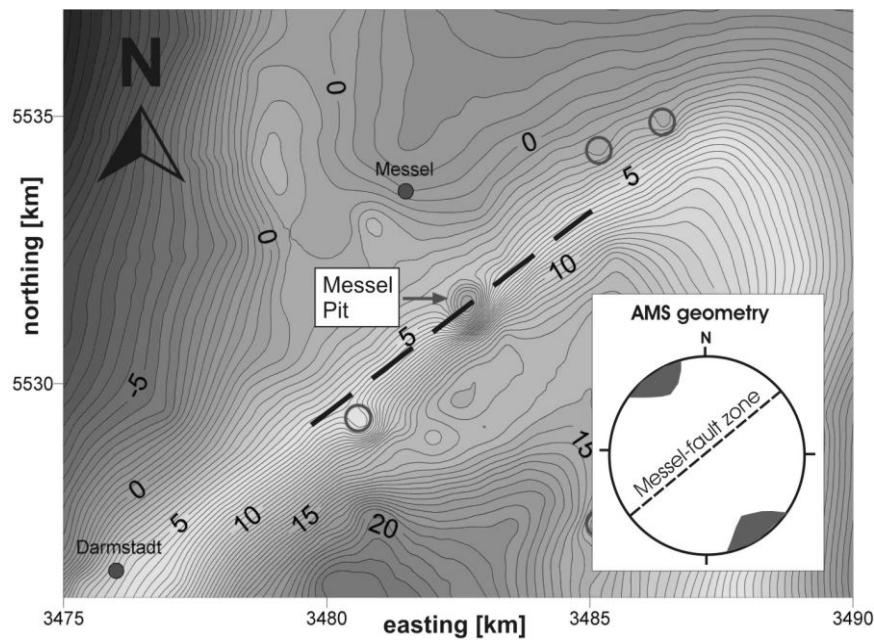


**Fig. 20** Map of gravitational anomalies (in mGal) of surroundings of the Sprenglinger Horst (after BUNESS et al., 2004). The NE-SW oriented Messel fault zone represents a transition from low to high gravity values (JACOBY et al., 2000). The trend of the faultzone is characterised by the occurrence of maar-volcanoes (circles). The sketched, preferred orientation of the magnetic lineations is perpendicular to the fault zone (bottom right).

In fact, the AMS data of the Messel volcanoclastics are cryptic and the interpretation speculative. However, it is supposable that a compaction-resulted, vertical stress field interacts with a tectonically horizontal paleostress field of the Rhine graben tectonics. Gravity measurements around the Spremlinger Horst area show a remarkable gradient which follows a possible ENE-striking crustal discontinuity (Fig. 20), the so-called “messel fault zone”. The real existence of this fault zone seems to be approved, but is still a current research subject (Felder, 2006; personal communication). However, the orientation of the magnetic lineation, perpendicular to the striking of the fault zone, argues for a genetic relation of the AMS lineation to this lineament.

## Chapter 3 Pyroclastic fragments

### 3.1 Why study the Messel volcanoclastic particles?

Powerful explosive eruptions make direct observations of processes in the vent, in the eruption column, or in pyroclastic density currents difficult. The understanding of eruptive and transport processes must be deduced from detailed stratigraphic and sedimentological studies. The previous rock magnetism chapter dealt with volcanoclastic rock units. To study the Messel volcanoclastic material in more detail, it is essential to evaluate the volcanoclastic particles.

Generally, lithics deposited near source and close to the vent are considered to provide little reasonable information about eruptive conditions, due to different transport history and refragmentation processes (Houghton et al., 2000). Nevertheless, as it will be shown in this chapter, small-scale properties of near-vent deposits within the Messel volcano deliver insights into the thermal and magmatic conditions. Volcanoclastic particle studies of diatremefacies are rarely applied to continuously vertical successions, due to scarcity of appropriate outcrops. Therefore, the Messel drilling, which recovers a continuous core section of volcanoclastic units of a maar-diatreme offers a unique opportunity for a detailed study on fragmented rocks. Thereby, image-analytical data of juvenile fragments elucidate and assist to the rockmagnetic properties by differentiation of size, fraction volume (area) and flattening ratio (deformation) of the particles. Geochemical investigations on juvenile lapilli deposited in vertical successions allow identifying different magma compositions and thus commenting on eruption phases and some depositional aspects during formation of these rocks.

### 3.2 Analytical methods

#### 3.2.1 Image analysis

Quantitative image analytical investigations of size and abundance of lithics have been performed with the software DIAna V3 (digital image analysis, version 3) which is trademark of Johannes Duyster, BASys (Bildanalysesysteme) Karlsruhe, Germany. One-meter half-cores (10 cm in diameter) and thin sections of 1-inch-plugs have been digitalised and measured with the particles manual modus because of small colour differences and poor, automatic particles identification. The accidental clasts fractions of 27 images (>250 single measurements) have been measured and illustrated in percent; size (mean long axis and mean area), fraction volume (area sum) and shape (flattening ratio) reflect quantities of nine image samples compared with their rockmagnetic parameters (MS, NRM).

Core measurements with a particle size resolution of >2-3 mm have been implemented within an area frame of 100 cm<sup>2</sup> (200-700 single measurements). For calculation of flattening ratios, only juvenile particles >5 mm have been considered. Achieving a more detailed resolution

and measuring of all particles, area sums, mean areas and mean long axes of lithics (with sizes  $>0.6 \text{ mm}^2$  or  $>1 \text{ mm}$ ) have been calculated on thin section images within an area frame of  $600 \text{ mm}^2$  (130-250 single measurement). For comparison and quality control data of the relatively small area frames of the thin sections, area sums of the lithics have been also measured on 20 core images. It is consequent that the 2D cross sections do not really reflect the true size values. However, magnetic fabric studies proved the weak anisotropy texture of the volcanoclastic rock samples with small P' values mostly ranging between 1.005 and 1.020. Therefore, it is inferred that the ratios bear only small mistakes by using 2D instead of 3D values. The volumetric proportion of clasts in a rock is equal to the area proportion of the clasts in any section (Delesse, 1847; Higgins, 2002).

### 3.2.2 Geochemical analysis

When dealing with volcanoclastic material, the geochemical composition of the magmatic phase can be studied by the juvenile fraction. Because of large amounts of small-sized particles in these rocks, it is difficult to acquire whole-rock chemistry of the juvenile material. Avoiding the time-consuming selection of single juvenile particles to produce sufficient rock powder for preparing XRF-tablets and to be ascertained that the geochemical results are limited to one juvenile particle, averaged microprobe scan analyses of single particles have been used for the evaluation of major element distribution (Fig. 21).

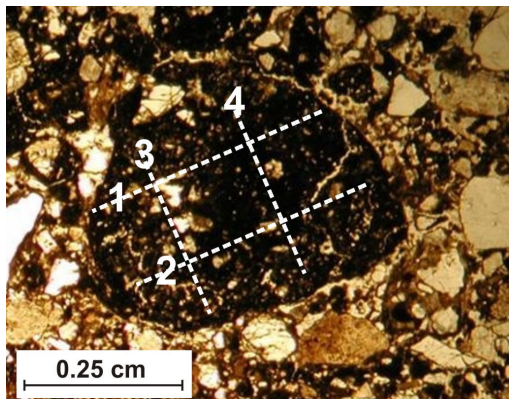


**Fig. 21** Photomicrograph of a juvenile lapillus. Major element measurements are aligned to the sketched lines averaging bulk major element composition.

Major elements of juvenile fragments have been analysed with CAMECA SX50 electron microprobe (Institute for Mineralogy, University of Würzburg), using 15 kV accelerating voltage, 15 nA beam current and  $25 \mu\text{m}$  beam size, as well as international rock standards (natural or synthetic silicates and oxides) for calibration and data quality control. Matrix correction has been carried out by using the CAMECA PAP-program. Analytical error for major elements is less than 1 % relative. For minor elements with concentrations  $<5 \text{ wt.}\%$ , the analytical error increases with decreasing element content. The detection limits are between 0.1 and 0.05 wt.%. Averaged values of 2-4 linear scans (Fig. 21) within juvenile particles represent bulk geochemical analysis of 7 samples (3 outside and 4 inside the  $\Delta F$ -anomalies). At least 3 particles per sample have been investigated, reflecting approximately 200-500

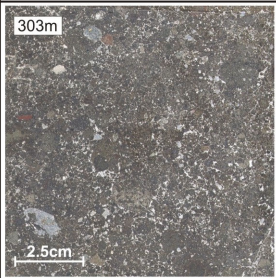
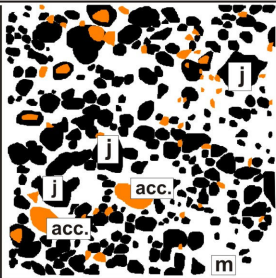
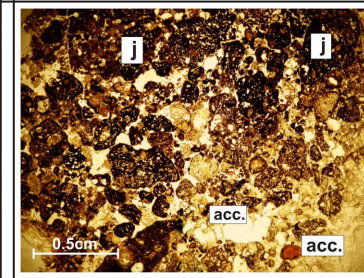
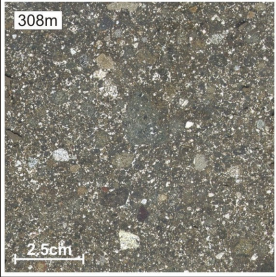
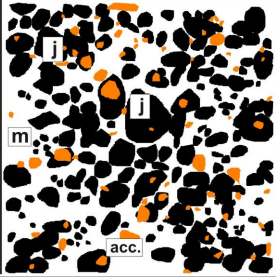
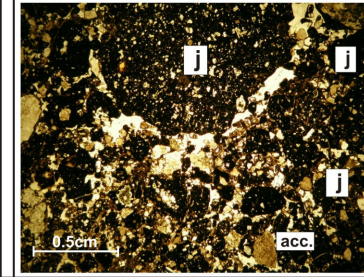
single measurements per sample. Because of total oxide values ranging between 70-99 wt.% due to different contents of primary or secondary fluid phase, every single analysis was normalised to 100 %. Despite of the relatively low total oxide values occurring in some single measurements, the comparison of element analyses of samples inside and outside the  $\Delta F$ -anomalies is still significant.

Trace elements were analysed by inductively coupled plasma mass spectrometry (ICP-MS) at the Institute for Mineralogy (University of Würzburg), using calibration of NIST 612 50 ppm glass and values from Pearce et al. (1997). The analyses reflect mean values of 4-17 single measurements for at least 3 particles per sample. Data evaluation was carried out with the program GLITTER version 3.0, whereby the 1-sigma errors determined by counting statistics are on average 5-10 % (Rb, Sr and Y), 13-18 % (Zr, Nb, Cs, Ba, La, Ce, Pr, Nd, Sm, Eu, Gd, Tb, Dy, Ho, Er, Tm, Yb, Lu) and 9-11 % (Hf, Ta, Pb, Th, U). The minimum detection limits (99 % confidence) of values up to 2500 ppm are reliable, the high values for Ti and P are only information values and without specification for errors and detection limits.

### 3.3 Results of the fragment studies

#### 3.3.1 Image analytical results

The Messel maar lapilli tuffs (240-373 m) predominantly consist of clast-supported fragments, with a minor ash matrix fraction. The clasts or lithics are classified as either juvenile or accidental (Fig. 22). The (sub-)rounded juvenile fragments are mostly characterised by low vesicularity (<10 %) and phenocrysts (5-10 %) disseminated within a black and glassy matrix. The juvenile lapilli are unsorted and vary in grain size. They are mostly in the range of 0.2-1 cm, rarely exceeding 2 cm in diameter. Accidental clasts are mostly angular, but may show small, rounded components, too. Their grain sizes are mostly in the same range as the juvenile fragments and very rarely show blocks of several decimetres in diameter. The lapilli tuffs are hardly differentiable on a macro- and microscopic scale. In the following, quantitative image analyses of the lithics are compared with MS and NRM measurements. Because the material can not be distinguished in units used for magnetic investigations, differentiations are made for volcanoclastics deposited above (section I), inside (section II) and below (section III) the  $\Delta F$ -anomalies. For instance, the onset of the magnetic anomalies at depths between 300-310 m deduced by borehole ( $\Delta F$ ) and single plug data (NRM) (Fig. 19) is not a significant marker featured by petrographical core studies of samples from outside (section I) and inside (section II) the  $\Delta F$ -anomalies (i.e. 303 m and 308 m, Fig. 22). The combination of image analytical investigations on cores and thin sections reveal small-scaled information of the Messel volcanoclastic particles which could not be observed by lithological descriptions after Felder et al. (2004).

	core samples		thin sections	description
section I				<ul style="list-style-type: none"> <li>- mostly clast-supported, structureless, poorly sorted and juvenile-rich lapillituffs</li> <li>- (sub-)rounded, juvenile fragments with low vesicularity (&lt;10%) and low richness of phenocrysts (5-10%)</li> <li>- angular to rounded accidental clasts</li> <li>- frequently altered ash matrix</li> </ul>
section II				<ul style="list-style-type: none"> <li>- as above, but with higher concentrations and larger grain sizes of juvenile fragments</li> </ul>

**Fig. 22** Photographs of two core and thin section samples at the magnetic boundary zone outside (303 m, section I) and inside (308 m, section II) the  $\Delta F$ -anomalies. Lithics are defined as juvenile fragments (j) and accidental clasts (acc.). The ash matrix (m) represents the indefinable portion of very small particles.

*Lithics and MS*

Accidental clast fraction throughout the lapilli tuffs mainly ranges between 5 % and 35 % (Fig. 23). Values of nearly 100 % reflect larger blocks of crystalline basement which are within the measured 100 cm<sup>2</sup> area. Comparing susceptibilities with the accidental clast fraction, no dependency is evident. A negative correlation of the parameters would suggest “MS dilution” due to high abundances of accidental clasts. The MS increase with depth would imply a decrease of the accidental clast fraction. The quantitative image analyses rule out this hypothesis. Generally, the volcanoclastic rocks are difficult to differentiate and can be regarded as virtually homogeneous.

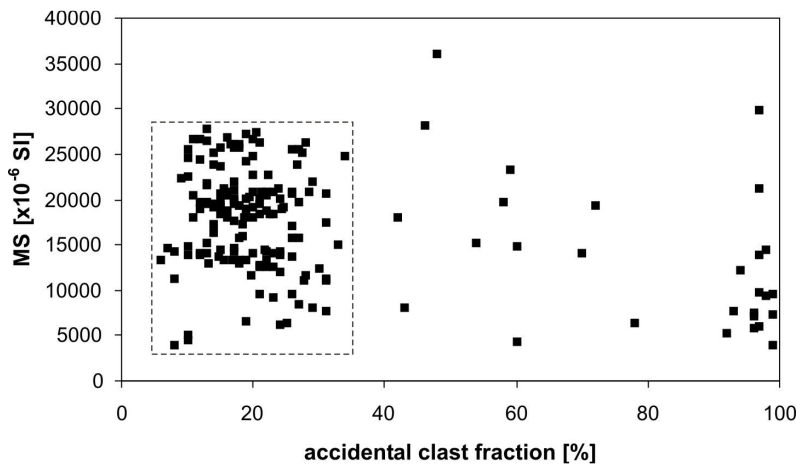


**Fig. 23** Cross-plot of magnetic susceptibilities (MS) and proportion of the accidental clast fraction.

In figure 24a, the particle size of the juvenile and accidental clasts is shown as its mean area or mean long axis. In section I between 250-290 m, the juvenile particle size constantly

remains below 1 mm<sup>2</sup> (mean area) and/or slightly higher than 1 mm (mean long axis). Following the image analytical logs downwards between 290-360 m (section I and II), the juvenile fragment sizes show increasing values from 0.8 mm<sup>2</sup> to 2.7 mm<sup>2</sup> and 1.2 mm to 2.2 mm, respectively. The transition to the diatreme breccia between 360-370 m (section II and III) is marked in turn by drop of the curves to low values between 0.6-1.0 mm<sup>2</sup> or 1.0-1.2 mm. The accidental clast logs only reveal low variability in the mean grain sizes ranging between 0.7-1.6 mm<sup>2</sup> or 1.3-1.6 mm. Comparing the particle grain sizes with the MS behaviour of the samples, it is obvious that both mean area and mean long axis of the juvenile fragments follow the downhole, linear MS trend with increasing values in section I and II as well as the remarkable drop of the parameters in direction to the diatreme-breccia (section II and III). This situation is also reproducible by MS borehole data (Fig. 17).

#### *Lithics and NRM*

Image analytical measurements of juvenile area sums (i.e. juvenile fraction) indicate relatively low values between 130-230 mm<sup>2</sup> for the upper part of the lapilli tuffs (section I), and high values roughly between 300-400 mm<sup>2</sup> for the lower part (section II) (Fig. 24b). The values from the transition to the diatreme breccia (section II to section III) decrease again to roughly 200 mm<sup>2</sup>. Area sums of the accidental clasts are relatively low between 10-100 mm<sup>2</sup>. Thus, the calculated matrix portion behaves in the opposite direction and is high (c. 380 mm<sup>2</sup>) in section I and low (c. 160-280 mm<sup>2</sup>) in section II. The values increase again in section III up to 380 mm<sup>2</sup> within the transition to the diatreme breccia. The juvenile log curve reflects the NRM trend, which is also implicative for the  $\Delta F$ -intensity curve given in figure 19. The image analytical log data of the accidental clasts show the non-dependency to the juvenile fraction and confirm the absence of the “MS dilution” hypothesis, even by small-scale investigations on thin sections.

The mean flattening ratio (length/height) of juvenile fragments also differs for the lower (section II and III) and upper part (section I) of the lapilli tuffs. As their lengths are twice their heights in section I, the mean flattening ratios increase from 2.5 to 3.0 in section II and decrease again to roughly 2.5 from the transition to the diatreme breccia (section II to section III). Comparing the magnetisation log data with image analytical data, it is obvious that both area sums and mean flattening ratios of juvenile fragments show high values, where the material with high NRM intensities was deposited at higher temperatures (>>300°C).

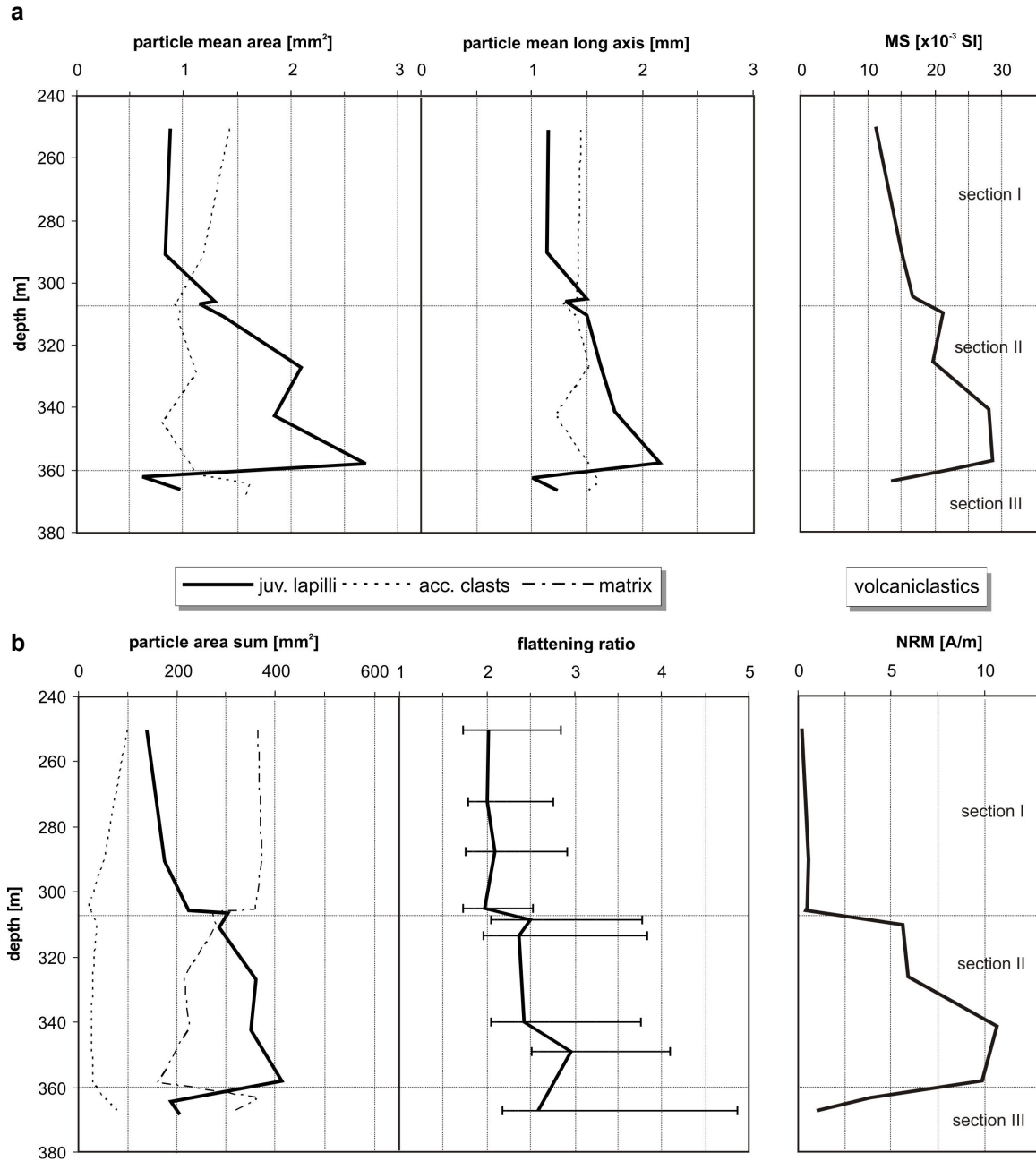


**Fig. 24** Logs of image analytical data with corresponding rockmagnetic parameters in depth of 250-365m. **a)** Juvenile and accidental particle analyses with mean areas and mean long axes. Juvenile curves follow the MS trend from low to high values (section I and II) and drop to the transition of the diatreme breccia (section III) **b)** Juvenile, accidental and matrix curves of area sums of the volcaniclastic rocks. Mean flattening ratios (length/height) are displayed for juvenile particles >0.5mm (beams). Area sums and flattening values of the juvenile particles are highest in section II, following the volcaniclastic NRM (or  $\Delta F$ ) trend.

### 3.3.2 Geochemical analysis

Major and trace element analyses have been performed on juvenile fragments of the upper (section I) and lower part of the lapilli tuffs (section II and III). In the following, the geochemical results describe the magmatic character of the Messel juvenile fragments, embedded within volcaniclastic rock assemblages of relatively low and high emplacement temperatures from inside ( $\gg 300^\circ\text{C}$ ) and outside ( $< 300^\circ\text{C}$ ) the  $\Delta F$ -anomalies.



### Major elements of juvenile fragments

MgO variation diagrams of juvenile fragments (from depths of 250 m and 324 m) show oxide analyses of major elements with exemplary element distribution fields from samples outside (section I and III) and inside (section II) the  $\Delta F$ -anomalies (Fig. 25). Measurements inside the  $\Delta F$ -anomalies (308 m, 324 m, 339 m, 351 m) generally display high MgO values in the range between 10-25 wt.%, indicating a more primitive geochemical character than MgO values of 5-15 wt.%, belonging to samples deposited outside the  $\Delta F$ -anomalies (250 m, 303 m, 364 m). For simplification of data illustration, mean values are supposed to approximate bulk element composition of the magma. They plot on and very close to the alkali basalt-tholeiite line after Mac Donald and Katsura (1964) and can be mainly classified as alkali basaltic, as shown in the sodium-potassium versus silica diagram (Table 4; Fig. 26a). The analyses show groupings of the juvenile samples deposited inside and outside the  $\Delta F$ -anomalies. Due to the subdivision of the alkalic magmas (Fig. 26b), the section II group (308 m, 324 m, 339 m, 351 m) mainly belongs to sodic series, the section I to potassic (250m and 303m) and the section III group to sodic (364m) series.

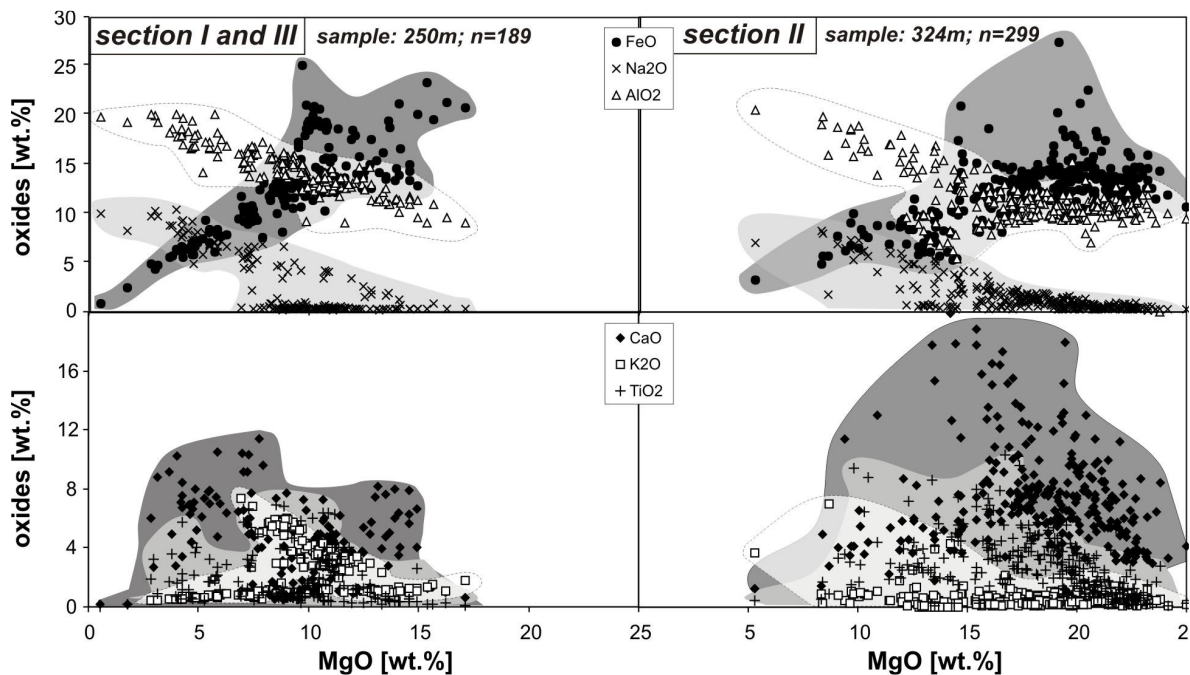


**Fig. 25** MgO variation diagrams of juvenile lapilli scans with major element distribution fields typical for samples from section I and III (outside the  $\Delta F$ -anomalies) as well as section II (inside  $\Delta F$ -anomalies).

In addition to the differences in MgO content between 8-12 wt.% and 14-18 wt.% as well as SiO<sub>2</sub> content between 43-45 wt.% and 47-52 wt.%, variation diagrams of Al<sub>2</sub>O<sub>3</sub>, K<sub>2</sub>O and CaO demonstrate bulk analytical differences for juvenile fragments inside the  $\Delta F$ -anomalies, section II (11.0-13.5 wt.%, ~0.5 wt.% and 7.0-8.5 wt.%), and outside the  $\Delta F$ -anomalies, section I and III (13.5-15.0 wt.%, mainly 2.0-3.0 wt.% and 4.0-5.5 wt.% (Fig. 27). Concerning the oxide analyses of Fe (10-13 wt.%), Ti (2.0-3.5 wt.%) and Na (1.5-5.5 wt.%),

groupings only occur by cross plots with MgO or SiO<sub>2</sub>. The sample in depth of 364 m (section III) possibly typifies a separate magmatic character, due to the exceptional position within the variation diagrams and partly apparent deviation of geochemical results from samples of section I.

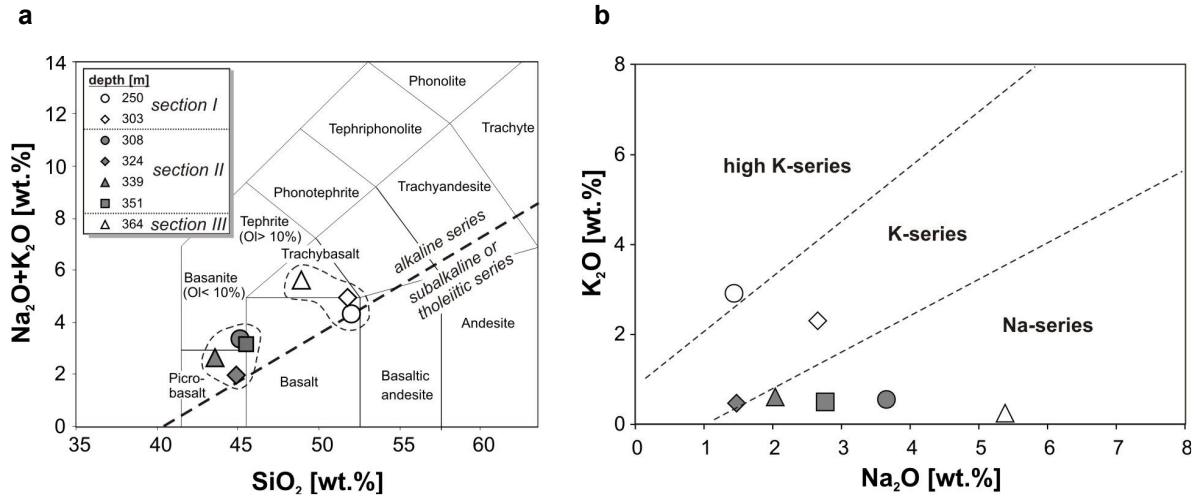
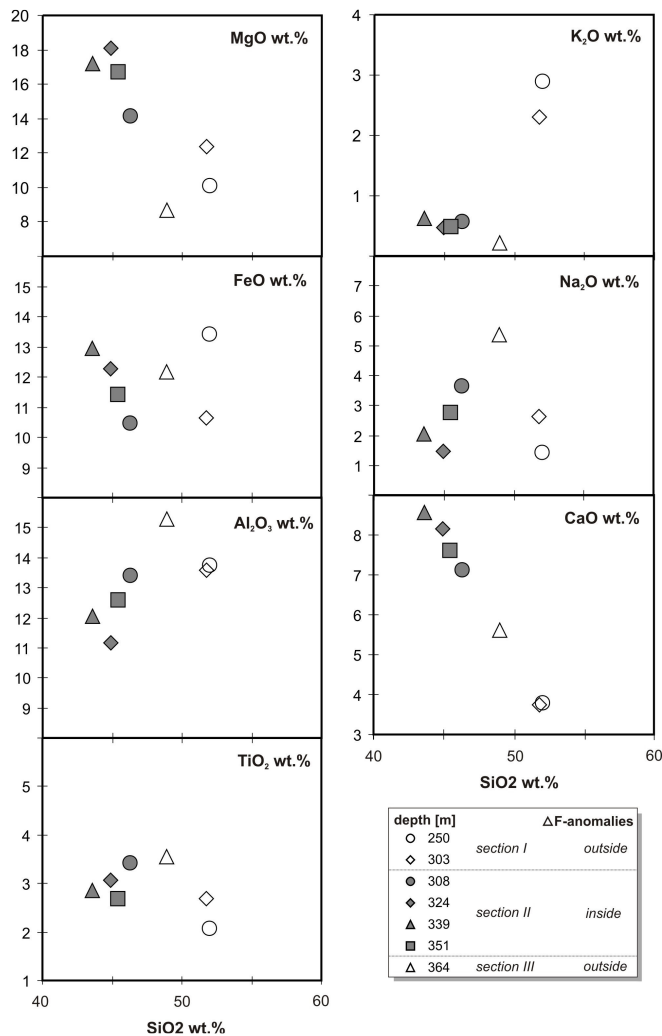


**Fig. 26** a) Total alkalis (Na<sub>2</sub>O+K<sub>2</sub>O wt.%) versus silica diagram with groupings of the juvenile material from section I, II and III (after Middlemost, 1980) b) K<sub>2</sub>O versus Na<sub>2</sub>O (wt.%) diagram, showing the subdivision of the alkalic magma series into high-K, K and Na sub-series (after Middlemost, 1975).



PYROCLASTIC FRAGMENTS

**Table 4** Major and trace element analyses (wt.% and ppm) of juvenile lapilli deposited in section I, II and III (out- and inside the  $\Delta F$ -anomalies).

$\Delta F$ anomaly type	outside			inside			
	250	303	364	308	324	339	351
sample depth (m)	<i>section I</i>		<i>section III</i>	<i>section II</i>			
SiO <sub>2</sub>	51.99	51.75	48.92	46.25	44.92	43.60	45.43
TiO <sub>2</sub>	2.08	2.68	3.55	3.42	3.07	2.85	2.69
Al <sub>2</sub> O <sub>3</sub>	13.76	13.58	15.30	13.43	11.15	12.07	12.60
MgO	10.10	12.38	8.65	14.14	18.10	17.18	16.70
CaO	3.79	3.73	5.61	7.13	8.14	8.55	7.62
MnO	0.09	0.22	0.13	0.16	0.23	0.26	0.24
FeO	13.43	10.64	12.17	10.49	12.28	12.96	11.42
Na <sub>2</sub> O	1.44	2.65	5.38	3.65	1.47	2.03	2.77
K <sub>2</sub> O	2.90	2.31	0.24	0.57	0.47	0.62	0.50
P	20678	3446	9930	14085	9332	15053	8666
Ti	72416	8562	19377	33521	24599	37584	32986
Rb	54	23	18	79	49	48	30
Sr	1259	330	864	956	794	1544	814
Y	158	14	65	111	50	127	70
Zr	1339	192	412	601	524	785	552
Nb	615	91	189	317	323	486	288
Cs	33	6	4	12	12	19	26
Ba	1439	300	519	1582	853	2320	1567
La	582	70	255	440	222	546	241
Ce	953	123	472	684	376	875	415
Pr	97	12	44	71	37	91	43
Nd	374	43	149	249	127	312	149
Sm	58	6	25	40	20	48	24
Eu	17	2	7	13	6	14	7
Gd	45	4	19	32	15	36	18
Tb	6	1	3	4	2	5	3
Dy	33	3	14	23	12	25	14
Ho	6	1	2	4	2	4	3
Er	16	1	6	10	5	11	7
Tm	2	0	1	1	1	1	1
Yb	13	1	4	8	4	9	7
Lu	2	0	1	1	1	1	1
Hf	20	4	9	10	9	12	9
Ta	33	5	10	15	15	23	13
Pb	15	10	5	10	9	31	24
Th	46	12	37	37	39	59	32
U	22	3	8	11	7	19	7
Nb/Zr	0.46	0.47	0.46	0.53	0.62	0.62	0.52
Ce/Zr	0.71	0.64	1.15	1.14	0.72	1.11	0.75
La/Zr	0.43	0.37	0.62	0.73	0.42	0.69	0.44
Rb/Zr	0.04	0.12	0.04	0.13	0.09	0.06	0.05

### Trace elements of juvenile fragments

When plotted in a REE-diagram the juvenile material display extreme enrichments in incompatible elements with averaged  $(La/Yb)_n$ -ratios of 32 (Fig. 28a). Other incompatible trace element ratios (e.g.  $Nb/Zr \approx 0.57$ ) are similar for all samples. The analyses do not provide a well-pronounced grouping character of the juvenile composition in all sections, inside and outside the  $\Delta F$ -anomalies. However, it appears that REE curves of fragments inside the anomalies show possible groupings for the samples from 308 m and 339 m as well as 324 m and 351 m. The samples at 250 m and 303 m deposited in section I display end members with the lowest and highest REE concentrations; the sample at 364 m reflects an intermediate REE pattern between 250 m and 303 m. Generally, all samples have high light-REE values, showing a typical REE trend of volcanic suits of potassic continental rift zone magmatism (Fig. 28a). For instance, schematized REE patterns of leucitites, lamproites or kimberlites (data from Bergmann, 1987 and Wilson, 1989) of the western branch of the East African Rift (EAR) are comparable with the Messel REE pattern. Lamproites or kimberlites plot into the upper part of the leucitic composition field. Here, the REE curves of the Messel juvenile fragments resemble these undersaturated, potassic rocks. The ratios of Th/Yb versus Ta/Yb display respectively high values for the juvenile components and plot within the field of intra-plate basalts deriving from enriched mantle source (Fig. 28b). The ratios are again comparable with the potassic lavas of the EAR (Mitchell and Bell, 1976). Trace element compositions of the Messel juvenile fragments can be tectonically associated to within-plate basalts with exemplary Zr/Y ratios of 6-8 and Zr content roughly between 200-1300 ppm.

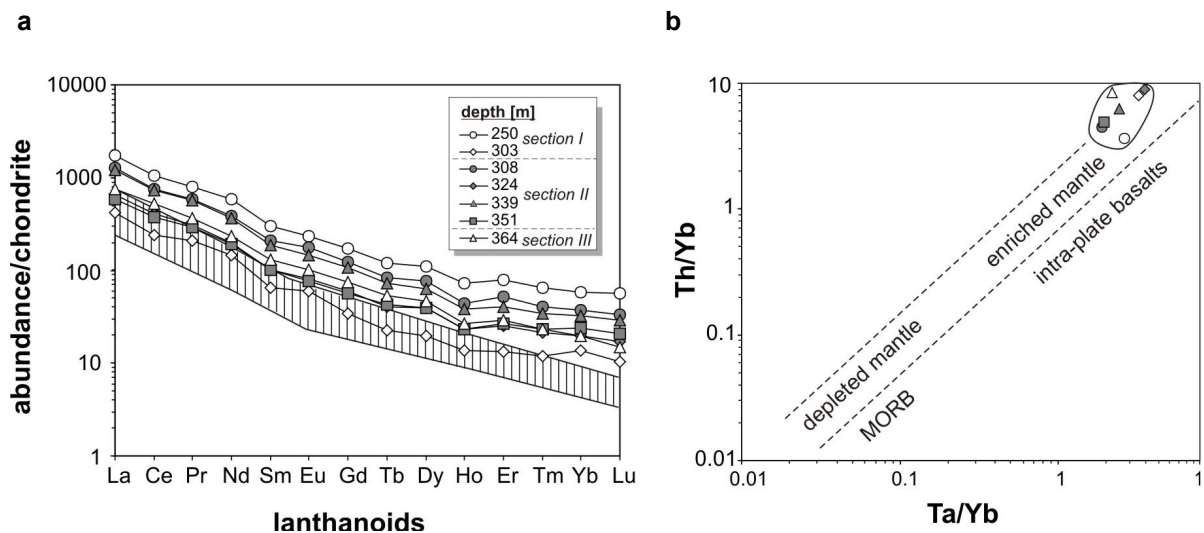


**Fig. 28 a)** REE-diagramm of the juvenile material and the schematised pattern of the leucitic composition field of volcanic rocks of the western branch of the East African Rift (EAR). **b)** Th/Yb versus Ta/Yb plot showing the magmatic mantle source character of the juvenile lapilli.

### 3.4 Interpretation of the analytical measurements

The Messel drilling project 2001 recovered a lapilli tuff body (240-373 m) within a maar-diatreme-structure. Besides the low magnetised rocks of the transition to the diatreme breccia (section III), the tuffs can be subdivided into a low magnetised upper part (section I) and a strongly magnetised lower part (section II). Rock magnetic experiments explain the differences in acquisition of remanent magnetisations (NRM and TRM) by differently availed depositional temperatures (section I  $<300^{\circ}\text{C}$  and section II  $\gg 300^{\circ}\text{C}$ ). Small-scale image analytical investigations on juvenile fragments prove to be valuable for understanding the rock magnetic character (MS trend and NRM signature) of the tuffs and show distinct differences in their particle grain size, degree of relative fraction dominance and shape. Juvenile fragments of section II are generally larger, more frequent and have higher flattening ratios than in section I (Fig. 7). The clear subdivision of the tuffs is also accomplished by major element analyses of the juvenile fraction. Particles deposited in section I and III have higher  $\text{SiO}_2$ ,  $\text{Al}_2\text{O}_3$  and  $\text{K}_2\text{O}$ , but lower  $\text{MgO}$  and  $\text{CaO}$  concentrations than samples deposited in section II. The chemical analyses of juvenile fragments from section III (diatreme-breccia) possibly correspond to a separate group. In the following, these data of image analytical and geochemical investigations on juvenile fragments will be discussed in the context of heat and magma source conditions.

#### 3.4.1 Heat source

In context with rock magnetic studies, image analytical results suggest that the juvenile fragments deposited at higher temperatures (section II) favoured a more effective delay in cooling process (heat loss) of the material than the volcanoclastic rocks deposited at lower temperatures (section I and III). During eruption and subsequent deposition of the material within the Messel diatreme-structure, the temperatures of the tuffs in section II have been high enough (above Curie temperatures of near magnetite-composition) to acquire TRM. Besides large grain sizes and high fraction dominance of juvenile fragments in section II, high flattening ratios are observed in the high temperature-effected lapilli tuffs. In this part, abrupt changes in flattening ratios to higher values indicate higher degrees of fragment deformation which can serve as an approximate guide to relative viscosity (Peterson 1979; Fischer and Schmincke 1984). Besides crystallinity and volatile content, viscosity is a function of temperature and chemical composition. Due to petrographical investigations of the juvenile particles, the degree of crystallinity and volatile content does not change much, so that temperature and chemical composition most likely control their different rheological behaviour. Ignoring the geochemical character, high temperatures of the juvenile fragments very likely caused their higher degree of deformation. This statement agrees with the occurrence of agglutinated formations of some particles at roughly 350 m, showing here their highest degree of flattening ratios and very high NRM intensities, too. It is possible that the water/magma mass ratio, which can be one crucial parameter for the degree of fragmentation

of the material, has varied (Fischer and Schmincke, 1984; Lorenz, 1986; Wohletz, 1986; Vespermann and Schmincke, 2000). Larger particles in section II possibly result from lower mixing ratios. A pronounced water involvement can be inferred from section I. This is not only confirmed by the lower particle grain sizes and deduced low temperatures, but also by frequent occurrence of accretionary lapilli within the first meters at the top of the volcanoclastic body. Concerning the Messel explosivity (the efficient conversion of thermal energy into kinetic energy), the particles in section II indicate a rather strombolian eruption style with lower water/magma mass ratios; the particles deposited in section I (and section III) favour a more hydrovolcanic eruption style with higher water/magma mass ratios, typical for most maar-related deposits.

### **3.4.2 Magma source**

The chemical composition of the mainly alkaline magma appears to be more primitive ( $\text{Na}_2\text{O}+\text{K}_2\text{O} < 4 \text{ wt.}\%$  and  $\text{SiO}_2$  43-45 wt.%) in section II (inside the  $\Delta\text{F}$ -anomalies) of the tuffs and more differentiated ( $\text{Na}_2\text{O}+\text{K}_2\text{O} > 4 \text{ wt.}\%$  and  $\text{SiO}_2$  47-52 wt.%) in section I and III (outside the  $\Delta\text{F}$ -anomalies). The geochemical variation in all sections points to at least two different eruption phases. The geochemical division can not be clearly reproduced by trace element analyses of the juvenile fragments. However, REE data with very high LREE concentrations show a well-defined association to potassic continental riftzone-magmatism of typical within-plate basalts. Comparing certain incompatible element ratios (e.g. Nb/Zr and Rb/Zr; Tab. 4) of juvenile fragment samples inside and outside the  $\Delta\text{F}$ -anomalies, the results are relatively constant. This provides a useful test for the fractionation-controlled origin of the more silica-rich magma (outside the  $\Delta\text{F}$ -anomalies), because if trace element ratios are constant throughout a suite then significant crustal contamination is unlikely to have occurred (Wilson, 1989). Despite the absence of radiogenic isotope data to confirm a liquid line of descent, the constancy of these ratios provides strong evidence for fractional crystallisation process and derivation from a similar magma source (Wilson, 1989). Due to juvenile melt composition, Th/Yb versus Ta/Yb ratios favour an enriched mantle source.

The data suggest a clear sub-division of the lapilli tuffs into a two-condition eruption phase at the end of the Messel volcanic activity. Image analytical and major element data support the rockmagnetic results of the lapillituffs and separate the volcanoclastic material into a relatively hot, undifferentiated eruption phase and a colder, differentiated phase. Size, shape and amount of the juvenile particles account for the temperature evolution and heat conditions during/after deposition of the Messel lapilli tuffs.

## Chapter 4 Potential field modelling

Magnetic and gravity exploration, also referred to as “potential fields” exploration, is used to give geoscientists an indirect way to “see” beneath the Earth’s surface by sensing different physical properties of rocks (magnetization and density, respectively). Thus magnetic and gravity data are interpreted in conjunction with other geoscience information to provide constraints on the subsurface structure. Potential field surveys are relatively inexpensive geophysical methods and can quickly cover large areas of ground. The evaluation of the gravity and magnetic exploration can be carried out by 3D potential field modelling.

This chapter deals with gravity and magnetic field modelling of the Messel subsurface. Ground survey data from the GGA Institute and the University of Mainz have been used for the models. The ambiguity of potential field interpretation will be reduced by considering results of several geoscientific methods: lithological results of several Messel boreholes, seismic information, density parameters from the 2001 research well and results of the core and/or plug magnetic measurements. After introducing the potential field measurements which were performed around the Messel Pit, the methodology of the computer-based 3D modelling, the results and interpretation of the combined models are presented.

### 4.1 Potential field data of Messel Pit

For preparation of the exact drill location of the Messel project 2001, the GGA Institute and the University of Mainz intensely investigated the Messel area with geophysical methods (Fig. 29a). The techniques are of use for the different physical parameters of the rocks, e.g. magnetisation (magnetics), density (gravity) or elastic properties (seismics). Based on the potential field data (gravity and magnetic measurements, Jacoby et al. 2005), the well was located close to the residual gravity minimum expected to correspond to the maximum sediment thickness and close to the magnetic minimum as well (Fig. 29b). With respect to the geoscientific information of the drilling, the potential field methods allow the reconstruction of the Messel maar-structure.

#### 4.1.1 Gravity measurements

Gravimetry deals with measuring and interpretation of gravity as the magnitude of the gravity acceleration on or near the surface of the earth (e.g. Torge, 1989) which is approximately  $9.81 \text{ m/s}^2$  on surface of Germany. Gravimetric investigations detect gravity anomalies caused by lateral density variations of different rocks. Positive gravity anomalies point to source rocks of high densities, and negative anomalies point to low densities. In principal the interpretation of gravity anomalies is ambiguous and the observed anomaly is a superposition of the gravity effects of all rock types. Furthermore, it has to be considered that the measured gravity does not solely depend on distribution of the “light” (in contrast to “heavy”) sedimentary rocks, but

also on the mass distribution of the whole geological environment of the Messel Pit. Determining the exact local gravity anomaly, intensive data processing is necessary to consider local disturbances such as terrain reduction of the pit, corresponding to approximately 15 % of the local gravity anomaly (Buness et al., 2004). On the other hand, the regional gravity field caused by structures of the Odenwald or Rhine Graben, for instance, has to be also filtered out of the measured gravity data set. This regional gravity field, surrounding the Messel Pit and showing a SW-NE trending gravity gradient (“Messel fault zone”), has been already introduced when dealing with the interpretation of magnetic fabrics and AMS geometries of the volcanoclastic rock units (Fig. 20). Subtracting the regional gravity portion, a slightly elliptical shape of the local field occurs with a SW-NE elongation of 1500 m and a SE-NW extension of 1100 m (Fig. 29a, middle). The observed gravity minimum of -7 mGal ( $1 \text{ mGal} = 10^{-5} \text{ m/s}^2$ ) is typical for maar volcanoes of this dimension and signals the location of the maximum thickness of the low-dense sediments (Gabriel, 2003; Buness et al., 2004; Schulz et al., 2005). Density estimation by weighing the cores of the Messel “oil shales” proved to be very low ( $1.33 \text{ g/cm}^3$ ) compared to the surrounding densities ( $2.65 \text{ g/cm}^3$ ). Due to averaged density values of  $2.0 \text{ g/cm}^3$  in a depth between 240-373 m, the lapilli tuffs contribute only to a small part of the measured gravity anomaly of the Messel Pit.

#### **4.1.2 Magnetic measurements**

The most applicative geophysical method used for investigations of remnants of subsurface volcanic structures is magnetics. Differences in rock magnetic properties can result in anomalies of the measured Earth’s magnetic field. Thereby, the amplitude mostly corresponds to less than 1 % of its field which is around 48,000 nT in our latitudes. As shown and described in the rock magnetism chapter, only the rocks containing (ferri)magnetic minerals make a contribution to magnetic anomalies in the borehole or on the surface.

The Messel anomaly is dominated by the remanent magnetisation which volcanoclastic rocks acquired during their deposition and formation. The detected magnetic anomaly associated to the subsurface of the Messel structure was recorded by Laubersheimer (1997). After figure 29a (left), the anomaly is negative and its minimum (-300 nT) approximately 150 m south of the gravity minimum. The origin of the negative sign of the magnetic field can be reproduced by negative inclinations mainly measured on rock units of the lower half of the lapilli tuffs and inside the downhole magnetic anomalies (chapter 2), respectively. Thus, the volcanoclastic rocks have been deposited at a time when the Earth’s magnetic field was inversely poled.



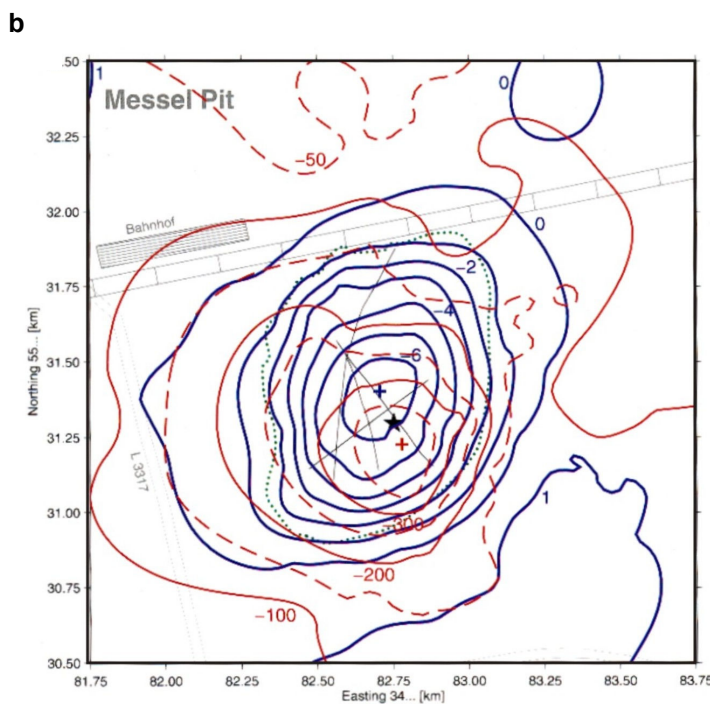
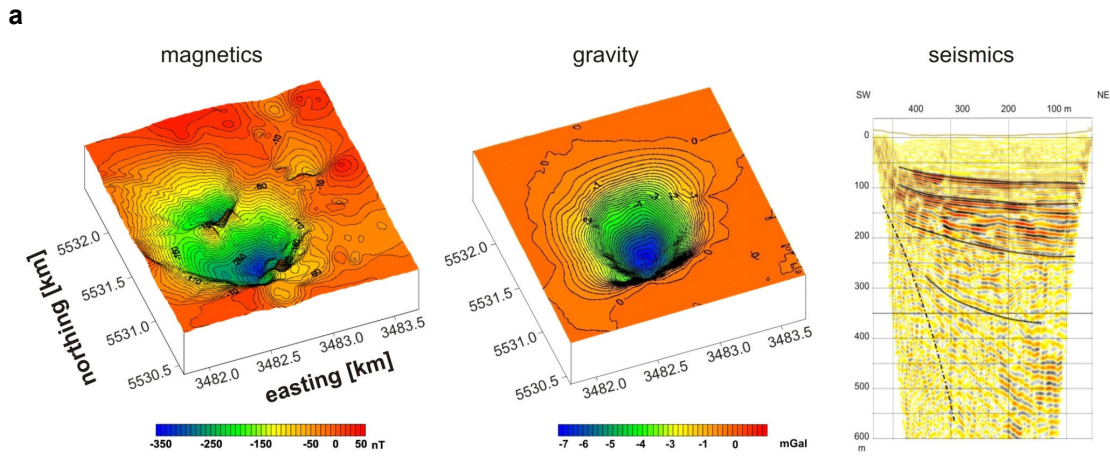


**Fig. 29 a)** Magnetic, gravity and seismic measurements (after Bunes et al., 2004) have been used for identifying the circular-shaped Messel structure. Potential field data of the Messel Pit collected by Mainz University show negative anomalies of both the local magnetic field relative to 48.000 nT and the local residual gravity field. Seismic reflection data reveal the funnel-shaped subsurface and the layering of the Messel lacustrine sediments. **b)** Overlapped contour lines of gravity (blue) and magnetic (red) measurements (after Jackoby et al., 2005). Four reflection profiles are shown as black thin lines. The potential field minima are marked by crosses, the borehole location is centred in between.

## 4.2 Methodology

The interpretation of potential field data can be carried out by qualitative (anomaly imaging) and quantitative (forward modelling) methods. Gravity and magnetic modelling can be considered as independent applications, but also as combined methods with one geological structure defined as best fit option. By the reason of typical maar-structures with relatively well-known geometries and an approximated vertical, cylindrical maar-sediment-body with a diameter/thickness ratio of roughly 4:1, 3D model calculations are necessary and preferred (Gabriel, 2003). The following paragraphs describe the proceedings and considerations in the context of the Messel maar modelling.

#### 4.2.1 Elevation model

Due to the aforementioned relief corrections when dealing with gravity modelling, an appropriate elevation model is inevitable. The model represents the topography of the Messel area in grid format, i.e. it illustrates the interpolation of single measurements with corresponding geographic coordinates and numerical descriptions of altitude. For the adequate amount of data, elevation parameters have been mainly obtained by remote sensing (data from University of Mainz) technique combined with a minority of data from direct GPS or ground survey measurements (GGA Institute). The approximate elevation variations of the data sets correspond to a few meters only, so that all measurements are integrated in one elevation model. Data processing was done with the surface mapping program *Surfer* which may convert the data into post, contour and shaded image maps (Fig. 30). It has to be mentioned that the Messel surface changes continuously due to on-going excavations of the fossil-bearing oil shales and marginal depositions of solid waste material from the nearby Ytong-factory. The elevation model integrated in the 3D potential field modelling reflects a “snapshot” of the Messel Pit surface. In addition to new geoscientific information in the future, the elevation model has to be renewed to correct the interpretation of the Messel subsurface.

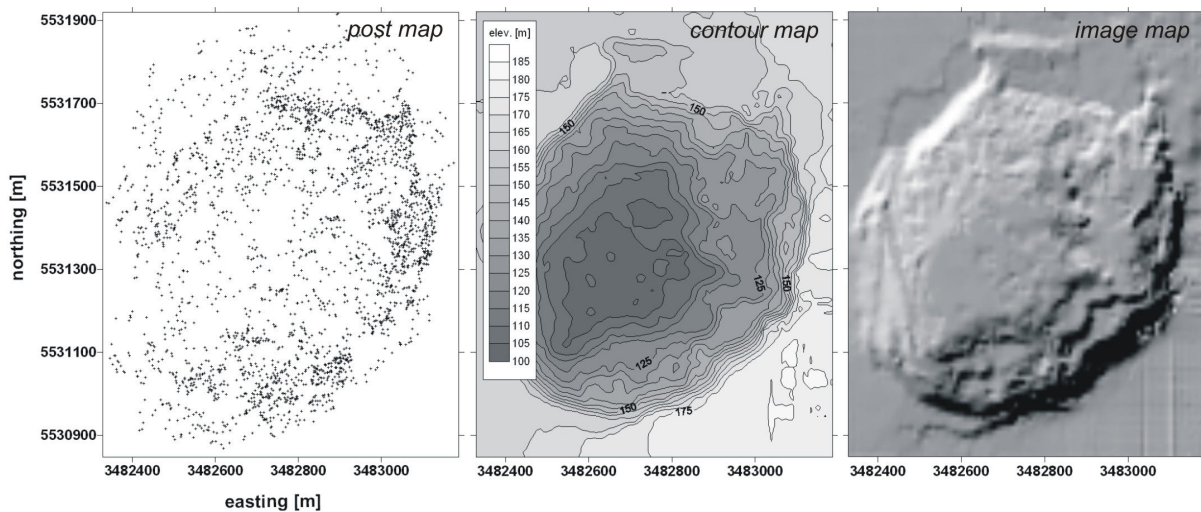


**Fig. 30** Illustrations of elevation data of the Messel Pit shown by post (left), contour (middle) and image maps (right). The topographic parameters are used for potential field modelling.

#### 4.2.2 Modelling with IGMAS

IGMAS (*Interactive Gravity and Magnetic Application Systems*), the program used in this study, is an interactive, graphical computer system for interpretation of potential fields (gravity and magnetics) by means of numerical simulation (Götze, 1984; Götze and Lahmeyer, 1988; Schmidt, 1996). The modelling procedure is based on “trial and error” methods. The algorithm used for potential field calculation is based on triangulated polyhedrons (Götze, 1978).

The data structure, which is required for the description of three dimensional model geometry, has to be simple and flexible enough to cover the wide field of gravity or magnetics modelling. It should facilitate representations of geological information, such as vertical or horizontal cross sections, surface and depth contour maps, 3D visualization, as well as volume and mass calculations. These requirements lead to the following basic elements of the input data: The structures (geological bodies) to be modelled are bounded by triangulated surfaces (layer boundaries), which limit domains with constant density, susceptibility or remanent magnetisation (Fig. 31). The definition of these triangulated surfaces may be given by defining polygons (lines) along vertical, parallel cross sections. The triangulation between the vertical planes is done automatically. The data input is two-dimensional, whereas the construction of the final 3D model structures is performed by IGMAS and does not require detailed knowledge about topology, data structures or triangulation techniques. Interactive modification of model parameters, e.g. geometry, density and magnetic parameters, access to the numerical modelling process and direct visualization of calculated and measured fields of gravity and magnetics. A basic requirement for modelling is the existence of ideas and hypothesis on the investigated area, i.e. the availability of quantitative or qualitative constraints.

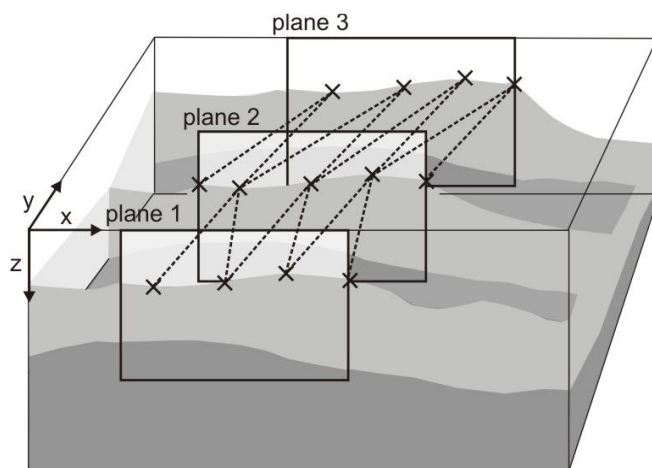


**Fig. 31** Sketch of constructed vertical planes (1-3) used for definition and location of the vertex coordinates (crosses). The planes are always parallel to each other, but spacing is variable. In order to achieve greatest flexibility, these vertical planes should be defined perpendicular to the dominating strike direction of the structures to be modelled.

#### *Constraints of Messel modelling*

As all potential methods of geophysics, gravity forward modelling is subject to the principle of equivalence: Due to relative changes of geometry and density distributions, variable substructure models may provide the same gravity field. Therefore, known geophysical and geological constraints have to be considered during modelling. After Bunes (2005), structural information with high resolution is provided by four reflection seismic profiles crossing in the centre of the Messel gravity field (Fig. 29b). The bowl-shaped maar-structure is proved by all profiles. Thereby, the majority of the reflections are associated with the sediment infill, whereas in relation the seismic information of the margins is weak. In this respect, gravity and seismic measurements complement one another: Gravity does not have the ability to detect horizontal layer boundaries, but makes a contribution to detection of lateral density contrasts.

Besides the subsurface geometrical constraints of the Messel maar, the significance of gravity models depends on the quality of available density information. In this connection, recorded density logs performed during the drilling project 2001 have been very instrumental (Wonik, 2005). They reflect horizontal layer boundaries, particularly the transition from the lacustrine sediments to the volcanoclastic sequences (Buness et al., 2005). The densities used in this model represent values of 1.5 m long weighted cores, determined by Felder et al. (2004). In addition to the research drilling 2001, lithological information from approximately 30 drill holes supports the suggestive dimensions of the sedimentary units belonging to the upper part of the entire maar-diatreme-structure.

The magnetic anomaly on the surface reflects the magnetic moments, i.e. the product of magnetisation and volume (thickness of volumetric elements). The form of the magnetic anomaly depends on intensity and direction of the magnetisation, the distance to the magnetised volumetric elements as well as the ratio of remanent to induced magnetisation of the rocks. Generally, magnetic models solely are ambiguous, because different modelled bodies may result in the same modelled anomaly. Limitation of this ambiguity succeeds with additive information, such as rock magnetic, geological or geophysical statements to the structure to be modelled. Hereby, magnetic models have the same constraints considered by gravity models. Fortunately, the *Messel* drilling 2001 recovered volcanoclastic rocks, accounting for the magnetised material and the magnetic anomaly on the surface. The thickness of the magnetised body being modelled arises from the 2001 drill hole. After Lorenz (1974, 1986 and 2000), the lateral extension is limited due to typical maar geometries with funnel-shaped diatreme-wall dips of approximately 80°.

#### *Vertical planes of Messel model*

The aim of the 3D modelling is to combine the gravity and magnetic field planes to fashion a single maar-diatreme-structure. The Messel area to be modelled has been divided into 20 vertical planes. Due to the circular shaped structure, modelling flexibility is given in all directions, i.e. the planes do not have to be defined perpendicular to a dominating strike direction. The East-West-oriented planes (1, 2, 3..., and 20) align parallel from South to North. Their spacing is 100 m, except at the margins of the maar-structure, where the intervals are 50 m (plane 5-9 and 15-18) because potential field isolines are narrowest and parameter contrasts highest. A 2D maar-model is illustrated by an exemplary vertical section (plane 10), striking through the 2001 research borehole (Fig. 32). According to lithological and log data information, 9 different lithozones are used for gravity and magnetic modelling. The geometrical dimensions and rock-physical parameters (density, magnetisation) of the selected bodies account for the modelled potential field curves. These curves are supposed to best fit the measured field curves, defining an approximate parabola (with its vertex oriented downwards, i.e. negative field anomalies) in the centre of the maar-diatreme-structure.

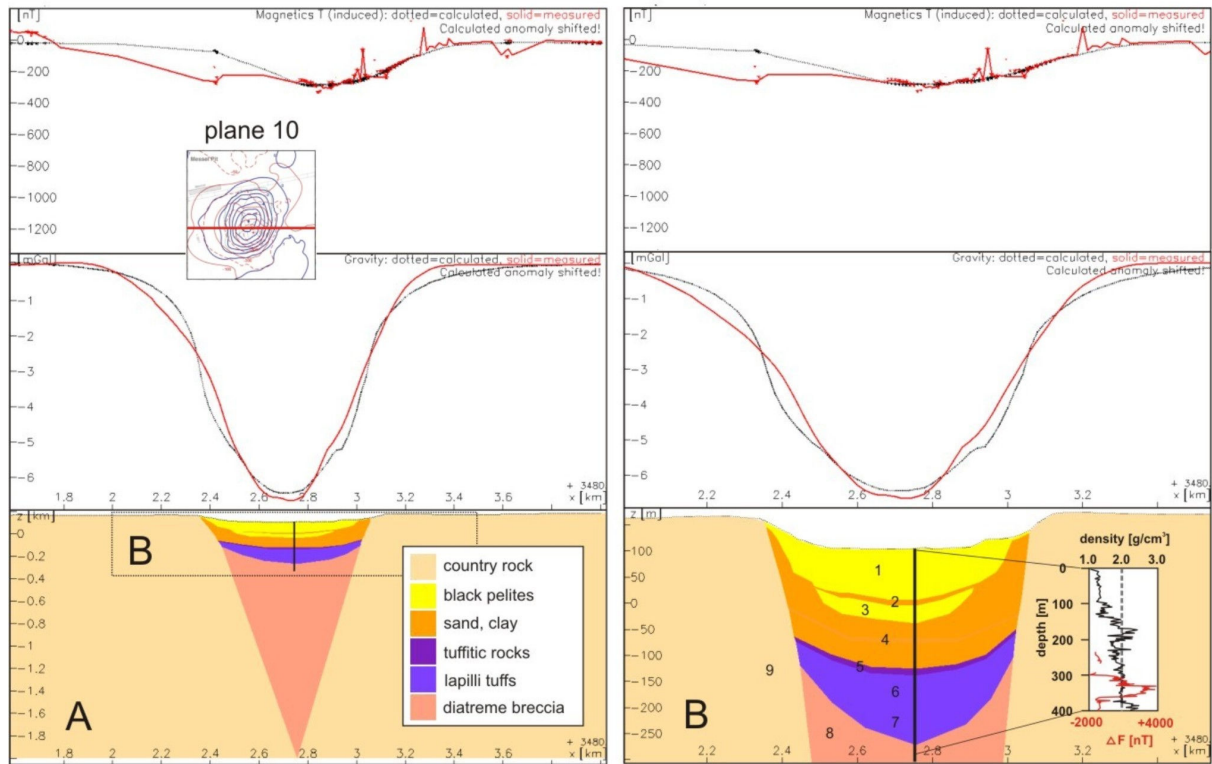
### 4.3 Results of the 3D modelling

Figure 32 shows a vertical section through the 3D model demonstrating that the gravity model is well-contoured relative to the magnetic model, where some artefacts not only occur at the diatreme margins, but also within its central parts. After Laubersheimer (1997), the magnetic measurements on the surface ascribe possible interference caused by the magnetic field of the maar-diatreme structure and the field of the solid waste material of the nearby Ytong-factory (NE-margin) or excavated and heated material of the “oil shales” (W-margin). However, the shape of the magnetic anomaly and thus its existence is not questioned. While the selected geometries of the lacustrine bodies (pelites or “oil shales” and sand/clay) are relatively well-defined by 30 boreholes, the dimensions of the tuffitic rocks and lapilli tuffs are assumed in direction to the diatreme margins. The 3D model shows its highest contrasts in rock properties at the margins or transition to the country rocks.

In the gravity model, the lowest density values are reflected by the black pelites ( $1330 \text{ kg/m}^3$  and  $1500 \text{ kg/m}^3$ ) and the upper sand/clay units ( $1630 \text{ kg/m}^3$ ). Intermediate densities between  $2030\text{-}2100 \text{ kg/m}^3$  have the lower sand/clay units, tuffitic rocks and the upper lapilli tuff sequences. The highest densities ( $2500 \text{ kg/m}^3$ ) exist in the lower lapilli tuffs and the diatreme breccia. All densities reflect values determined by direct core weighting (Felder and Harms, 2004).

In the magnetic model, magnetisation parameters only concern the tuffitic rocks and lapilli tuffs (Tab. 5). Rock magnetic studies (chapter 2) on these volcanoclastics proved the existence of negative polarities in the material. Thus the Tertiary magnetic field orientation was opposite to the today’s Earth’s magnetic field. However, the magnetic pole axis was very similar to the today’s axis. This implies that a Tertiary inversely remanent magnetisation with an induced magnetisation (IM) of similar intensity cancel out each other. In the Messel magnetic model, the effective inverse remanence is the remanence which prevails the induced magnetisation. For instance, the ratio of natural remanent (NRM) to induced magnetisation (IM)  $\text{NRM/IM} = Q \approx 6.8$  implies the predominance of  $M_{\text{rem}} \approx -5.63 \text{ A/m}$ . The difference of  $M_{\text{rem}}$  and  $M_{\text{ind}} (\approx 0.81 \text{ A/m})$  results in the effective magnetisation  $M_{\text{res}} \approx -5 \text{ A/m}$  (Tab. 5, 6). The averaged magnetisation inclination of the upper and lower halves of the lapilli tuffs is  $I = 40^\circ$ . As all averaged rock magnetic parameters (NRM, MS, IM, Q and I) for the lapilli tuff units are calculated by plug measurements, the parameters for the overlying tuffitic are assumed mean values drawn by downhole magnetic log curves from Wonik (2005). With respect to the magnetisations used in the magnetic model, the tuffitic rocks and the upper lapilli tuffs have the lowest ( $-1.5$  and  $-1.0 \text{ A/m}$ ), the lower lapilli tuffs ( $-5.0 \text{ A/m}$ ) the highest magnetisations. Due to the solid logging data and deduced geophysical parameters (averaged values) for the bodies (Fig. 32, Tab. 6), best fit models are mainly based on modification of geometrical data. In doing so, Messel volcanoclastic rocks have their greatest dimensional variability, due to the solely magnetic model influence and single borehole information. The slightly bowl-shaped structure-model is consistent with post-eruptive conditions, affected by

compaction and subsidence of the crater infill (Lorenz et al., 2003). To keep the model as simple as possible, the tuffitic rocks and the lapilli tuffs are symmetric in 2D illustrations from the centre to the margins, and the structure is not accompanied by intrusive bodies. This assumption is in agreement with the interpretation of the seismic profiles (Buness et al., 2005), albeit the steep dip of the diatreme wall (approximately 80°) can not be proved by seismic reflection survey. In addition to the geophysical parameters (density, magnetisation) used for modelling, table 6 outlines the calculated volumes and masses of the Messel lithozones.



**Fig. 32** Vertical sections of the complete (left) and zoomed (right) diatreme model, striking through the research borehole 2001. The measured (red) and modelled (black) curves correspond to the gravity (bottom curves) and magnetic (top curves) fields. Logging data (density, magnetisation) of the lithozones provide the geophysical parameters for the model.

**Table 5** Averaged rock magnetic parameters calculated for the magnetisations used in the magnetic model.

No.	lithozone	NRM [A/m]	MS [ $10^{-3}$ S]	IM [A/m]	Q=NRM/IM	I [°]	polarity
5	tuffitic rocks	-2.0	8.5	0.3	6.6	-40?	-
6	upper lapilli tuff	-1.62	15.3	0.6	2.7	-77...+39, $\emptyset = -40$	-
7	lower lapilli tuff	-5.63	20.8	0.81	6.8	-30...-56, $\emptyset = -40$	-

**Table 6** Geophysical parameters of the Messel 2001 lithozones and calculated volumes and masses.

No.	lithozone	density [kg/m <sup>3</sup> ]	~ magnetisation [A/m]	volume [10 <sup>-3</sup> km <sup>3</sup> ]	mass [10 <sup>9</sup> kg]
	surrounding (ref.)	2670	0		
1	upper black pelites	1330	0	32.6	43.4
2	upper sand/clay	1630	0	10.1	16.5
3	lower black pelites	1500	0	5.2	7.8
4	lower sand/clay	2100	0	48.1	101.0
5	tuffitic rocks	2070	-1.7	3.7	7.7
6	upper lapilli tuff	2030	-1	9.1	18.5
7	lower lapilli tuff	2250	-5	22.4	50.4
8	diatrema breccia	2250	0	144.0	324.0
9	country rock	2550	0		

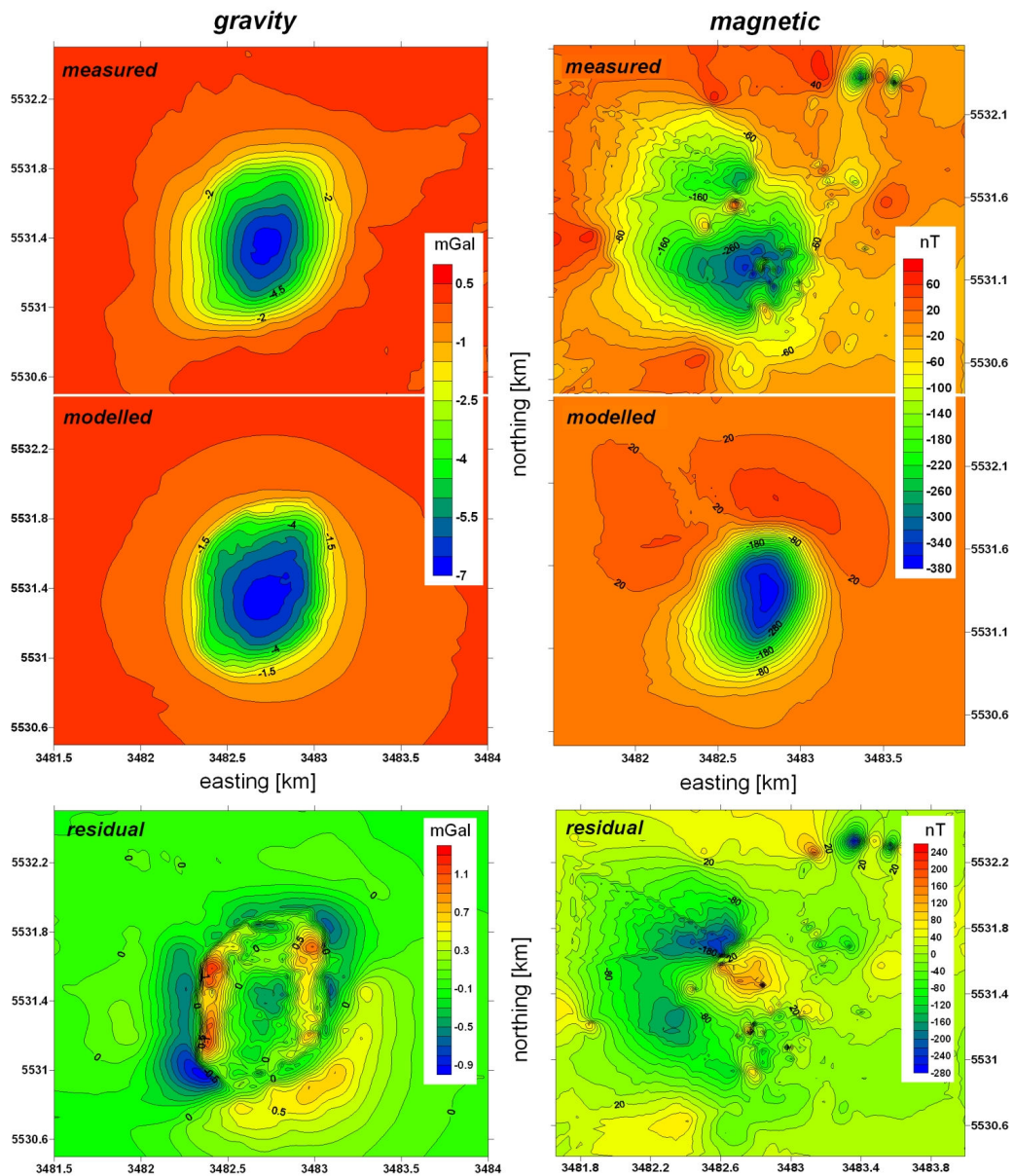


**Fig. 33** Measured and modelled potential field anomalies as well as their residuals. Highest contrasts are illustrated in red (positive) and blue (negative). The gravity model shows its greatest differences around the circular shaped anomaly, the magnetic model at the northern part of the main anomaly.

Measure of model quality is provided by gravity and magnetic maps, signifying the difference between the measured and modelled fields (Fig. 33). Reasonable modulation is achieved when deviations are in the range of measurement errors ( $\pm 0.3$  mGal) and geology is not visible in corresponding map illustrations. In the Messel case, both measured and modelled gravity fields show similar negative anomalies with a slight SW-NE elongation. The differences – defined as measured field minus modelled field – are of maximal  $\pm 1$  mGal and are located at the western and eastern parts of the modelled diatreme-structure. The residuals are relatively high, but the main focus was restricted to the crater infill. Here, the gravity differences are between  $+0.3$  and  $-0.3$  mGal. Furthermore, near surface structures embedded in the country rock, have not been considered in this model. The attempt of density inversion did not significantly improve the modelling results and thus has been rejected.

Concerning the more complex measured magnetic anomaly, the aforementioned qualitative constraints do not allow the construction of a two-body-model. It is very speculative, if the negative peak of approximately  $-260$  nT results from the existence of an additional volcanic body (e.g. dyke) which has to be negatively polarised and located north of the main anomaly peak of  $-380$  nT (Fig. 33). If so, its magnetic influence is shown in deviations, mainly occurring in the western parts of the modelled planes. The magnetic field displays differences of the measured and modelled fields in the range of  $\pm 200$  nT. The residual intensities are relatively low when compared to measures or modelled field contrasts of roughly  $440$  nT from the maar-centre to its margins (maximal deviation).

#### **4.4 Interpretation of the 3D modelling**

The combined interpretation of the surface potential field measurements, interpretation of the seismic lines, the results of the borehole logging and the lithological core information confirm a maar-diatreme-structure model. The gravity model fit well with the measured anomalies; the magnetic model is more simplified but well-approximated. While the gravity model mainly attributes to the density parameters selected for the lacustrine sediments (upper part of the maar-structure), the magnetic model is based on magnetisation intensities of the volcanoclastic material (lower part of the maar-structure). Figure 34a shows one representative vertical section through the gravity and magnetic models, and confirms their well-defined accordance between measured and modelled potential fields. In this section, the diatreme-structure appears to be slightly asymmetrical with a flatter diatreme wall angle of the lacustrine sediments at the SW margin. The lapilli tuffs display here their greatest thickness. According to current research studies on the volcanoclastic rocks, the western half of the maar-structure is assumed to be the preferred depositional area (pers. communication, Felder, 2006). Thereby, it does not necessarily implicate that the magnetised material is dominant in the volcanoclastic facies. The volcanoclastic source investigations are based on country rock studies which are supposed to clarify possible vent movements and involvement of the rocks surrounding the



diatreme-structure. The so-called “flying carpet” illustration shows the modelled 3D “snapshot” of the Messel subsurface (Fig. 34b).

Finally, it has to be mentioned that the magnetic model includes the calculated magnetisations deduced by one single borehole information. As described in the rock magnetic chapter the NRM's are produced by different emplacement temperatures. The same thermal history and acquisition of the TRMs are not ascertained in the Messel lateral volcanoclastic successions. Consequently, the correctness of the modelled geometry of the volcanic edifice is questioned. The complexity of these deposits with their appropriate magnetisations can only be clarified by additional information of cored boreholes, drilled in direction to the Messel maar-margins.

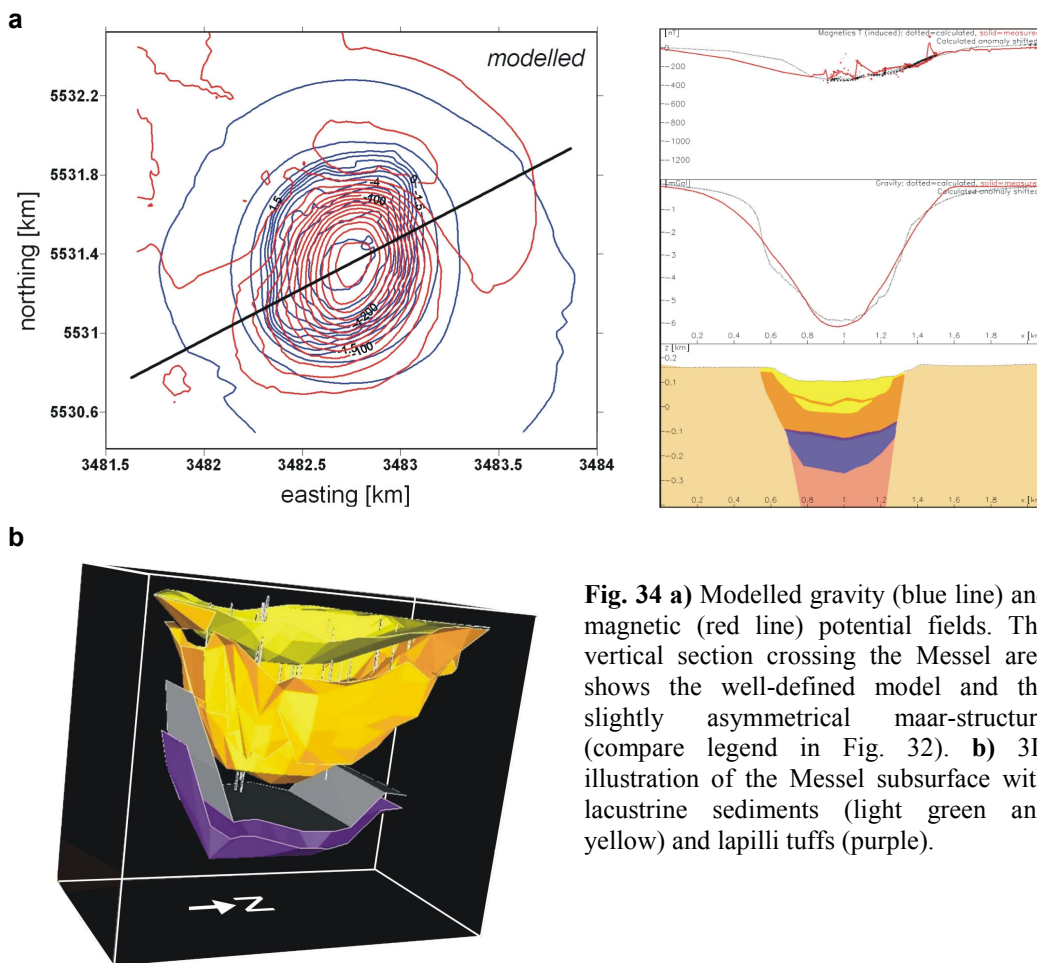


**Fig. 34 a)** Modelled gravity (blue line) and magnetic (red line) potential fields. The vertical section crossing the Messel area shows the well-defined model and the slightly asymmetrical maar-structure (compare legend in Fig. 32). **b)** 3D illustration of the Messel subsurface with lacustrine sediments (light green and yellow) and lapilli tuffs (purple).

## Chapter 5 Conclusions

According to scientists dealing with maar-related problems, interpreting explosive eruption and primary depositional processes of intra-crater deposits can be very difficult in the field (e.g. Houghton et al., 2000; Skilling, 2006). The reconstruction of eruption and formation processes depends on the distribution (size and spatial) of clasts in primary volcanoclastic deposits. However, processes of re-sedimentation (unconsolidated deposits) and re-fragmentation (i.e. epiclastic processes) of consolidated deposits complicate the information of eruption mechanisms. Primary deposits can also be very difficult to identify in intra-crater settings, because rapid deposition and short transportation distances give rise to a dominance of massive, poorly sorted facies which are very difficult to classify. Furthermore, steep-sided and thus gravitationally unstable margins of diatreme-related volcanoes and multiple eruptions that commonly destroy or disrupt wallrock or earlier deposits point out the complexity of common infilling of the craters. To obtain any reliable data on primary deposits from intra-crater sequences, it is essential to understand and extract the crater formation and the volcano-specific (eruption-related) processes.

In this context, rock magnetic investigations on the Messel volcanoclastics have shown that they are very instrumental in identifying primary deposits due to the extraction of informational data and the interpretation of the prevailing magnetic record of the historic Earth's magnetic field.

The used rock magnetic methods in combination with small-scale image analytical and geochemical methods explain the downhole and ground magnetic anomalies of Messel. The interdisciplinary studies also provide insights into emplacement conditions of the intra-crater pyroclastics.

Based on borehole and rock magnetic data, the Messel lapilli tuffs can be separated into one strongly and one slightly magnetised (lower and upper half) volcanic body. MS and NRM data of specimens approve the onset of the magnetised part below 307 m of the surface. Rock magnetic experiments (k(t)-curves, iron oxide analyses, hysteresis, IRM, demagnetisation experiments) performed on samples throughout the volcanoclastic units have shown similarities in the composition (near magnetite) and grain size (PSD) of the ferrimagnetic components. Therefore, with respect to the lack of ferrimagnetic diversity in the material, the differently acquired remanence magnetisations can be only explained by heat differences during/after emplacement of the volcanoclastic particles.

The origin of the remarkable magnetic signature could be clarified by thermal magnetic experiments. Although the whole volcanoclastic material was able to acquire similar remanent magnetisations, the lower half of the lapilli tuff only shows high remanence magnitudes and reflects strong TRMs. The TRM experiments, presented here, indicate that the magnetised part have been deposited at temperatures  $\gg 300$  °C, the non-magnetised part  $< 300$  °C.

Moreover, pyroclastic fragment investigations argue for the different heat and magma source conditions under the terms of particle grain size, amount and geochemistry of the juvenile fragments. Based on the results of the previous chapters and the knowledge of (Messel) maar-related concerns (e.g. Zimanowski et al., 1997; Lorenz et al., 2003; Lorenz and Kurszlauskis, 2007; Schmincke, 2004), the last eruption phases of the Messel volcanic activity and its post-eruptive events can be described and illustrated (Fig. 35) as follows:

Magma ascended along a conduit within the pipe, associated to the SW-NE oriented Messel fault zone. The Messel volcanoclastics do not represent deposits of the direct feeding system. Therefore, the conduit or conduits have to be displaced from the Messel centre where the borehole 2001 exists. Deposition of the volcanoclastic rocks in direction to the centre occurred in temporal and spatial successions. The melt penetrated through layered deposits of the diatreme-breccia or older eruption phases and encountered groundwater in depths of several tens of meters (up to hundred meters) below the pre-existing and partly subsided maar-crater. The magma/water interaction resulted in a (phreato)magmatic eruption (eruptive phase 1). It is very likely that the eruption column was relatively low and the intra-crater depositional process rapid, so that the material was still relatively hot to acquire high remanence intensities (TRM) and stable (negative) NRM inclinations. In this connection, image analyses have shown the predominance of relatively large juvenile fragments, their high frequency of occurrence and a relatively small ash proportion. The particle investigations argue here for the most pronounced temperature effect (maintenance of heat in juvenile particles), a relatively low W/M (water/magma) mass ratio and low fragmentation index. Moreover, juvenile fractions with an undifferentiated geochemical character (primary magma) tend to erupt at high temperatures (basaltic melt c. 1200 °C). This assumption supports the hot eruptive phase and the maintenance of still high temperatures after deposition of the material. The absence of layer boundaries, especially between the magnetised and non-magnetised lapilli tuff sequences, implicates a fast, subsequent impulse of eruptive phase 2. In this stage, the erupted material has been deposited at lower temperatures and is characterised by a slightly smaller amount of juvenile fragments as well as smaller grain sizes. All criteria infer a high amount of water involved in the eruptive system relative to the first eruptive phase, which resulted in a more energetic event (higher degree of magma fragmentation) and thus in a possibly higher eruption column. Thereby, relatively rapid and effective heat loss of the juvenile particles is given by their slightly smaller grain sizes which correlate with their thermal diffusion time (Gudmundsson, 2003). Possibly, the longer ballistic aerial duration time and the geochemically more differentiated character of the juvenile fraction (evolved magma) are favours for the colder eruptive phase 2. Thus, the intra-crater deposits acquired weak remanent magnetisations. The primary origin of deposition is not questioned because of the lack of totally disordered paleomagnetic data and dominant negative inclinations in most parts of the deposited material.

Similar trace element ratios of the magma involved in both eruption stages indicate a magmatic source from the same magma chamber. However, the major element pattern of the juvenile fragments favours magmas from different magma chamber levels.

The clear major element differentiation from the first eruptive phase provides the potential of a newly evolved magma conduit (eruptive phase 2b). Vent migration is a possible and observed phenomenon in maar-related volcanoes (Sohn and Park, 2005), but speculative and incomprehensible with the rapid and successive Messel eruption stages. Post-eruptive phases signal the final stages of the Messel maar formation. They are dominated by erosive processes of the crater walls, compaction of the material and subsidence processes (Lorenz et al., 2003; Lorenz and Kurszlaukis, 2007). Due to the relatively high groundwater level and lacking surface drainage, the Messel maar crater was filled with a lake. Lake beds and other maar-related deposits accumulated and were affected by further subsidence and slumping processes as long as compaction of the underlying diatreme fill continued.

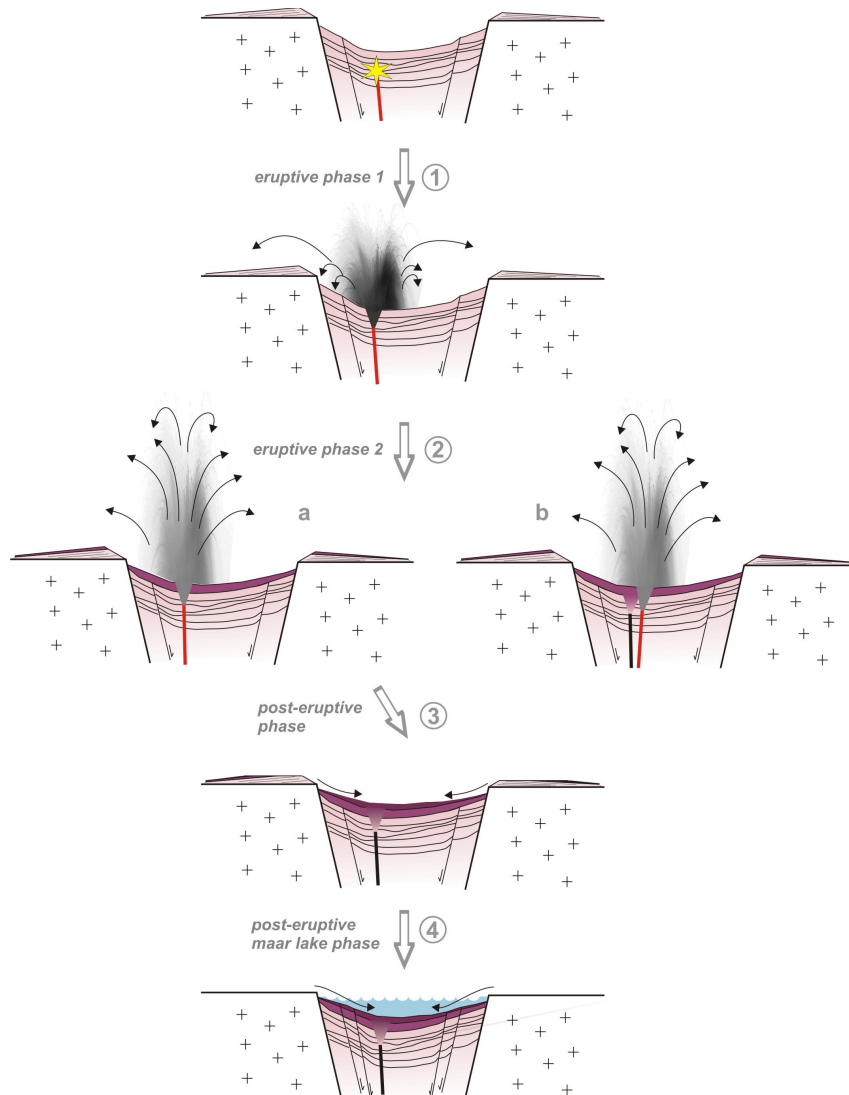


**Fig. 35** Schematic cross sections through the upper level of the Messel maar-diatreme-volcano in syn- and post-eruptive stages, showing the deposition of the magnetised and non-magnetised lapilli tuff sequences as well as the evolution of the Messel basin up to the maar-lake stadium.

The dynamic model, presented here, implies a relatively stable feeder conduit located somewhere distant from the core recovery in the borehole sections. Although the material lacks distinct bedding, experimental studies favour at least two intra-crater fills of different time and spatial distribution. The relatively juvenile-rich pyroclastic phases imply the deficiency of groundwater which indicates the prevention of very powerful thermohydraulic explosions at the end of Messel volcanic activity. The dominance of post-explosive magmatic activity is known from several maar volcanoes and can lead to sills in bedded volcanoclastics in the upper diatreme or could reach the maar crater, forming scoria cones or lava flows and lava lakes (Houghton and Schmincke, 1989; Houghton et al., 1996; Houghton et al. 1999; Aranda-Gomez et al., 1992; Aranda-Gomez and Luhr, 1996; Lorenz, 1986; Lorenz and Kurszlaukis, 2007; Martin and Nemeth, 2007). In addition to the Messel volcanoclastic material, however, massive volcanic edifices within the crater infill can be excluded. This is confirmed by the absence of geophysical indicators (e.g. seismics, magnetics) during exploration of the Messel Pit as well as log interpretation of the downhole magnetic field measurements.

For the first time, thermal magnetic temperature studies on pyroclastic successions within a diatreme-structure could clarify the existence of downhole magnetic anomalies by different emplacement temperatures. Although it was thought that maar-related deposits of phreatomagmatic origin deal with relatively low eruption temperatures, the lower half of the Messel pyroclastics argue the converse.

Generally, when dealing with magnetic anomalies which are implicative for a subsurface diatreme-structure, it has to be considered the existence of pyroclastic rock units, which are affected by high emplacement temperatures, and their acquisition of high thermal remanent magnetisations. These TRMs can produce magnetic anomalies, detectable by ground survey and borehole measurements. The Messel potential field 3D model explains the magnetic anomaly on the surface. Thereby, the remanent magnetisations of the volcanoclastics account for the ground magnetic anomaly to approximately 83 %, the induced magnetisations to 17 %.

### *Perspectives*

The Messel drilling project 2001 with full core recovery provides a wide variety for on-going research interests. The comparison of the volcanoclastic material with volcanic rocks of the neighbouring volcanoes (e.g. Prinz of Hessen, Großzimmern) or dyke intrusions will enhance chances for the volcanological interpretation of the entire "Sprendlinger Horst volcanic field" existence. With respect to the pyroclastic edifice of the maar-volcano, detailed investigations on accidental clasts and their geological origin related to the geological environment will improve knowledge about the eruptive processes occurred at the end of Messel activity.

It is possible that the aforementioned two eruption phases can be sub-classified into several short eruptive events by means of differently occurring clasts of the country rock. Observing

the magnetic signature (or NRMs) pronounced to the lower half of the lapilli tuffs (eruptive phase 1), magnetic peaks may reflect such different eruptive impulses. Due to very similar results of the TRM experiments, the hot deposited material only reflects small temperature difference ( $\Delta T \approx 50 \text{ }^\circ\text{C}$ ) between its highest and lowest NRM intensity (Fig. 36). According to the distribution field of these TRM curves, the maximal temperature difference between low (2 A/m) and high (10 A/m) NRM samples is  $<70 \text{ }^\circ\text{C}$ . Admittedly, the determination of absolute temperatures within the hot deposited rocks is problematic due to the Messel exponential TRM curves and their insignificance at temperatures above the Curie point. However, maar-related pyroclastic rocks are rarely exposed to very high temperatures (e.g.  $>600 \text{ }^\circ\text{C}$ ), especially in settings where the interaction of magma and water (coolant) prevails. Modelling more exact emplacement temperatures of the volcanoclastic units appears to be a very complex challenge. The particle variability with different physical and chemical properties complicates the system when dealing with geodynamic problems in volcanoclastic or pyroclastic rocks. Moreover, the particle information of the Messel borehole is due to one single cut into the subsurface structure; there is no lateral distribution of the volcanoclastic rocks and the corresponding particles available. However, a possible approach to understand the temperature evolution mainly within the lower half of the hot deposited lapilli tuffs can be a computer-based modelling. The results of the rock magnetic, image analytical, geochemical and potential field modelling may support the appropriate data input in those models.

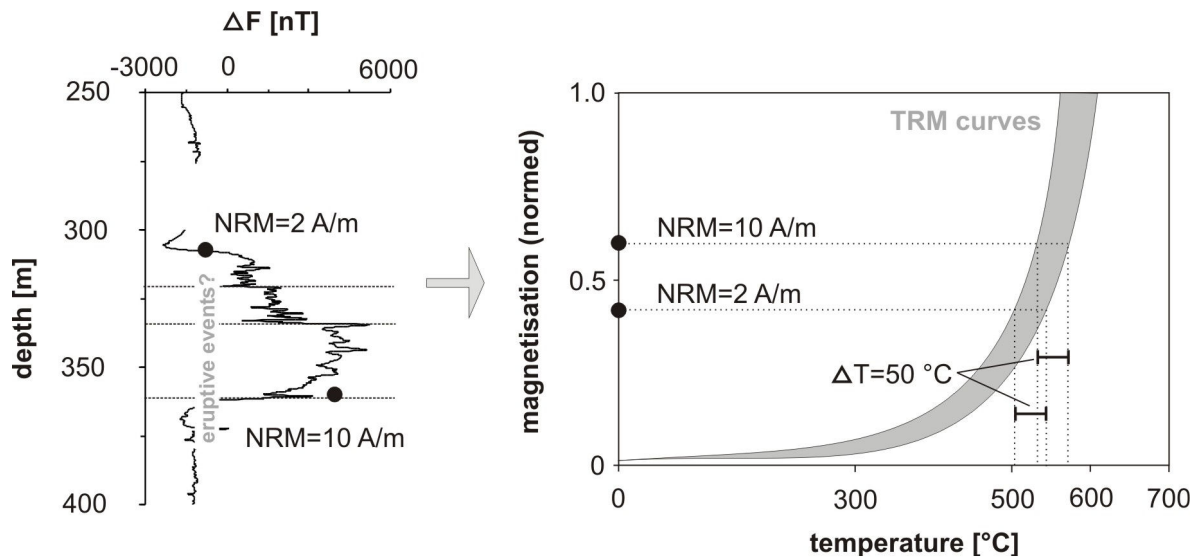


**Fig. 36** Illustration of the magnetic signature with  $\Delta F$  intensity peaks indicating different eruptive events. Due to initial NRMs and corresponding TRM curves, the maximal temperature differences of samples from the hot eruptive phase are  $50 \text{ }^\circ\text{C}$ .

## References

- Alva-Valdivia, L.M., Rosas-Elguera, J., Bravo-Medina, T., Urrutia-Fucugauchi, J., Henry, B., Caballero, C., Rivas-Sanchez, M.L., Goguitchaichvili, A. and Lopez-Loera, H., 2005. Paleomagnetic and magnetic fabric studies of the San Gaspar ignimbrite, western Mexico - constraints on emplacement mode and source vents. *Journal of Volcanology and Geothermal Research*, 147, 1-2, 68-80.
- Aranda-Gomez, J.J. and Luhr, J.F., 1996. Origin of the Joya Honda maar, San Luis Potosi, Mexico. - *Journal of Volcanology and Geothermal Research*, 74, 1-18.
- Aranda-Gomez, J.J., Luhr, J.F. and Pier, J.G., 1992. The La-Breña-El-Jaguey-Maar Complex, Durango, Mexico .1. Geological Evolution. *Bulletin of Volcanology*, 54, 393-404.
- Baier, J., Lücke, A., Negendank, J.F.W. and Zolitschka, B., 2000. Changes in biogeochemical parameters in response to anthropogenic and climatic influences on the palaeo-ecosystem of Lake Holzmaar (West-Eifel, Germany) focussing on the time-period 6300 varve years BP to 1550 varve years BP. *Terra Nostra*, 2000/6, 29-34.
- Bergmann, H., 1987. Lamproites and other potassium-rich igneous rocks: a review of their occurrence, mineralogy and geochemistry. In: J.G. Fitton and B.G.J. Upton (Editors), *Alkaline igneous rocks*. Geological Society Special Publications, 30, 103-190.
- Bloxham and Gubbins, 1998. The evolution of the Earth's magnetic field. *Scientific American*, 261 (6), 30-37.
- Bogaard, P.J.F. and Woerner, G., 2003. Petrogenesis of basanitic to tholeiitic volcanic rocks from the Miocene Vogelsberg, central Germany. *Journal of Petrology* 44, 569-602.
- Büchel, G., 1987. Geophysik der Eifelmaare. 1.: Erkundung neuer Maare im Vulkanfeld der Eifel mit Hilfe geomagnetischer Untersuchungen. *Mainzer geowiss. Mitt.*, 16, 227-274.
- Büchel, G., 1988. Geophysik der Eifelmaare. 2: Geomagnetische Erkundung von Trockenmaaren im Vulkanfeld der Westeifel. *Mainzer geowiss. Mitt.*, 17, 357-376.
- Büchel, G., 1993. Maars of the Westeifel, Germany. In: Negendank J.F.W. (Ed.): *Paleolimnology of European maar lakes*. Lecture Notes Earth Science, 49, 1-13.
- Büchel, G., Jacoby, W., Lorenz, V. and Zimanowski, B., 1987. Geophysical aspects of the formation of Eifel maars. *Terra Cognita, EUG IV, G 11, 54: 365*.
- Bücker, C., Wonik, T. and Schulz, R., 2003. Physikalische Eigenschaften einer Tertiären Maarfüllung – Ergebnisse von Bohrlochmessungen in den Forschungsbohrungen Baruth (Sachsen). *Zeitschrift für Angewandte Geologie*, 1, 43-51.
- Buness, H., 2005. Seismische Experimente am Nordostrand der Grube Messel in der Umgebung der Inklinometerbohrung IN28. *Courier Forschungsinstitut Senckenberg*, 255, 57-65.
- Buness, H., Gabriel, G., Pucher, R., Rolf, C., Schulz, R. and Wonik, T., 2004. Grube Messel: Die Geophysik blickt unter die Abbausohle. *Natur und Museum*, 134, 65-76.

- Butler, R.F., 1992. Paleomagnetism: Magnetic Domains to Geologic Terranes. Blackwell Scientific Publications, 319 pp.
- Büttner, R. and Zimanowski, B., 1998. Physics of thermohydraulic explosions. - *Physical Review E*, 57, 5726-5729.
- Cassidy, J., Locke, C.A., 2004. Temporally linked volcanic centres in the Auckland Volcanic Field, New Zealand *Journal of Geology and Geophysics*, 47, 287-290.
- Cassidy, J., France, S.J. and Locke, C.A. Gravity and magnetic investigation of maar volcanoes, Auckland volcanic field, New Zealand. *Journal of Volcanology and Geothermal Research*, (in press).
- Daubree, M., 1893. Versuche über die mechanische Wirkung heißer, stark gepresster und rapid bewegter Gase auf Gesteine. *Zeitschrift für praktische Geologie*, 1893, 284-295.
- Daubree, M., 1891. Recherches expérimentales sur le rôle possible des gaz à hautes températures, doués de très fortes pressions et animés d'un mouvement fort rapide, dans divers phénomènes géologiques. - *Bulletin Sociale Géologique France* 3, 19, 313-354.
- Day, R., Fuller, M., and Schmidt, V., 1977. Hysteresis properties of the titanomagnetites, grain size and compositional dependence. *Physics Earth Planetary Interiors* 13, 260-267.
- De Wall, H., 2005. Die Anisotropie der magnetischen Suszeptibilität – eine Methode zur Gefügeanalyse. *Zeitschrift Deutscher Geologischer Gesellschaft*, 155 (2-4), 287-298.
- De Wall, H., Kontny, A. and Vahle, C., 2004. Magnetic susceptibility zonation a melilititic dyke complex (Riedheim dyke, Hegau volcanic field, Germany) evidence for multiple magma pulses? *Journal of Volcanology and Geothermal Research*, 131, 143-163.
- Delesse, M.A., 1847. Procédé mécanique pour déterminer la composition des roches. *Comptes rendus de l'Académie des Sciences (Paris)*, 25, 544-545.
- Dezes, P., Schmid, S.M. and Ziegler, P.A., 2004. Evolution of the European Cenozoic rift system; interaction of the Alpine and Pyrenean orogens with their foreland lithosphere. *Tectonophysics*, 389, 1-33.
- Downes, H., 1987. Tertiary and Quaternary volcanism in the Massif Central, France. *Geological Society Special Publications*, 30, 517-530.
- Dunlop, D.J. and Ozdemir, O., 1997. *Rock magnetism: Fundamentals and frontiers*. Cambridge University Press, 573 pp.
- Eberle, D., 1985. Interpretation von bohrlochmagnetometrischen Messungen in drei Komponenten. *Geologisches Jahrbuch*, E28, 219-235.
- Felder, M., Harms, F.J. and Wolf, K., 2004. Lithologie und genetische Interpretation der vulkano-sedimentären Ablagerungen aus der Grube Messel anhand der Forschungsbohrung Messel 2001 und weiterer Bohrungen. *Courier Forschungsinstitut Senckenberg*, 252, 151-203.
- Fischer, R.V., 1961. Proposed classification of volcanoclastic sediments and rocks. *Geological Society American Bulletin*, 72, 1409-1414.



- Fischer, R.V., 1966. Rocks composed of volcanic fragments. *Earth Science Review*, 1, 287-298.
- Fisher, R.V. and Schmincke, H.U., 1984. *Pyroclastic rocks*. Springer Verlag, Berlin, New York, 472 pp.
- Frisch, W. and Meschede, M., 2005. *Plattentektonik. Kontinentverschiebung und Gebirgsbildung*. Wissenschaftliche Buchgesellschaft, Darmstadt, 196 pp.
- Gabriel, G., 2003. Die gravimetrische Anomalie Baruth (sachsen) – Aussagen über die Struktur eines verdeckten Maars. *Zeitschrift für Angewandte Geologie*, 1, 18-25.
- Glatzmaier, G.A. and Roberts, P.H., 1996. Rotation and magnetism of Earth's inner core. *Science*, 274, 1887-1891.
- Goes, S., Spakman, W. and Bijwaard, H., 1999. A lower mantle source for Central European volcanism. *Science*, 286, 1928-1931.
- Götze, H.J. and Lahmeyer, B., 1988. Application of three-dimensional interactive modeling in gravity and magnetics. *Geophysics*, 53/8, 1096-1108.
- Götze, H.J., 1978. Ein numerisches Verfahren zur Berechnung der gravimetrischen Feldgrößen drei-dimensionaler Modellkörper. *Arch. Met. Geoph. Biokl., A*, 25, 195-215.
- Götze, H.J., 1984. Über den Einsatz interaktiver Computergraphik im Rahmen 3-dimensionaler Interpretationstechniken in Gravimetrie und Magnetik. *Habilitations-Schrift*, Technische Universität Clausthal, 121 pp.
- Harms, F., Nix, T. and Felder, M., 2003. Neue Darstellungen zur Geologie des Ölschiefer-Vorkommens Grube Messel. *Natur und Museum* 133, 140-148.
- Hawthorne, J.B., 1975. Model of a kimberlite pipe. - In: Ahrens, L.H., Dawson, J.B., Duncan, A.R., Erlank, A.J. (eds.): *Proc. 1st Int. Kimberlite Conf.*, Cape Town 1973. *Phys. Chem. Earth*, 9, 1-15.
- Heiken, G. and Wohletz K., 1985. *Volcanic Ash*, University of California Press, Berkeley, 245 pp.
- Higgins, M.D., 2002. Closure in crystal size distributions (CSD), verification of CSD calculations, and the significance of CSD fans. *American Mineralogist*, 87, 171-175.
- Houghton, B.F. and Schmincke, H.U., 1989. Rothenberg scoria cone, East Eifel; a complex strombolian and phreatomagmatic volcano. *Bulletin of Volcanology*, 52(1), 28-48.
- Houghton, B.F., Wilson, C.J.N. and Pyle, D.M. 2000. *Pyroclastic Fall Deposits*. In: *Encyclopedia of volcanoes*. Edited by H. Sigurdsson, B.F. Houghton, S.R. McNutt, H. Rymer, and J. Stix. Academic Press, San Diego, California, 555–570.
- Houghton, B.F., Wilson, C.J.N. and Smith, I.E.M., 1999. Shallow-seated controls on styles of explosive basaltic volcanism: a case study from New Zealand. *Journal of Volcanology and Geothermal Research*, 91(1), 97-120.
- Houghton, B.F., Wilson, C.J.N., Rosenberg, M.D., Smith, I.E.M. and Parker, R.J., 1996. Mixed deposits of complex magmatic and phreatomagmatic volcanism: An example from Crater Hill, Auckland, New Zealand. *Bulletin of Volcanology*, 58(1), 59-66.

- Hrouda, F., 1994. A technique for the measurement of thermal changes of magnetic susceptibility of weakly magnetic rocks by the CS-2 apparatus and KLY-2 Kappabridge. *Geophysical Journal International*, 118, 604-612.
- Illies, J.H., 1975. Recent and paleo-intraplate tectonics in stable Europe and the Rhinegraben rift system. *Tectonophysics*, 29, 251-264.
- Jackoby, W., Wallner, H. and Smilde, P., 2000. Tektonik und Vulkanismus entlang der Messel-Störungszone auf dem Sprendlinger Horst: Geophysikalische Ergebnisse. *Zeitschrift Deutscher Geologischer Gesellschaft*, 151, 493-510.
- Jacoby, W., Sebazungu, E., Wallner, H., Gabriel, G. and Pucher, R., 2005. Potential field data for the Messel Pit and surroundings. *Courier Forschungsinstitut Senckenberg*, 255, 1-9.
- Jelinek, V., 1981. Characterization of the magnetic fabrics of rocks. *Tectonophysics*, 79, 63-67.
- Jung, S. and Hoernes, S., 2000. The major- and trace-element and isotope (Sr, Nd, O) geochemistry of Cenozoic alkaline rift-type volcanic rocks from the Rhoen area (central Germany): petrology, mantle source characteristics and implications for asthenosphere-lithosphere interactions. *Journal of Volcanology and Geothermal Research*, 99, 27-53.
- Kontny A., Vahle C. and de Wall H., 2003. Characteristic magnetic behaviour of subaerial and submarine lava units from the Hawaiian Scientific Drilling Project (HSDP-2). *Geochemistry, Geophysics, Geosystems*, 3, 8, 10.1029 / 2002GC000304.
- Kontny, A. and de Wall, H., 2000. The use of low and high k(T)-curves for the characterization of magneto-mineralogical changes during metamorphism. *Physics and Chemistry of the Earth*, A25/5, 421-429.
- Kurszlaukis, S., Büttner, R., Zimanowski, B. and Lorenz, V., 1998. On the first experimental phreatomagmatic explosion of a kimberlite melt. – *Journal of Volcanology and Geothermal Research*, 80, 323–326.
- Larroque, J.M. and Laurent, P., 1988. Evolution of the stress field pattern in the south of the Rhine Graben from the Eocene to the present. *Tectonophysics*, 148, 41-58.
- Laubersheimer, F., 1997. Vermessung magnetischer Anomalien über Ölschieferbecken bei Messel: Quantitativer Vergleich verschiedener Vorkommen auf dem Sprendlinger Horst. Diploma thesis, Univ. Mainz, (unpublished).
- Le Penec, J.L., Chen, Y., Diot, H., Froger, J.L. and Gourgaud, A. 1998. Interpretation of anisotropy of magnetic susceptibility fabric of ignimbrites in terms of kinematic and sedimentological mechanisms: An Anatolian case-study. *Earth and Planetary Science Letters*, 157, 1-2, 105-127.
- Lorenz, V. and Büchel, G., 1980. Zur Vulkanologie der Maare und Schlackenkegel der Westeifel. *Mitteilungen Pollichia*, 68, 29-100.
- Lorenz, V. and Kurszlaukis, S., 2007. Root zone processes in phreatomagmatic pipe emplacement model and consequences for the evolution of maar-diatreme volcanoes. *Journal of Volcanology and Geothermal Research*, 159, 4-32.

- Lorenz, V., 1974. On the formation of maars. *Bulletin of Volcanology*, 37, 183-204.
- Lorenz, V., 1975. Formation of phreatomagmatic maar-diatreme volcanoes and its relevance to the formation of kimberlite diatremes. - In: Ahrens, L.H., Dawson, J.B., Duncan, A.R., Erlank, A.J. (eds.): *Proc. 1st Int. Kimberlite Conf., Cape Town 1973, Phys. Chem. Earth*, 9, 17-27.
- Lorenz, V., 1982. Zur Vulkanologie der Tuffschlote der Schwäbischen Alb. - *Jber. Mitt. oberrhein. geol. Ver.*, 64, 167-200.
- Lorenz, V., 1985. Maars and diatremes of phreatomagmatic origin, a review. *Trans. Geol. Soc. South Africa*, 88, 459-470.
- Lorenz, V., 1986. On the growth of maars and diatremes and its relevance to the formation of tuff rings. *Bulletin of Volcanology*, 48, 265-274.
- Lorenz, V., 2000. Formation of maar-diatreme-volcanoes. *Terra Nostra*, 2000/6, International Maar Conference, Daun/Vulkaneifel, Extended Abstract, 284-291.
- Lorenz, V., Suhr, P. and Goth, K., 2003. Maar-Diatrem-Vulkanismus – Ursachen und Folgen. Die Guttauer Vulkangruppe in Ostsachsen als Beispiel für die komplexen Zusammenhänge. *Zeitschrift Geologischer Wissenschaft*, Berlin, 31/4-6, 267 – 312,
- Lorenz, V., Zimanowski, B. and Büttner, R., 2002. On the formation of deep-seated subterranean peperitelike magma-sediment mixtures. *Journal of Volcanology and Geothermal Research*, 114, 107-118.
- Lücke, A., Moschen, R., Schleser, G.H., 2005. High temperature carbon reduction of silica: A novel approach for oxygen isotope analysis of biogenic opal. *Geochimica et Cosmochimica Acta*, 69, 1423-1433.
- Lücke, A., Schleser, G.H., Zolitschka, B. and Negendank, J.F.W., 2003. A continuous Lateglacial and Holocene organic carbon isotope record of lacustrine palaeoproductivity and climatic change derived from varved lake sediments of Lake Holzmaar, Germany. *Quaternary Science Reviews*, 22, 569-580.
- Mac Donald G.A. and Katsura T., 1964. Chemical Composition of Hawaiian Lavas. *Journal of Petrology*, 5, 82-133.
- Martin, U. and Nemeth, K., 2007. Blocky versus fluidal peperite textures developed in volcanic conduits, vents and crater lakes of phreatomagmatic volcanoes in Mio/Pliocene volcanic fields of Western Hungary. *Journal of Volcanology and Geothermal Research*, 159, 164-178.
- McElhinny, M. W. and McFadden P. L., 2000. *Paleomagnetism: Continents and Oceans*, Academic Press, San Diego, California, 386 pp.
- McElhinny, M.W. and Lock, J, 1990. IAGA global palaeomagnetic database. *Geophysical Journal International*, 101, 763-766.
- Merril, R.T., McElhinny, M.W. and McFadden, P.L., 1996. *The magnetic field of the Earth: Paleomagnetism, the Core and the deep Mantle*. Academic Press, San Diego, 531 pp.

- Mertz, D.F. and Renne, P.R., 2005. A numerical age for the Messel fossil deposit (UNESCO world natural heritage site) from  $^{40}\text{Ar}/^{39}\text{Ar}$  dating. *Courier Forschungsinstitut Senckenberg*, 255, 67-75.
- Michon, L., van Balen, R.T., Merle, O. and Pagnier, H., 2003. The Cenozoic evolution of the Roer Valley rift system integrated at a European scale. *Tectonophysics*, 367, 101-126.
- Middlemost, E.A.K., 1975. The basalt clan. *Earth Science Review*, 11, 337-364.
- Middlemost, E.A.K., 1980. A contribution to the nomenclature and classification of volcanic rocks. *Geological Magazine*, 117, 51-57.
- Mitchell, R.H. and Bell, K., 1976. Rare earth element geochemistry of potassic lavas from the Birunga and Toro-Ankole regions of Uganda, Africa. *Contributions to Mineralogy and Petrology*, 58, 293-303.
- Nairn, A.E.M. and Negendank, J., 1967. Paleomagnetic investigations of Tertiary and Quaternary rocks: IV. The Tertiary rocks of Southwest Germany. *Geologische Rundschau*, 62, 126-137.
- Noll, H., 1967. Maare und maar-ähnliche Explosionskrater in Island. Ein Vergleich mit dem Maar-Vulkanismus der Eifel. *Sonderveröff. Geol. Inst. Univ. Köln*, 11, 1-117.
- Ort, M.H., Rosi, M. and Anderson, C.D., 1999. Correlation of deposits and vent locations of the proximal Campanian Ignimbrite deposits, Campi Flegrei, Italy, based on natural remanent magnetization and anisotropy of magnetic susceptibility characteristics. *Journal of Volcanology and Geothermal Research*, 91, 2-4, 167-178.
- Ort, M.H., Wohletz, K., Hooten, J.A., Neal, C.A. and McConnel, V.S., 2000. The Ukinrek Maars eruption, Alaska, 1977: a natural laboratory for the study of phreatomagmatic processes at maars. - *Terra Nostra*, 2000/6, Int. Maar Conf., Daun/Vulkaneifel, Extended Abstract, 396-400.
- Palmer, H.C., MacDonald, W.D., Gromme, C.S. and Ellwood, B.B., 1996. Magnetic properties and emplacement of the Bishop tuff, California. *Bulletin of Volcanology*, 58, 101-116.
- Peterson, D.W., 1979. Significance of flattening of pumice fragments in ash-flow tuffs. In: C.E. Chapin and W.E. Elston (Editors), *Ash-flow tuffs and associate igneous rocks*. Special Paper Geological Society America, 195-204.
- Pirrung, M., Fische, C., Büchel, G., Gaupp, R., Lutz, H. and Neuffer, F.O., 2003. Lithofacies succession of maar crater deposits in the Eifel area (Germany). *Terra Nostra*, 15, 125-132.
- Puchnerova, M., Kubes, P., Lanc, J., Szalaiova, V., Santavy, J., Zboril, L., 2000. Results of geophysical exploration of the maar structures in the southern Slovakian Basin. *Terra Nostra* 2000/6, 410-417.
- Radhakrishnamurty, C., Likhite, S.D., Deutsch, E.R. and Murthy, G.S., 1982. On the complex behaviour of titanomagnetites. *Physical Earth Planetary Interior*, 30, 281-290.

- Rolf, C., Pucher, R., Schulz, R. and Wonik, T., 2005. Magnetische Untersuchungen an Kernen der Forschungsbohrung Messel 2001 – Erste Erkenntnisse zum Erwerb magnetischer Remanenzen in den Pyroklastika. Courier Forschungsinstitut Senckenberg, 255, 47-55.
- Roll, A., 1979. Versuch einer Volumenbilanz des Oberrheintalgrabens und seiner Schultern/Volume balance of the Upper Rhine Graben and its shoulders. Geologisches Jahrbuch Reihe A: Allgemeine und Regionale Geologie BR Deutschland und Nachbargebiete, Tektonik, Stratigraphie, Palaeontologie, 52, 3-82.
- Schmidt, S., 1996. 3D Modeling of Geoid and Gravity using GIS-functions - Österreichische Beiträge zu Meteorologie und Geophysik, 14, 137-144.
- Schmincke, H.U., 2004. Volcanism. Berlin, Springer Verlag, 334 pp.
- Schulz, R., Buness, H., Gabriel, G., Pucher, R., Rolf, C., Wiederhold, H. and Wonik, T., 2005. Detailed investigation of preserved maar structures by combined geophysical surveys. Bulletin of Volcanology, 68, 95-106.
- Schumacher, M.E., 2002. Upper Rhine Graben: role of preexisting structures during rift evolution. Tectonics 21, 1-17.
- Scrope, G.P., 1825. Considerations on volcanoes. London, 1–270.
- Skilling, I., 2006. Interpreting explosive eruption and primary depositional processes from kimberlitic intra-crater deposits. Extended Abstract for Kimberlite Emplacement Workshop, Saskatoon, Saskatchewan, Canada, 7-14 September 2006.
- Soffel H., 1991. Paläomagnetismus und Archäomagnetismus, Berlin, Springer Verlag, 276 pp.
- Sohn, Y.K and Park, K.H., 2005. Composite tuff ring/cone complexes in Jeju Island, Korea: possible consequences of substrate collapse and vent migration. Journal of Volcanology and Geothermal Research, 141, 157-175.
- Song, X. and Richards, P., 1996. Seismological evidence for differential rotation of the Earth's inner core. Nature, 382, 221-224.
- Steininger, J., 1819. Geognostische Studien am Mittelrhein. 1-223, Mainz (Kupferberg).
- Steininger, J., 1820. Die erloschenen Vulkane in der Eifel und am Niederrheine. 1-180, Mainz (Kupferberg).
- Steininger, J., 1821. Neue Beiträge zur Geschichte der rheinischen Vulkane. Mainz (Kupferberg), 1-116.
- Steininger, J., 1822. Gebirgskarte der Länder zwischen dem Rheine und der Maas. Mainz (Kupferberg), 1-82.
- Tarling, D.H. and Hrouda, F., 1993. The Magnetic Anisotropy of Rocks. London (Chapman and Hall), 217 pp.
- Torge, 1989. Gravimetry. Walter de Gruyter, Berlin, 465 pp.
- Toth, C., 1992. Geophysical prospecting of maar-type basaltic craters in Hungary. 54<sup>th</sup> Meet Eur Assoc Explor Geophys, 668-669.

- Vespermann, D. and Schmincke, H.U., 2000. Scoria cones and tuff rings. In: H. Sigurdson (Editor), *Encyclopedia of Volcanoes*. Academic Press, 683-694.
- Wedepohl, K.H., Gohn, E. and Hartmann, G., 1994. Cenozoic alkali basaltic magmas of western Germany and their products of differentiation. *Contributions to Mineralogy and Petrology*, 115, 253-278.
- White, R. and McKenzie, D., 1989. Magmatism at rift zones; the generation of volcanic continental margins and flood basalts. *Journal of Geophysical Research*, 94, 7685-7729.
- Wilson, M. and Downes, H., 1991. Tertiary-Quaternary extension-related alkaline magmatism in Western and Central Europe. *Journal of Petrology*, 32, 811-849.
- Wilson, M. and Downes, H., 2006 (in press). Tertiary-Quaternary intra-plate magmatism in Europe and its relationship to mantle dynamics. In: R.A. Stephenson and D. Gee (Editors), *European lithosphere dynamics*. Geological Society of London, *Memoirs*, xx-xx pp.
- Wilson, M., 1989. *Igneous petrogenesis. A global tectonic Approach*. International Thompson, London, 466 pp.
- Wohletz, K.H., 1986. Explosive magma-water interactions; thermodynamics, explosion mechanisms, and field studies. *Bulletin of Volcanology* 48, 245-264.
- Wonik, T. and Salge, S., 2000. Eine Apparatur für geophysikalische Messungen in Kleinkalibrigen Bohrungen bis 1300 m Tiefe. *Geologisches Jahrbuch*, E52, 129-160.
- Wonik, T., 2005. Erste Ergebnisse der geophysikalischen Messungen in der Forschungsbohrung Messel 2001. *Courier Forschungsinstitut Senckenberg*, 255, 11-20.
- Wood, C.A., 1974. Reconnaissance geophysics and geology of the Pinacate Craters, Sonora, Mexico. *Bulletin of Volcanology*, 38, 149-172.
- Zanella, E., De Astis, G. and Lanza, R., 2001. Palaeomagnetism of welded, pyroclastic-fall scoriae at Vulcano, Aeolian Archipelago. *Journal of Volcanology and Geothermal Research* 107, 1-3, 71-86.
- Zanella, E., De Astis, G., Dellino, P., Lanza, R. and La Volpe, L., 1999. Magnetic fabric and remanent magnetisation of pyroclastic surge deposits from Volcano (Aeolian Islands, Italy). *Journal of Volcanology and Geothermal Research*, 93, 217-236.
- Ziegler, P.A., 1992. European Cenozoic rift system. *Tectonophysics* 208, 91-111.
- Zimanowski, B., 1998. Phreatomagmatic explosions. In: A. Freundt and M. Rosi (Editors), *From Magma to tephra, Developments in Volcanology 4*. Elsevier, Amsterdam, 25-54.
- Zimanowski, B., Büttner, R., Lorenz, V. and Haefele, H.-G., 1997. Fragmentation of basaltic melt in the course of explosive volcanism. *Journal of Geophysical Research*, 102, 803-814.
- Zolitschka, B., Schaebitz, F., Lücke, A., Clifton, G., Corbella, H., Ercolano, B., Haberzettl, T., Maidana, N., Mayr, C., Ohlendorf, C., Oliva, G., Paez, M.M., Schleser, G.H., Soto, J., Tiberi, P., Wille, M., 2006. Crater lakes of the Pali Aike Volcanic Field as key sites of paleoclimatic and paleoecological reconstructions in southern Patagonia, Argentina. *Journal of South American Earth Sciences*, 21, 294-309.